UNIVERSITÀ DEGLI STUDI DI PAVIA

DOTTORATO IN SCIENZE CHIMICHE E FARMACEUTICHE E INNOVAZIONE INDUSTRIALE
(XXXVI Ciclo)

Coordinatore: Chiar.mo Prof. Giorgio Colombo

Synthesis of Substituted Tetralins via Novel Electrochemical Decarboxylative Cycloalkylation

Tesi di Dottorato di
Enrico Lunghi

AA 2023/2024

Tutor
Chiar.mo Prof. Giuseppe Zanoni

Co-tutor
Dr. Massimo Verzini

To Flavia, Francesco and Carlo.

Making you proud is the only thing i live for.

Summary

1. Chapter I: Organic electrochemistry

1.1 Hystorical evolution and early application of organic electrochemistry

Organic electrochemistry originated in the mid-19th century with Faraday's electrolysis of acetic acid to hydrocarbons[1] and Kolbe's electrochemical decarboxylative dimerization[2] (Figure 1a). Other important synthetic strategies discovered during this period include Simons' fluorination process[3] (Figure 1b) and Shono's oxidation of amines[4] (Figure 1c).

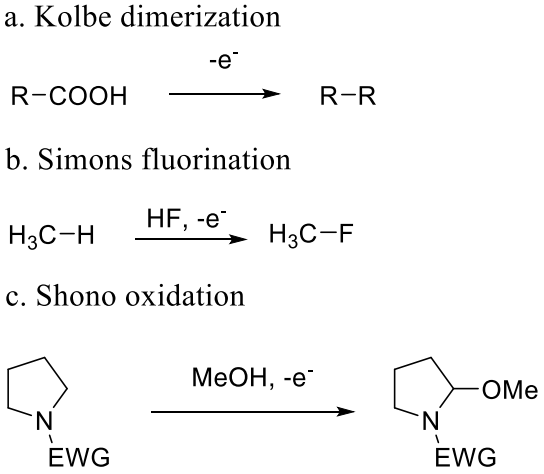

Figure 1: a. Kolbe dimerization reaction. b. Simons fluorination. c. Shono oxidation.

Although studies on electrocatalyzed organic transformations continued in the 20th century, in recent years, new electrochemical synthetic strategies have gained increasing interest both in academia and industry. The fundamental process underlying electrocatalysis is electron transfer, in which an electron is either added to or removed from a molecule[5]. Electron transfer is reversible only when the resulting species is stable under reaction conditions. In other cases, electron transfer triggers subsequent chemical processes, such as dissociation or the formation of

new bonds. Electrochemical methods are an excellent strategy for generating reactive species under mild conditions[6]. Cationic and anionic radicals can be generated through electron transfer processes on neutral organic compounds. Carbocations, free radicals, and carbanions can be generated through subsequent associative or dissociative processes. These reactive carbon species are used in various synthetic transformations, particularly in carbon-carbon bond formation. There are two main strategies for generating reactive intermediates in electrochemical reactions:

1. Generation of an intermediate in the presence of a reactive partner, in situ method (Figure 2a);

2. Generation in the absence of a reactive partner, pool method[7] (Figure 2b).

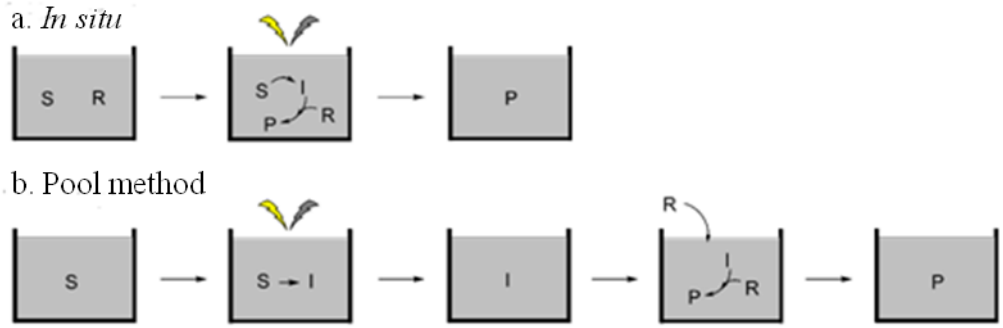

Figure 2: a. In situ method. b. Pool method.

The first approach, chosen in this research work, is more commonly used because reactive intermediates are generally transient species with short lifetimes, making in situ capture more effective[8]. The pool method, in which the reactive intermediate is accumulated before being trapped by a suitable partner, has recently been applied to flow techniques under the

name cation flow[9]. In classical organic chemistry, many methods have been developed for intramolecular control of selectivity. For example, directing groups directly coordinated to metal centers are widely used to control the reaction pathway[10], but similar approaches are not employed in the electrochemical field. This significant difference poses a unique challenge offered by electrochemical methods, which can be overcome by employing appropriate strategies that will be described in the following section.

1.2 Reactivity modulation and auxiliary groups

In electrochemical processes, the tendency of substrates to undergo electron transfer depends on their oxidation and reduction potentials[11]. The transfer of an electron is favored when the oxidation potential is less positive and the reduction potential is less negative. In order to achieve electron transfer-driven reactions, it is necessary to selectively activate the appropriate position within the molecule for the redox event. The use of suitable functional groups that guide and facilitate the process allows for intramolecular control of selectivity. A highly efficient method for selectivity control is based on the use of appropriate functional groups that make the electron transfer process easily predictable. These functional groups, introduced by Yoshida[12], are called electroauxiliaries (*EA*). Electroauxiliaries serve two important functions:

a. They promote the electron transfer process by making the oxidation potential less positive.

b. They selectively activate the desired molecular position for the subsequent chemical process after ET.

From the perspective of Frontier Molecular Orbital theory[13], an oxidative process involves the extraction of an electron from the highest energy occupied orbital (HOMO) of the substrate (Figure 3). Increasing the energy of the HOMO is the simplest method to activate the substrate for oxidation[14]. In the case where multiple substrates are oxidizable, the selectivity of the redox process depends on the difference in the HOMO energies of the different substrates. If the HOMOs are very close in energy to each other, it will not be possible to selectively oxidize one substrate in the presence of others. By using an appropriate *EA*, it is possible to increase the energy of the substrate's HOMO and achieve a selective process (Figure 4).

In the case where multiple sites on a single molecule are susceptible to oxidation, a similar strategy can be applied: the introduction of

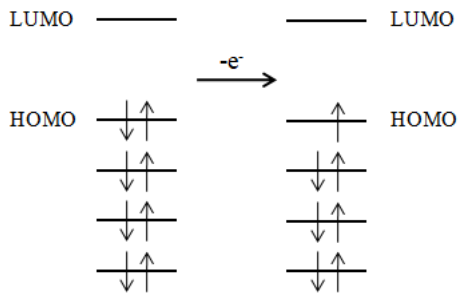

Figure 3: Oxidation of a non-activated substrate.

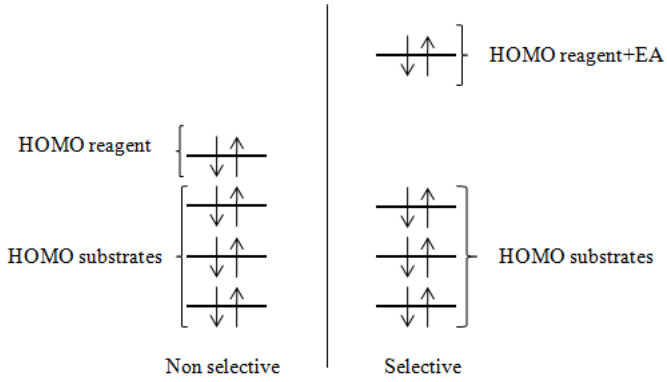

Figure 4: Differences between a non-selective oxidation process (left) and a selective oxidation process (right).

an *EA* can selectively activate a functional group towards oxidation.

There are different types of electroauxiliaries that should be evaluated based on the nature of the substrate of interest. In this research work, carboxylic acids have been chosen as EAs.

1.2.1 Carboxylic acids

Carboxylic acids are highly efficient electroauxiliaries due to their moderate oxidation potential[15]. Thanks to their high stability and ease of preparation, these functional groups are excellent substrates for electrochemical reactions[16–18]. As described earlier, Faraday and Kolbe (Figure 5a) were the first to use carboxylic acids as substrates for electrochemical reactions. Shortly after, Hofer and Moest demonstrated that, for certain tertiary carboxylates, the electrogenerated radicals are further oxidized to carbocations, which can be trapped by nucleophilic species at the oxygen[19] (Figure 5c). The first example of Kolbe dimerization applied to highly complex molecules was proposed by Corey in the synthesis of pentacyclosqualene[20] (Figure 5b). Recently, Baran et al.[21] developed an optimized variant of the Hofer-Moest reaction (Figure 5d). The protocol allows for the coupling of a

carbocation generated from a carboxylic derivative with various alcohols, using a silver salt as a sacrificial oxidant.

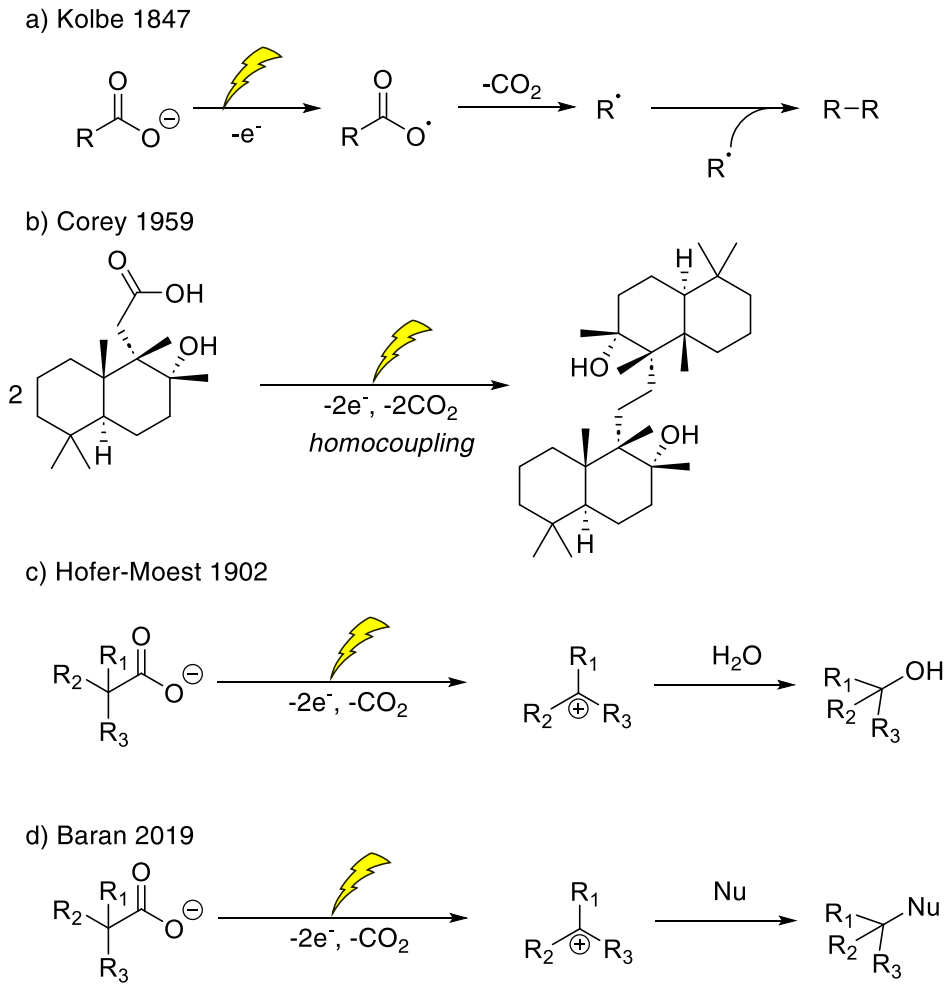

Figure 5: a: Kolbe decarboxylation reaction. b: Corey synthesis of pentacyclosqualene. c: Hofer-Moest decarboxylation process. d:Baran Hofer-Moest-like process.

The electrochemical oxidation of carboxylates has been extensively studied, and if the reaction conditions are not specifically controlled, a wide range of products can be obtained (Figure 6). After the anodic oxidation of the carboxylate ion 1 and subsequent loss of CO_2, the radical 2 is formed. The radical can undergo a second oxidative event, resulting in the formation of the carbocation 3, which can be trapped in situ by a nucleophile Y (Hofer-Moest process). Instead of undergoing further redox events, the radical 2 can react with another radical through

two different pathways. The first pathway involves the dimerization of the reactive intermediate, leading to the formation of the homocoupling product 5 (Kolbe reaction). In the second pathway, two radicals 2 can disproporionate, resulting in the formation of an unsaturated product 7 and a saturated product 6. By appropriately modifying the reaction conditions, it is possible to favor one of the possible pathways.

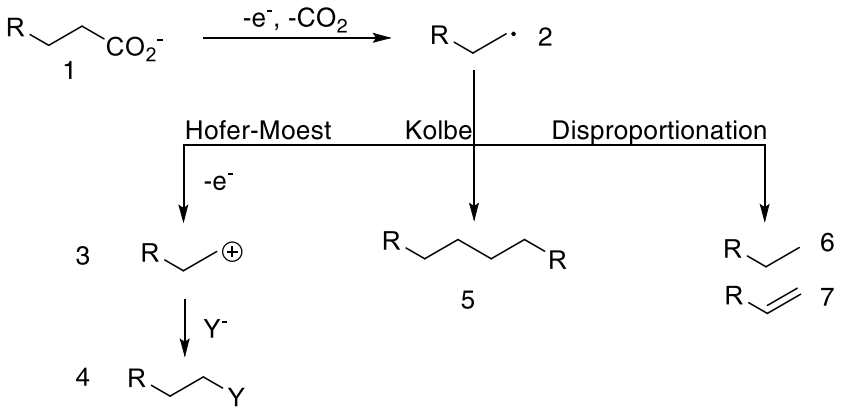

Figure 6: Different pathways of an electrochemical decarboxylation reaction.

1.3 Indirect electrolysis

Indirect electrochemical conversions represent a hybrid approach combining direct electrochemical conversions and homogeneous redox reactions. Instead of the traditional heterogeneous electron transfer between the electrode and substrate, a homogeneous redox reaction takes place in solution involving an electrochemically activated species and the substrate (Figure 7). This activated species can be generated and regenerated either in the same electrochemical cell (in-cell process) or in a separate cell (ex-cell process). The in-cell approach allows for the use of catalytic amounts of the redox mediator, as it can be continuously regenerated at the electrode during the reaction. Careful selection of reaction conditions ensures that only the mediator undergoes oxidation or reduction at the electrode, while the substrate, intermediates, and products do not interfere with the electrochemical regeneration of the catalyst. On the other hand, the ex-cell process involves transferring the activated species to a separate vessel, which requires greater stability of the activated species and may complicate the purification process. Mechanistically, two types of redox electron transfer processes can occur: outer-sphere and inner-sphere pathways. In outer-sphere mechanisms, the mediator facilitates electron exchange between the substrate and the electrode. In inner-sphere pathways, a chemical reaction occurs between the mediator and substrate, followed by bond cleavage to regenerate the mediator and the oxidized or reduced form of the substrate (Figure 8). Selective electron transfer is achieved by adjusting the electrode potential to that of the mediator, ensuring that the mediator is selectively oxidized or reduced in the presence of the starting material. However, caution must be exercised to avoid excessive current density, which could lead to unintended side reactions by consuming the mediator too rapidly[22].

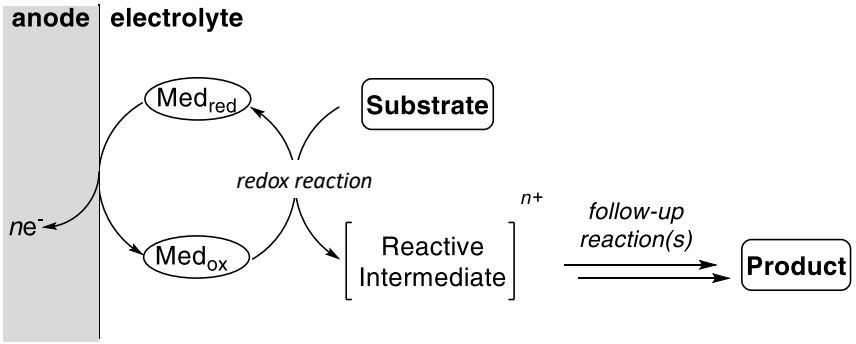

Figure 7: Use and mechanism of action of a mediator in electrolysis.

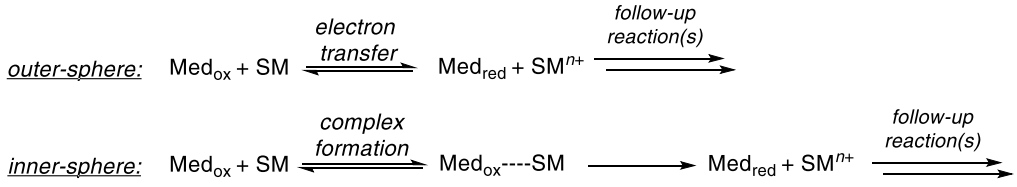

Figure 8: Outer sphere electron transfer vs inner sphere electron transfer process.[22]

Based on the aforementioned considerations, homogeneous electron transfer processes offer several advantages compared to their heterogeneous counterparts: (1) They eliminate the kinetic inhibition observed in heterogeneous electron transfer, allowing for the avoidance of overpotentials and acceleration of reactions. This is especially significant for large biomolecules with hindered redox centers due to steric shielding. (2) Electron transfer mediators can exhibit higher or different selectivity, expanding the range of possible reactions. (3) When direct electrochemical conversion leads to electrode passivation, the use of a mediator can prevent direct interaction between the substrate and the electrode surface. (4) Conducting the electrolysis at potentials lower than the redox potential of the starting material enables milder reaction conditions and minimizes the occurrence of side reactions. This is particularly beneficial when sensitive functional groups that should not react are present[22].

1.4 Electrosynthesis in APIs production

Instances of electroorganic syntheses of relatively intricate compounds had already been documented in the 1950s, with groundbreaking contributions like the creation of pentacyclosqualene by Corey and colleagues[20]. In numerous cases, electrochemistry has been employed to circumvent the use of costly or hazardous substances, particularly during preparative synthesis on a pilot scale or larger. For instance, Pfizer and the Electrosynthesis Company developed an electrochemical procedure for the reductive deacetoxylation of 11-ketorockogenin diacetate 8 (Figure 9a)[23]. The resultant 11-ketotigogenin 9 serves as a valuable intermediate in the synthesis of corticosteroids and related compounds. Although the conventional reduction method, involving treatment with calcium/ammonia, yielded satisfactory results, it posed significant safety and environmental concerns during large-scale preparations[24]. By utilizing a carbon felt cathode in a divided cell, cathodic reduction facilitated the removal of the two acetate groups under mild conditions, leading to moderate to good yields after 2 to 4 F mol^{-1}. Alternatively, an undivided cell could be employed by utilizing a sacrificial Mg anode. Electrochemical reductive deacetoxylation has also been employed in the synthesis of alkene 11 (Figure 9b), a crucial intermediate in the production of the antibiotic Ceftibufen[25]. This particular transformation was previously described using a large excess (8 equiv.) of Zn metal as the reducing agent at a low temperature (0 °C)[26]. The electrochemical approach circumvented the generation of significant amounts of metal salts and could be successfully demonstrated on a pilot scale (2.8 kg), achieving yields of up to 97%.

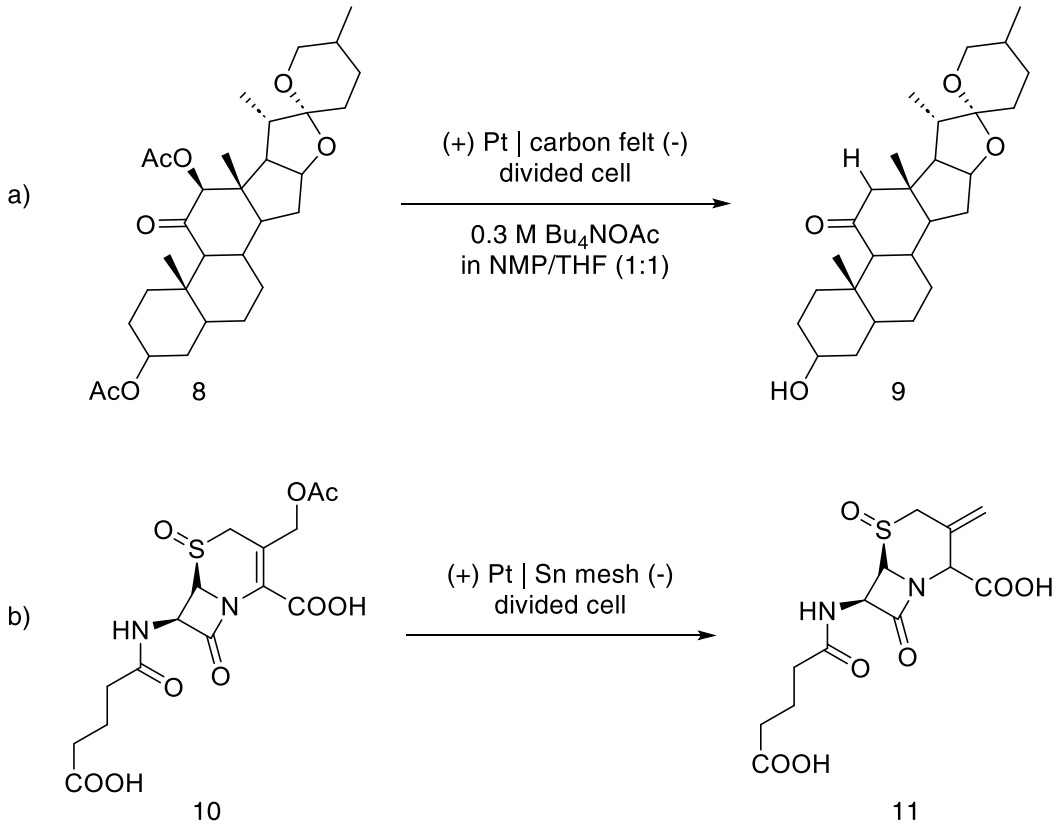

Figure 9: Electrochemical reductive deacetoxylation of APIs intermediates.[52]

The oxidative incorporation of acetates can be accomplished through decarboxylative acetoxylation, a process that utilizes readily available carboxylic acids as starting materials. Particularly, the decarboxylative acetoxylation of amino acids offers a convenient approach for synthesizing α-substituted amines, as the acetate group serves as an effective leaving group in the presence of nucleophiles[27,28]. Traditionally, this process has involved the Kochi reaction, employing excess $Pb(OAc)_4$ as both an oxidizing agent and a source of acetate, along with a copper catalyst[29-31]. However, due to the significant environmental drawbacks associated with $Pb(OAc)_4$, a sustainable electrochemical strategy has recently emerged (Figure 10)[32]. The anodic decarboxylative acetoxylation of amino acids (12) was carried out in AcOH at 40 °C, utilizing NaOAc as the base. By applying electrolysis under a constant

current and utilizing cost-effective graphite and stainless steel electrodes, excellent yields of various acetates (13) were obtained. Notably, this strategy was successfully employed in the synthesis of several intermediates for active compounds. For instance, acetates 14 and 16, which are crucial intermediates in the production of the insecticide tetramethrin (15) and the antiepileptic drug phenytoin (17), respectively, were synthesized in good yields (Figure 10).

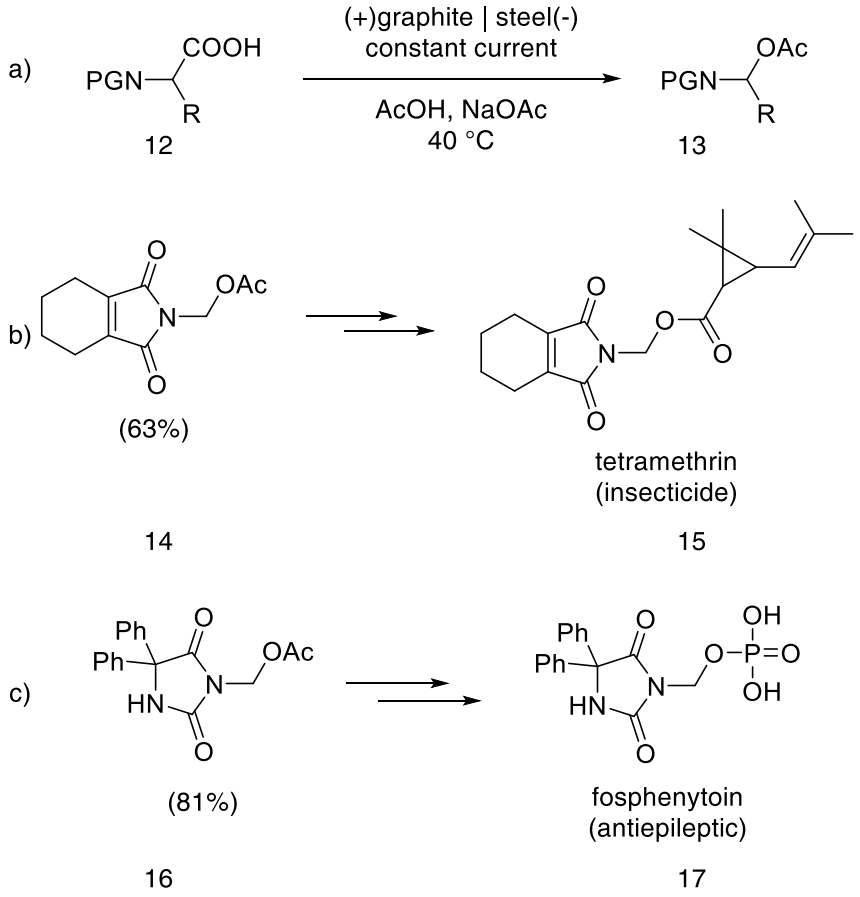

Figure 10: Anodic decarboxylative acetoxylation of amino acids and further transformations toward active ingredients.[52]

1.4.1 Scalable processes with flow electrolysis cells

The scaling up of electrochemical processes is widely understood and established[33,34]. In fact, some of the largest chemical processes known, such as the chloralkali process or aluminum production, rely on electrochemistry. While electrochemistry is generally recognized as a scalable technology, traditional setups with beaker cells containing two or three electrodes are only suitable for relatively small-scale laboratory experiments. Multigram transformations can be achieved with sufficient electrode surface area and mixing[35]. However, accomplishing kilogram-scale or larger reactions using batch cells is typically challenging. This difficulty arises from the limitations of mass transfer in many of these transformations and the dependence of process efficiency on the ratio between electrode surface area and reactor volume[36]. To address these issues, the use of flow electrolysis cells has been proposed as a solution (Figure 11). Flow devices are characterized by a narrow interelectrode gap, often less than 1 mm. This configuration provides electrode area-to-reaction volume ratios that are two orders of magnitude higher than those of batch cells, resulting in highly efficient electrolysis. Furthermore, the short distance between the electrodes significantly reduces the ohmic drop in the system, allowing electrolysis to be conducted with very low electrolyte concentration or even under electrolyte-free conditions. This aspect has the potential to greatly enhance the environmental sustainability of electrochemical processes. The benefits of flow electrolysis cells have been known for many years. In fact, flow devices were already described in the early 20th century for inorganic processes[37], and examples of organic electrosynthesis in flow cells were disclosed in the 1940s. Subsequently, several industrial electrochemical organic processes were developed using this technology. Noteworthy

examples include the synthesis of anthraquinone, adiponitrile, and benzaldehyde derivatives[38-43].

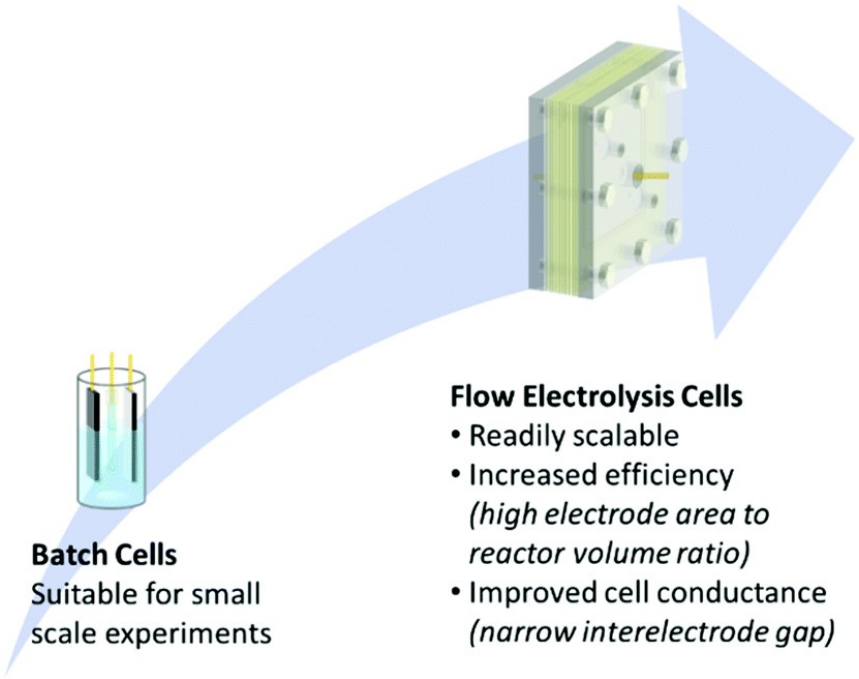

Figure 11: Flow technology enables large scale synthesis.[48]

Commonly used flow cell designs typically consist of two flat electrodes placed parallel to each other. These electrodes create a gap through which the reaction mixture, containing reactants and electrolytes, is pumped using suitable systems. This design offers a high electrode area to volume ratio and allows for easy enhancement of mass transfer properties by introducing turbulence promoters (Figure 12). Various commercially available parallel plate flow cells are used in laboratory-scale experiments. In addition, academic groups have published their own designs in recent years[44-49].

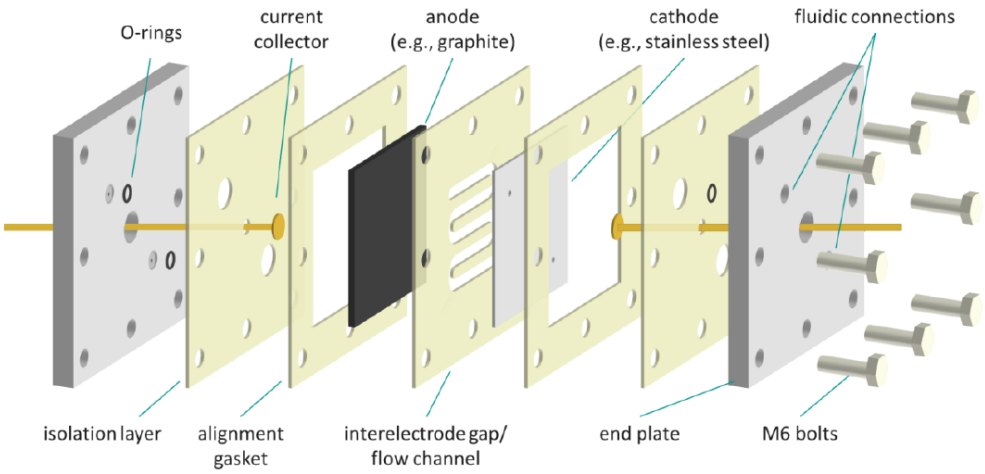

Figure 12: exploded image of a flow electrochemical cell.[48]

In previous pilot and industrial-scale organic electrochemical syntheses, the reaction mixture was processed using an electrolyte recirculation approach. This involves flowing the solution through the cell and back to a reservoir in a semi-batch process (Figure 13a). However, single-pass processing has gained significant interest in recent years (Figure 13b). It enables fully continuous processes and facilitates integration of electrochemical transformations with other synthetic or downstream steps. Developing single-pass continuous flow electrochemical reactions is more complex than the traditional recirculation approach. One challenge is gas generation at the counter electrode, which can reduce the available surface area for electrolysis[50-51].

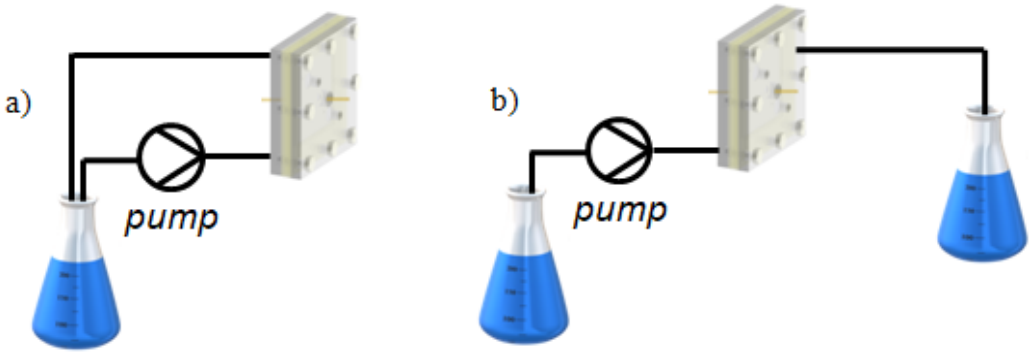

Figure 13: a: Flow recirculation electrolysis. b: Flow single pass electrolysis.

Single-pass processing in an electrolysis cell offers several advantages over electrolyte recirculation. The smaller volume of flow cells results in short residence times for the reaction mixture within the reactor, allowing for rapid screening of reaction conditions with minimal material waste. This is particularly advantageous for optimization compared to batch processes or semi-batch recirculation approaches. For example, a single-pass continuous flow reactor was successfully used for the electrochemical synthesis of acetate, an important intermediate for the synthesis of the dopamine antagonist ABT-670. The flow cell had a narrow interelectrode gap, enabling rapid screening of flow rates and currents to find optimal electrolysis conditions. The process achieved quantitative conversion and 94% isolated yield for the desired product. Importantly, the single-pass process could be sustained for several hours without any significant decrease in yield, allowing for the production of large quantities of material in a small-volume reactor[52].

1.5 Aim of the thesis

This work, developed in collaboration with Flamma S.p.A., Prof. Dr. David Cantillo and Prof. Dr. Oliver Kappe of the University of Graz, has the purpose to find a new electrochemical cyclization reaction for the synthesis of substituted tetralins (Figure 14).

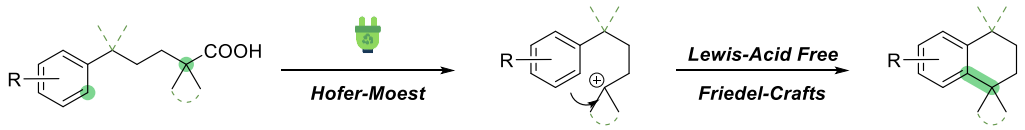

Figure 14: Electrochemical decarboxylative cycloalkylation.

The thesis can be divided in 6 different parts:

1) Synthesis of starting materials.

2) Batch optimization studies.

3) Batch electrolysis.

4) Flow experiments.

5) Mechanistic studies.

6) Computational studies.

Chapter II: Synthesis of substituted tetralins via electrochemical decarboxylative cycloalkylation

2.1 Results and discussion

A preliminary exploration of the experimental conditions was carried out based on the method reported by Baran and co-workers[21] using acid **2b** as the model substrate. Unfortunately, mixtures of decomposition products were observed in this case. In addition, these conditions required the use of stoichiometric amounts of Ag. Alternatively, conditions developed by Ley and Zhang were employed,[53] using an undivided cell, carbon felt and platinum plate as anode and cathode, respectively, nBu_4NOAc as the supporting electrolyte and HFIP as the solvent, to obtain the corresponding Friedel-Crafts product **2**, albeit in low yield (15%). Therefore, an optimization study, including screening of several supporting electrolytes, bases, solvents, electrodes, current density and amount of charge (F/mol), was performed (Table 1). All reactions were carried out in batch at room temperature using a commercial undivided cell (IKA ElectraSyn 2.0. 10 mL vial, see Supporting Information for details). The optimal conditions for the electrochemical decarboxylation-alkylation cascade used a graphite anode and a stainless-steel cathode, DCM/HFIP 14:1 solvent mixture, Bu_4NPF_6 supporting electrolyte, and 2,4,6-collidine (2 equiv) as a additive base. Under these conditions, a current of 7.5 mA (ca. 5 mA/cm^2) provided 65% GC yield (62% isolated) after 2.1 F/mol had been passed thorough the cell (entry 1).

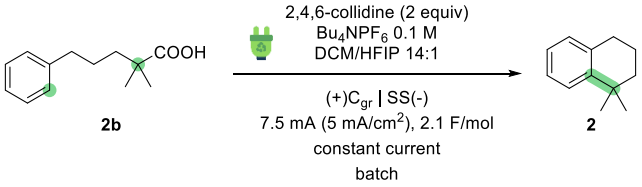

entry[a]	variation form optimal conditions	yield (%)[b]
1	**none**	**65 (62)[c]**
2	nBu_4NClO_4	21
3	nBu_4NBF_4	30
4	Pt anode	0
5	RVC anode	0
6	Zn cathode	60
7	Graphite cathode	59
8	5 mA	51
9	10 mA	38
10	2.5 F/mol	49
11	1.5 F/mol	48
12	Acetone/HFIP 14:1	0
13	MeCN/HFIP 14:1	0
14	DMSO/HFIP 14:1	0
15	2,6-lutidine	43
16	DBU	46
17	4-methoxypyridine	53
18	2,4,6-collidine (1 equiv)	40
19	2,4,6-collidine (4 equiv)	45

Table 1: Optimization of the electrochemical cycloalkylation.

[a] Conditions: 0.2 mmol **2b** in 10 mL reaction mixture, 10 mL ElectraSyn 2.0 vial, constant current. [b] Calibrated GC yield. [c] Isolated yield. C_{gr} = graphite; SS = stainless steel.

The nature ? of the anion present in the supporting electrolyte as well as the electrode materials proved to be critical in achieving high yields (entries 2 and 3). When Pt or reticulated vitreous carbon (RVC) were used as the anode material, no product was observed (entry 4 and 5). This was not surprising, as these materials typically favor radical (Kolbe) pathways, and the mechanism of this reaction was expected to follow a cationic intermediate (*vide infra*). A change in the cathode material had a minor effect in the reaction yield (entries 6 and 7). The yield of product **2** was significantly diminished by changing the current density (entries 8 and 9), amount of charge passed (entries 10 and 11), or the solvents employed in conjunction with HFIP (entries 12-14). Notably, no conversion was observed with solvents other than DCM. Deviation from 2,4,6-collidine as a base only provided lower yields (entries 15-17).

Increase or decrease in the amount of base was also detrimental (entries 18 and 19). Despite extensive optimization attempts, no more than 75% conversion and 65% yield (entry 1) could be achieved.

In attempt to enhance the performance of the reaction, the electrochemical procedure was transferred to a flow electrolysis cell. Flow cells exhibit very low interelectrode distance as well as high electrode surface area to reactor volume ratio and improved mass transfer.[54] These features typically provide more efficient transformations. We anticipated that the enhanced mass transfer in a narrow gap electrolysis cell might have a particularly positive influence on the conversion and selectivity of the reaction. Flow experiments were carried out in a previously described cell.[52] Initially, a recirculation approach, with a flow rate of 5 mL/min, was applied. Gratifyingly, after fine-tuning of the reaction conditions in a flow electrolysis cell featuring a 0.3 mm interelectrode gap, nearly quantitative yield of the desired product **2** was obtained (Figure 15). Notably, this excellent yield was obtained under a relatively low current (10 mA, ca. 1.6 mA/cm^2), in contrast with the batch results, which showed that decreased current density diminishes the yield (Table 1, entry 8).

Scheme 1. Optimized flow recirculation procedure.

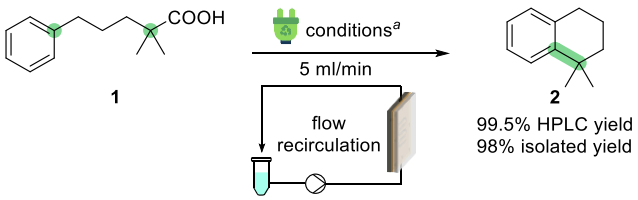

Figure 15: Flow recirculation experiments.

[a] Conditions: **2b** (0.2 mmol), 2,4,6-collidine (0.4 mmol), nBu_4NPF_6 (0.1 mmol), DCM:HFIP 14/1 (10.7 mL), undivided flow cell, 10 mA, 2.3 F/mol, (+)C_{gr} | SS(-), 5 ml/min, flow recirculation mode.

With the optimized reaction conditions in hand, the scope of the electrochemical decarboxylative cycloalkylation was evaluated both under batch and flow conditions (Figure 16). Unsurprisingly, the electrochemical process performed significantly better in the flow reactor than in the batch cell in all cases. Spirocyclic compound **3**, for example, which was obtained in modest yield in batch (13%), could be isolated in good yield (61%) in flow. The study of the reaction scope mainly focused on the introduction of methyl groups in the aliphatic chain, a characteristic feature of active ingredients containing the tetrahydronaphthalenes core such as synthetic retinoids,[55] as well as fluorine substituted aromatics. As expected, introduction of fluorine in the arene resulted in lower yield (**5**, 50% and 80% in batch and flow, respectively) compared to **2** due to the less nucleophilic character of the aromatic ring. On the other hand, decoration of the aliphatic chain with methyl groups did not have a significant impact on the reaction outcome (*i.e.,* **7** and **8**). As might be expected, compound **9** could not be obtained using this methodology, either under batch or flow conditions, likely due to the low oxidation potential of the aromatic ring, which may lead to oligomerization (a cyclic voltammogram of **2b** is collected in the Supporting Information).[56]

Interestingly, in substrates containing two phenyl groups in α-position to the carboxylate, alkene **4** was isolated. This is due to stabilization of the carbocation intermediate by the two aromatic groups, resulting in elimination of a β-proton as the preferred pathway.

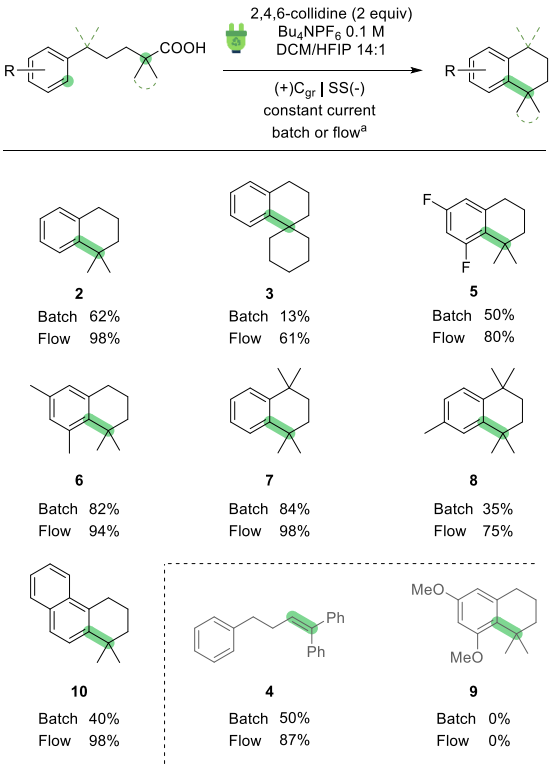

Figure 16: Scope.

[a] Conditions: **2b** (0.2 mmol), solvent (10.7 ml), constant current electrolysis. BATCH: 10 mL IKA ElectraSyn 2.0 vial, 7.5 mA, 2.1 F/mol. FLOW: 10 mA, 2.3 F/mol, 5 ml/min recirculation.

We next turned our attention into achieving a continuous, single-pass flow electrolysis protocol. Single-pass electrolysis can be very interesting from the process chemistry viewpoint, as it enables continuous generation of synthetic intermediates and products and the possibility of integrating several synthetic and purification steps into a continuous stream.[48] Moreover, the low reactor volume resulting from the narrow gap in flow cells typically provides low residence times of the reaction mixture within the reaction zone, enabling rapid screening of the reaction conditions. Indeed, a wide range of currents and amounts of charge could be readily screened (Figure 17). In this optimization experiment, a stock solution containing **2b**, 2,4,6-collidine (2 equiv) and nBu_4NPF_6 (0.1 M) in DCM/HFIP 14:1 was continuously pumped through the electrolysis cell.

The electrolysis parameters (cell current and pump flow rate, which determines the amount of charge) were successively adjusted and, after steady state conditions had been reached, aliquots of the crude mixture obtained from the reactor output were analyzed by HPLC (Figure 1; see Table S12 for additional data). As expected from the results in recirculation mode, lower current densities provided the best results. Notably, quantitative yield was observed under analogous electrolysis parameters (10 mA, 2.3 F/mol) to those used in recirculation mode (cf. Figure 16), also implying that both recirculation and single-pass operation presented the same current efficiency.

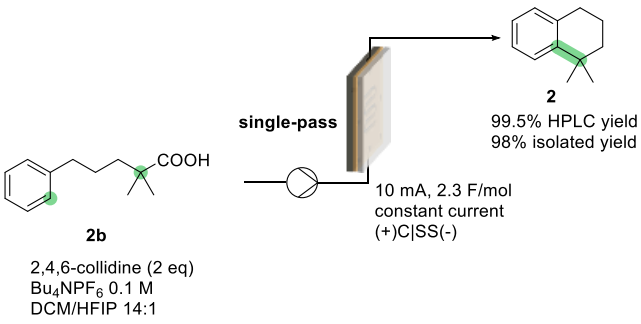

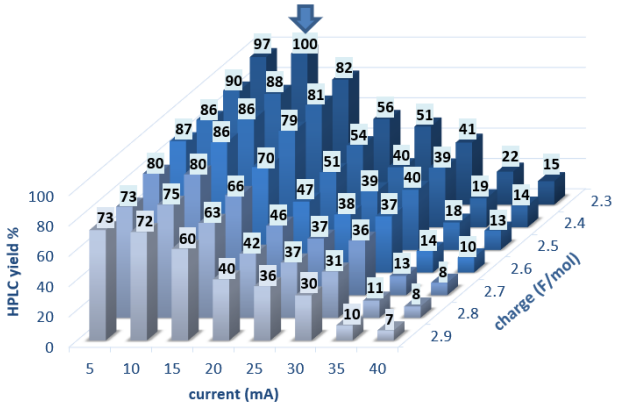

Figure 17: Optimization of flow single pass electrolysis.

Another relevant parameter in single pass flow electrochemical processing is the reactor stability, *i.e.*, the performance of the electrolysis cell over prolonged reaction times. In some cases, both electrode fouling and corrosion may affect reaction performance over time, preventing the obtention of the target amounts and quality of material in a continuous manner. Thus, under optimal reaction conditions (Figure 17, 10 mA, 0.108 mL/min, 2.3 F/mol), the single-pass continuous process was carried out uninterruptedly for 24 h. Gratifyingly, monitoring the crude reaction mixture obtained from the reactor output by HPLC confirmed that quantitative yield (> 98%) had been obtained over the entire period (see Figure S66); work up of the reaction produced 980 mg (7.2 mmol, 98%) of pure material.

Based on previous literature on the Hofer–Moest reaction,[21] radical trapping experiments and DFT calculations, a plausible mechanistic scenario for the electrochemical transformation was proposed (Figure 18). First, an experiment under optimal conditions, carried out using radical trapping agent TEMPO as an additive, provided no traces of the substrate-TEMPO adduct (Figure 18a), supporting that the reaction does not follow a radical mechanism. To probe for the formation of a carbocation, employment of MeOH as an additive (Figure 18b) led to the corresponding methyl ether, an intermediate observed by GC-MS.

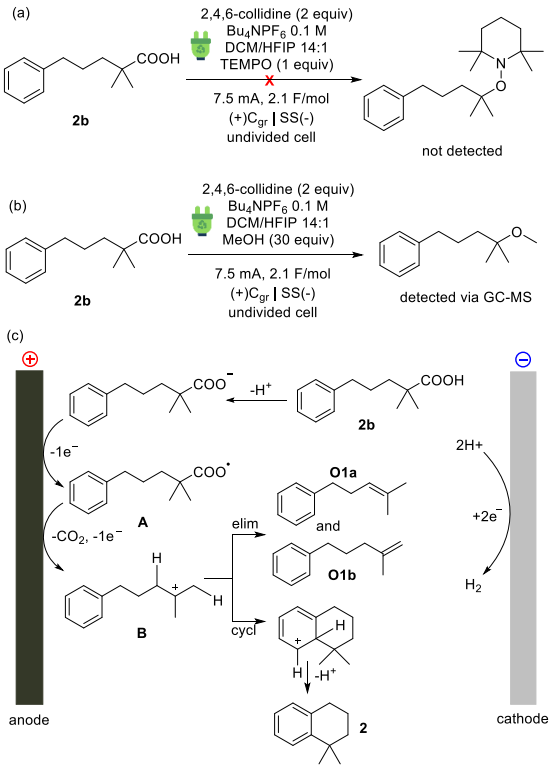

Figure 18: a) Trapping experiment with TEMPO. b) Trapping experiment with methanol. c) Proposed mechanism.

Based on this mechanistic evidence, electrochemical reaction likely commences with the deprotonation of carboxylic acid in the presence of 2,4,6-collidine. Anodic oxidation of the corresponding carboxylate generates radical intermediate **A**, which undergoes decarboxylation followed by a second anodic oxidation to form carbocation **B**. In the absence of other nucleophiles, the aromatic system traps the carbocation in a cycloalkylation, forming the product **2** by deprotonation. Intermediate **B** can also eliminate a β-proton, giving the elimination side products **O1a** or **O1b**. The cathodic reduction at the counter electrode is reduction of two protons to hydrogen, thus keeping the pH of the solution constant.

By looking closely to the mechanism we proposed above, we can clearly see that two side products were observed together with the cyclized one: namely the terminal bis-substituted olefin **O1b** and the tris-substituted one **O1a**. To further support the mechanistic hypothesis and

generatation of elimination products DFT calculations were performed. The mechanisms for both the cyclization and the elimination reactions steps were investigated using the Gaussian 16 program package in the framework of the density functional theory (DFT).[56] The cationic substrate was modelled without any simplifications to remain as close as possible to the real condition, while the role of the non-oxidizable base 2,4,6-collidine was replaced with pyridine. To better sample the conformational space for the starting cationic substrate we employed the semiempirical extended tight binding (*x*TB (*GFN2-xTB*)) approach (see Supporting Information for more details).[57] We next moved to the proper choice of functional and basis set for the DFT calculation. Soon we encountered problems in simulating the elimination reaction step. Different combinations between functional and basis sets were tested, but most of them proved unsuccessful (see SI for a full description of the computational benchmark). Given the reasonable existence of the elimination transition state, we used the M06-2X hybrid functional of Truhlar and Zhao, which includes double the amount of nonlocal exchange (2X).[58] This functional proved to be one of the first level choices for thermochemistry and thermochemical kinetics studies, by placing a particular attention also to noncovalent interactions given the presence of medium-range correlation contributions and a flexible functional form with extensive parameterization.[59] We next selected for each atom the same basis set 6-31+g(d,p).[60] To reproduce the effect of dichloromethane as a solvent, we included the Truhlar's solute electron density and a continuum solvation model (SMD).[61] For each structure, we performed frequency calculations to confirm the effective minimum or transition-state (TS) nature of the optimized system. Moreover, intrinsic reaction coordinate (IRC) calculations were performed to confirm the continuity of the reaction profile from TSs toward reactants, intermediates, or products.[62] Finally, single point calculations (SP) were

performed using the optimized structures using the long-range corrected hybrid density functional ωB97XD from Head-Gordon and co-workers, which already includes a version of Grimme's D2 dispersion model,[63] and def2-TZVP a valence triple-zeta polarization basis set from Ahlrichs and co-workers.[64] During the SP calculation we maintained the same SMD model for the dichloromethane solvent. The final reported energies were then thermally corrected to the free energy: all the next evaluations will be referred to this level of theory. Figure 19 shows the complete energetic profile for the two possible mechanistic pathways.

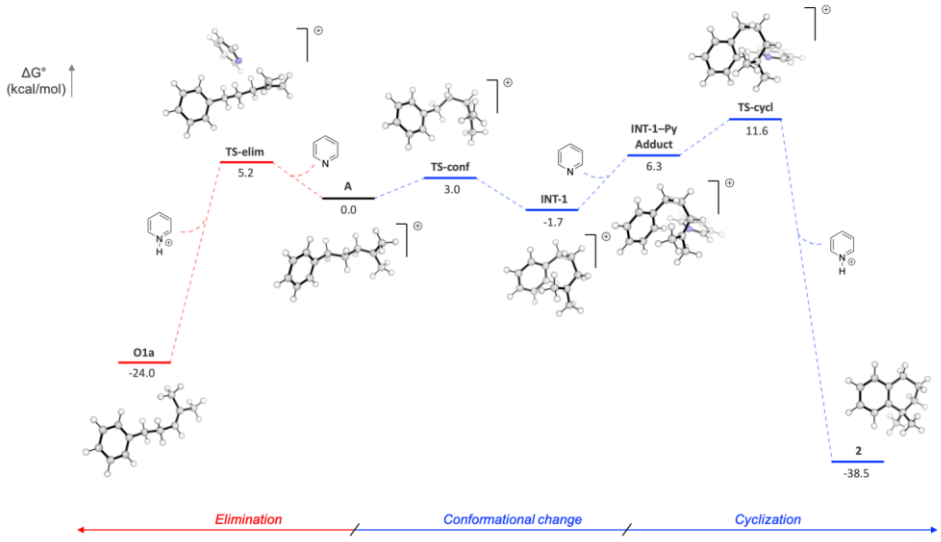

Figure 19: Electronic Free Energy Profile (kcal/mol) for both the cyclization and the elimination reactions. [SMD(DCM)-wB97XD/def2TZVP//SMD(DCM)-M06-2x/6-31+g(d,p)]

Our analysis begins from the elimination step, highlighted in red in Figure 19. Starting from the initial cation **A**, pyridine can either directly deprotonate at the terminal position, thus forming the disubstituted olefin, or deprotonate the more hindered internal position to form the trisubstituted alkene. Despite attempts in locating the transition state (TS) corresponding to terminal deprotation, we were only able to locate and optimize the TS leading to a more substituted internal olefin (**TS-**

elim). This step requires only 5.2 kcal/mol from the isolated reactants and appears to be thermodynamically favored since the final eliminated product **O1a** is 24.0 kcal/mol more stable than the initial **A**. Regarding this step, we strongly believe the most statistically probable terminal methyl groups are deprotonated, which is followed by a fast pyridine/pyridinium promoted "push-and-pull" equilibration occurs populating the most substituted internal olefin. We attempted to also simulate this equilibration, but we did not succeed in locating the isomerization transition state.

Regarding the cyclization step (Figure 19, blue line), we observed that a conformational modification has to occur in order to produce an intermediate **INT-1** capable to promote the cyclization. This conformational step occurs through **TS-conf** with an activation energy of 3.0 kcal/mol and shows a modification of the dihedral angle between the benzylic and homobenzylic carbons from 178.5° to 130.9° (in **TS-conf**) and finally to 60.3° in **INT-1**. This change in dihedral significantly shortens the distance between the tertiary carbon (where the cation charge is stabilized) and the carbon of the benzene ring where the cyclization occurs (from 5.62Å in **A**, to 2.87Å in **INT-1**). Starting from **INT-1** the income of pyridine forms the reactive adduct **INT-1-Py** which is then prone to promote the cyclization step. This occurs through **TS-cyc** with an activation energy of 5.3 kcal/mol from **INT-1-Py** and 13.3 kcal/mol from the conformational productive intermediate **INT-1**. During cyclization the distance between the reactive carbons is reduced from 2.87Å in **INT-1** to 2.26Å in **TS-cyc** and finally to 1.53Å in **2**. The removal of the proton from the benzene ring to re-establish aromaticity is mediated by pyridine. The re-aromatization step occurs concomitantly with cyclization, but it shows a strong asynchrony given the fact that first the cyclization occurs and only in a second time the re-aromatization occurs. This observation is corroborated by the distance between the

pyridine nitrogen and the proton to be removed. In **INT-1-Py** adduct this distance is 2.49Å, which is reduced to 2.31Å in **TS-cyc**. Only after the formation of the cycle, the distance decreases until the formation of N-H bond in pyridinium cation (1.02Å). This step is thermodynamically favored since the final cyclized product **2** is 38.5 kcal/mol more stable than the initial **A**.

To make a general discussion on the reaction profile we reported above, we can state that the reaction seems to be under the Curtin–Hammett control. Indeed, the formation of the eliminated product is less energetically expensive, but populates the less stable product. We can consider this step as the kinetic one. Vice versa, the cyclization step requires much nearly double the energy to overcome the transition state, but the cyclized product is much more stable than the eliminated one ($\Delta\Delta G° \approx 14.0$ kcal/mol). This means that the reaction equilibrates between the eliminated product, which is formed first, and the cyclized one, which is much more energetically costly but remains the most thermodynamically favored.

In summary, we have developed an electrochemical methodology for the synthesis of substituted tetrahydronaphthalenes via oxidative decarboxylative cycloalkylation of carboxylic acids. This electrochemical procedure, based on direct anodic oxidation, avoids the use of the corrosive reagents typically needed in Friedel–Crafts-type protocols, and uses carboxylic acids as readily available substrates. A significant enhancement of the reaction yield has been achieved when transferring the electrochemical procedure to a flow electrolysis cell, which can be operated both in recirculation and single-pass modes. Very good to quantitative yields have been obtained for tetrahydronaphthalenes decorated with fluorine and methyl groups.

Chapter III: Experimental section

3.1 General methods

NMR spectra were recorded on Bruker-400 MHz or Bruker-300 MHz spectrometer. The high resolution mass spectra were recorded on a Thermo LTQOrbitrap XL (ESI-). GC-MS analysis were performed on "Thermo scientific" Focus GC-DSQ II. Column chromatography was performed on silica gel Sigma-Aldrich High-purity grade (9385), pore size 60˚A (230-400 mesh). TLC was performed on GF-254 Merck (0.25 mm) per TLC Sigma-Aldrich. Electrolysis experiments have been performed on IKA Electrasyn 2.0. Flow electrochemical experiments have been performed using a peristaltic pump Vapourtech SF-10 and a self-assembled flow cell. All chemicals were used without purification as commercially available unless otherwise noted.

3.2 Abbreviations

BuLi: *n*-butyl lithium

TPPA: tris(N,N-tetramethylene) triamide phosphoric acid

i-Pr2NH: diisopropylamine

TEA: triethylamine

DIPEA: diisopropylethylamine

DBU: diazabicycloundecene

4-MeO-py: 4-methoxypyridine

KOH: potassium hydroxide

LiOH: lithium hydroxide

LDA: lithium diisopropylamide

HFIP: 1,1,1,3,3,3-Hexafluoro-2-propanol

DMSO: dimethylsulfoxide

Et_2O: diethylether

EtOH: ethanol

MeCN: acetonitrile

THF: tetrahydrofuran

DCM: dichloromethane

DMF: dimethylformamide

Bu_4NBF_4: tetrabutylammonium tetrafluoroborate

Bu_4NPF_6: tetrabutylammonium hexafluorophosphate

Bu_4NOAc: tetrabutylammonium acetate

Bu_4NOH: tetrabutylammonium hydroxide

Bu_4NClO_4: tetrabutylammonium perchlorate

C: graphite

GC: glassy carbon

RVC: reticulated vitreous carbon

Pt: platinum

SS: stainless steel

Ni: nickel

Zn: zinc

3.3 Synthesis of starting materials 2-10 (b or e or g)

Synthesis of **2b**-*Step 1*

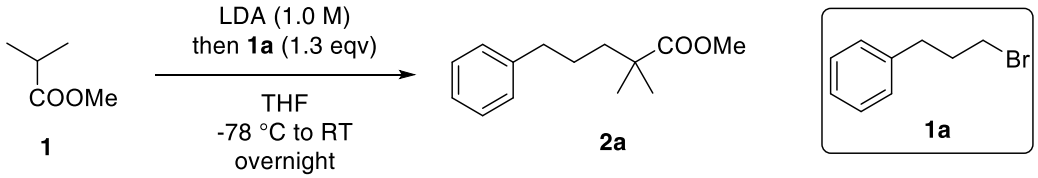

Figure S 1: Synthesis of methyl 2,2-dimethyl-5-phenylpentanoate

1.1 eq. of *n*-BuLi (55 mmol, 35 ml 1,6 M in hexanes) was added to a solution of freshly distilled diisopropylamine (1 eq, 50 mmol, 3.63 ml) in anhydrous THF (50 ml, 1.0 M) under nitrogen at 0 °C. The reaction mixture was then cooled to -78 °C and methyl isobutyrate **1** (0.9 eq, 45 mmol, 5.16 ml) was carefully added dropwise. The reaction was stirred at the same temperature for 30 min. and then bromide **1a** (1 eq, 50 mmol, 13.7 ml) was added dropwise. The mixture is stirred overnight slowly reaching RT.

The reaction was quenched adding one volume of a saturated solution of ammonium chloride in water. The organic phase was separated and the aqueous phase was extracted with ethyl acetate three times. Organic phases were reunited and washed 2 times with HCl 2 M and one time with brine. The organic phase was collected and dried over sodium sulphate then the solvent was evaporated under vacuum. The crude is a dark yellow oil and was used without purification for the next step.

MW: 220.14 g/mol

Synthesis of **2b**-*Step 2*

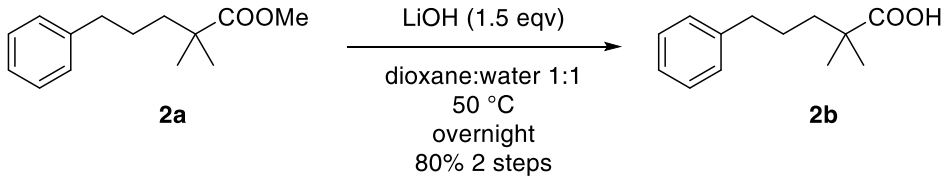

Figure S 2: Synthesis of 2,2-dimethyl-5-phenylpentanoic acid

The crude obtained from step 1 was dissolved in a 1:1 mixture water:1,4 dioxane (500 ml, 0.1 M). LiOH (1.5 eq, 2.0 g) was added to the reaction mixture and the temperature was brought to 50 °C under magnetic stirring for one night.

After the mixture was cooled to RT, 1,4 dioxane was removed under vacuum. The residue was washed three times with diethyl ether. Aqueous phase was then acidified with HCl 1 M (aq) until the pH was 3, then the same phase was extracted three times with ethyl acetate. The organic phase collected after the extraction of the acid phase was dried over sodium sulphate and the solvent was removed under vacuum.

The product **2b** results as a white solid and no further purification was required. Y% = 80% (8.2 g) over two steps.

MW: 206.28 g/mol

^{1}H NMR (300 MHz, Chloroform-*d*) δ 7.36 – 7.25 (m, 2H), 7.25 – 7.15 (m, 3H), 2.71 – 2.55 (m, 2H), 1.69 – 1.58 (m, 3H), 1.21 (s, 6H).

^{13}C NMR (101 MHz, Chloroform-*d*) δ 185.32, 142.27, 128.48, 128.42, 125.90, 42.21, 40.20, 36.40, 26.82, 25.03.

HRMS (ESI-): m/z $[M-H]^-$, calculated for $C_{13}H_{17}O_2^-$: 205.1234 ; found: 205.1225.

Synthesis of **3b**-*Step 1*

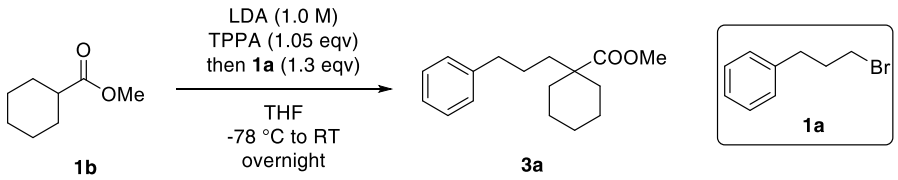

Figure S 3: methyl 1-(3-phenylpropyl)cyclohexane-1-carboxylate

1.1 eq. of *n*-BuLi (1 mmol, 625 µl 1,6 M in hexanes) was added to a solution of freshly distilled diisopropylamine (1 eq, 1 mmol, 141 µl) in anhydrous THF (1 ml, 1.0 M) under nitrogen at 0 °C. The reaction mixture was then cooled to -78 °C and a solution of ester **1b** (0.9 eq, 0.9 mmol, 143.8 µl) and TPPA (1.05 eq, 1.05 mmol, 261 µl) in dry THF (1 ml, 1.1 M) was carefully added dropwise. The reaction was stirred at the same temperature for 30 min. and then bromide **1a** (1 eq, 50 mmol, 91.7 µl) was added dropwise. The mixture is stirred overnight slowly reaching RT. The reaction was quenched adding one volume of a saturated solution of ammonium chloride in water. The organic phase was separated and the aqueous phase was extracted with ethyl acetate three times. Organic phases were reunited and washed 2 times with HCl 2 M and one time with brine. The organic phase was collected and dried over sodium sulphate then the solvent was evaporated under vacuum.The crude was purified on silica gel using 98:2 Hexane/EtOAc as mobile phase. The resulting yellow oil was used for the step 2. Y% : 77% (200 mg). The ^{1}H NMR analysis was correspondent to the one reported by Cala, Lara et al.[65]

MW: 260.37 g/mol

Synthesis of **3b**-*Step 2*

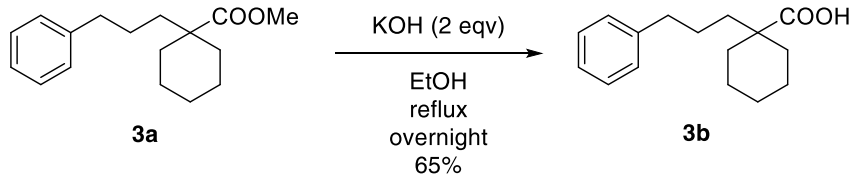

Figure S 4: Synthesis of 1-(3-phenylpropyl)cyclohexane-1-carboxylic acid

The ester **3a** (1 eq, 200 mg) was dissolved in ethanol (10 ml, 0.1 M). KOH (2 eq, 27.5 mg) was slowly added and the reaction was brought to reflux overnight under magnetic stirring.

The mixture was cooled to RT and the solvent was evaporated under vacuum. The residue was dissolved in water and the aqueous phase was extracted three times with diethyl ether. Aqueous phase was then acidified with HCl 1 M until the pH was 3, then the same phase was extracted three times with ethyl acetate. The organic phase collected after the extraction of the acid phase was dried over sodium sulphate and the solvent was removed under vacuum.

The product **3b** was obtained as an orange solid. No further purification was needed. Y% = 98% (185.7 mg)

MW: 246.35 g/mol

^{1}H NMR (400 MHz, Chloroform-*d*) δ 7.34 – 7.27 (m, 2H), 7.25 – 7.18 (m, 3H), 2.62 (t, *J* = 6.9 Hz, 2H), 2.17 – 2.03 (m, 1H), 1.73 – 1.53 (m, 5H), 1.51 – 1.38 (m, 1H), 1.34 – 1.19 (m, 2H).
^{13}C NMR (101 MHz, Chloroform-*d*) δ 183.85, 142.25, 128.47, 128.41, 125.88, 46.88, 36.33, 33.97, 26.02, 25.85, 23.28.

HRMS (ESI-): m/z $[M-H]^-$, calculated for $C_{16}H_{21}O_2^-$: 245.1547; found: 245.1544.

Synthesis of **4b**-*Step 1*

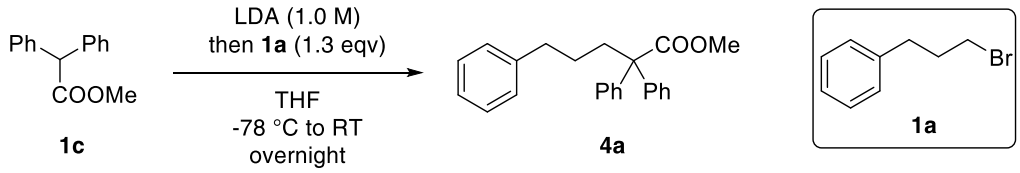

Figure S 5: Synthesis of methyl 2,2,5-triphenylpentanoate

1.1 eq. of *n*-BuLi (1 mmol, 625 µl 1,6 M in hexanes) was added to a solution of freshly distilled diisopropylamine (1 eq, 1 mmol, 141 µl) in anhydrous THF (1 ml, 1.0 M) under nitrogen at 0 °C. The reaction mixture was then cooled to -78 °C and ester **1c** (0.9 eq, 0.9 mmol, 228 µl) was carefully added dropwise. The reaction was stirred at the same temperature for 30 min. and then bromide **1a** (1 eq, 50 mmol, 91.7 µl) was added dropwise. The mixture is stirred overnight slowly reaching RT.

The reaction was quenched adding one volume of a saturated solution of ammonium chloride in water. The organic phase was separated and the aqueous phase was extracted with ethyl acetate three times. Organic phases were reunited and washed 2 times with HCl 2 M and one time with brine. The organic phase was collected and dried over sodium sulphate then the solvent was evaporated under vacuum.

The crude residue was used directly for the step 2 without further purification.

MW: 344.45 g/mol

Synthesis of **4b**-*Step 2*

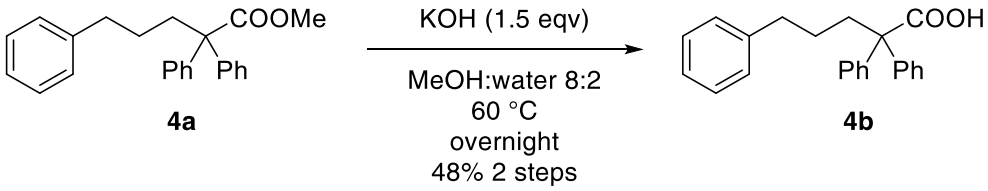

Figure S 6: Synthesis of 2,2,5-triphenylpentanoic acid

The crude ester **4a** (400 mg) was dissolved in methanol:water 8:2 (10 ml, 0.1 M). KOH (2 eq, 27.5 mg) was slowly added and the reaction was brought to reflux overnight under magnetic stirring.

The mixture was cooled to RT and the methanol was evaporated under vacuum. The residue was dissolved in water and the aqueous phase was extracted three times with diethyl ether. Aqueous phase was then acidified with HCl 1 M until the pH was 3, then the same phase was extracted three times with ethyl acetate. The organic phase collected after the extraction of the acid phase was dried over sodium sulphate and the solvent was removed under vacuum.

The crude was purified on silica gel (Toluene/Hexane=8/2 1% acetic acid) obtaining the product **4b** as white crystals. Y% = 60% (200 mg) over 2 steps.

^{1}H NMR (400 MHz, Chloroform-*d*) δ 7.35 – 7.22 (m, 12H), 7.21 – 7.04 (m, 2H), 2.59 (t, *J* = 7.7 Hz, 2H), 2.49 – 2.37 (m, 2H), 1.52 – 1.39 (m, 2H).

^{13}C NMR (101 MHz, Chloroform-*d*) δ 179.34, 142.25, 141.94, 129.01, 128.40, 128.25, 127.96, 126.99, 125.75, 60.13, 37.44, 36.12, 26.74.

HRMS (ESI-): m/z $[M-H]^-$, calculated for $C_{23}H_{21}O_2^-$: 329.1547; found: 329.1541.

Synthesis of **5e**-*Step 1*

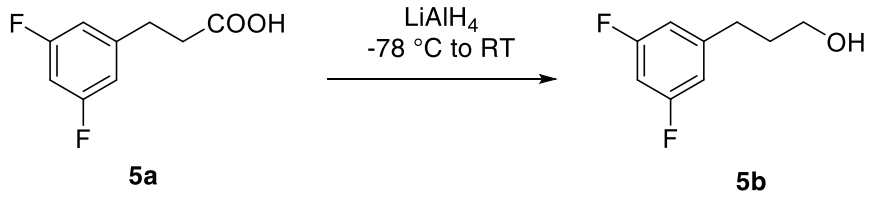

Figure S 7: Synthesis of 3-(3,5-difluorophenyl)propan-1-ol

The carboxylic acid **5a** was reduced to its corrispective alcohol **5b** following the procedure of Natori, Yoshiro et al.[66] obtaining the product in quantitative yield.

The crude resulting mixture was used without further purification for the following step.

MW: 172.17 g/mol

Synthesis of **5e** *-Step 2*

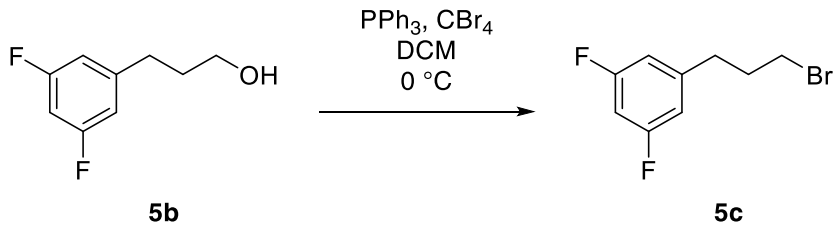

Figure S 8: Synthesis of 1-(3-bromopropyl)-3,5-difluorobenzene

The alcohol **5b** was brominated following the procedure of Natori, Yoshiro et al. [66]

The crude resulting mixture was filtered over a silica pad with hexane as mobile phase, then the solvent was evaporated under vacuum. The product was obtained as a clear oil in quantitative yield.

MW: 235.07 g/mol

Synthesis of **5e** *-Step 3*

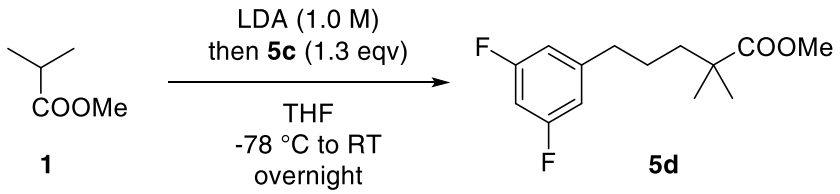

Figure S 9: Synthesis of methyl 5-(3,5-difluorophenyl)-2,2-dimethylpentanoate

1.1 eq. of *n*-BuLi (1 mmol, 625 µl 1,6 M in hexanes) was added to a solution of freshly distilled diisopropylamine (1 eq, 1 mmol, 141 µl) in anhydrous THF (1 ml, 1.0 M) under nitrogen at 0 °C. The reaction mixture was then cooled to -78 °C and ester **1** (0.9 eq, 0.9 mmol, 228 µl)

was carefully added dropwise. The reaction was stirred at the same temperature for 30 min. and then bromide **5c** (1 eq, 235 mg) was added dropwise. The mixture is stirred overnight slowly reaching RT.

The reaction was quenched adding one volume of a saturated solution of ammonium chloride in water. The organic phase was separated and the aqueous phase was extracted with ethyl acetate three times. Organic phases were reunited and washed 2 times with HCl 2 M and one time with brine. The organic phase was collected and dried over sodium sulphate then the solvent was evaporated under vacuum.

The crude was a dark yellow oil and was used without purification of the next step.

MW: 256.29 g/mol

Synthesis of **5e** *-Step 4*

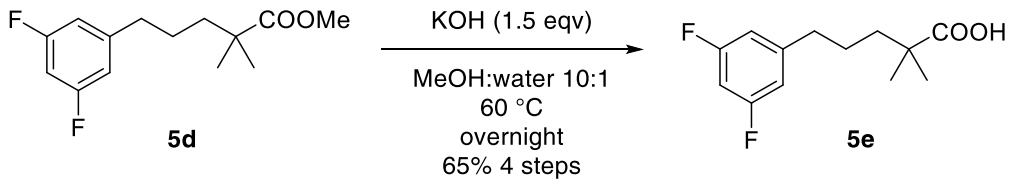

Figure S 10: Synthesis of 5-(3,5-difluorophenyl)-2,2-dimethylpentanoic acid

The crude ester **5d** (530 mg) was dissolved in methanol:water 8:2 (10 ml, 0.1 M). KOH (2 eq, 27.5 mg) was slowly added and the reaction was brought to reflux overnight under magnetic stirring.

The mixture was cooled to RT and the methanol was evaporated under vacuum. The residue was dissolved in water and the aqueous phase was extracted three times with diethyl ether. Aqueous phase was then acidified with HCl 1 M until the pH was 3, then the same phase was extracted three times with ethyl acetate. The organic phase collected after the extraction of the acid phase was dried over sodium sulphate and the solvent was removed under vacuum.

The resulting yellow oil does not need further purification. Y% = 65% (145 mg) over 4 steps.

MW: 242.27 g/mol

^{1}H NMR (400 MHz, Chloroform-*d*) δ 6.81 – 6.56 (m, 3H), 2.61 (t, *J* = 6.7 Hz, 2H), 1.60 (m 2H), 1.22 (s, 6H).

^{13}C NMR (101 MHz, Chloroform-*d*) δ 184.18, 164.15, 161.82, 161.69, 146.02, 145.93, 111.21, 111.15, 111.03, 110.97, 101.55, 101.29, 101.04, 42.02, 39.76, 35.96, 26.13, 24.95.

HRMS (ESI-): m/z $[M-H]^-$, calculated for $C_{13}H_{15}F_2O_2^-$: 241.1046; found: 241.1043.

Synthesis of **6e**-*Step 1*

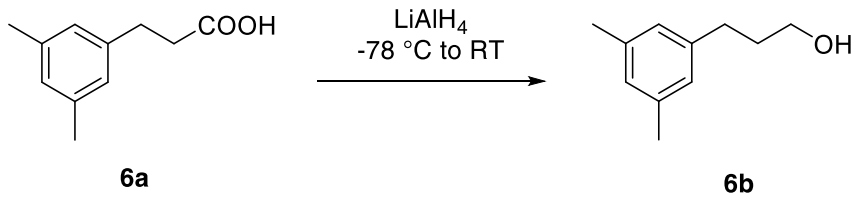

Figure S 11: Synthesis of 3-(3,5-dimethylphenyl)propan-1-ol

The carboxylic acid **6a** was reduced to its corrispective alcohol **6b** following the procedure of Cheung, Fung K.; et al.[67] obtaining the product in quantitative yield.

The crude resulting mixture was used without further purification for the following step.

^{1}H-NMR analysis matches with the one reported in literature by Cheung, Fung K.; et al.[67]

Synthesis of **6e**-*Step 2*

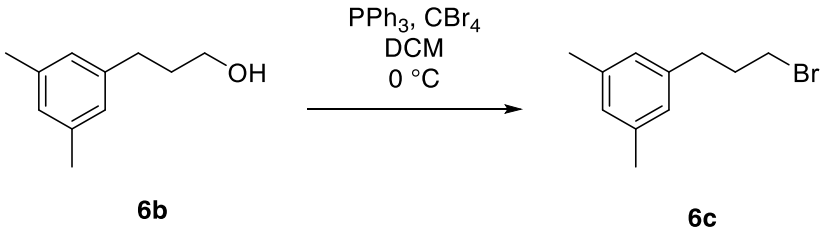

Figure S 12: Synthesis of 1-(3-bromopropyl)-3,5-dimethylbenzene

The alcohol **6b** was brominated following the procedure of Herold, Sebastian; et al.[68] obtaining the bromide **6c**.

The crude resulting mixture was filtered over a silica pad with hexane as mobile phase, then the solvent was evaporated under vacuum. The product was obtained as a clear oil in quantitative yield.

^{1}H-NMR analysis matches with the one reported in literature by Herold, Sebastian; et al.[68]

Synthesis of **6e** *-Step 3*

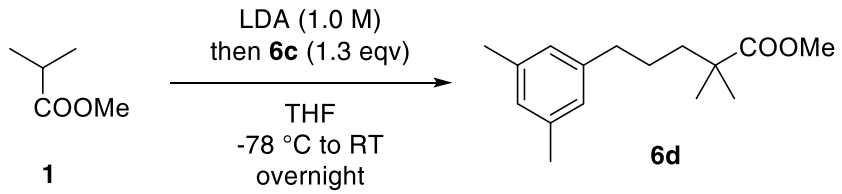

Figure S 13: Synthesis of methyl 5-(3,5-dimethylphenyl)-2,2-dimethylpentanoate

1.1 eq. of *n*-BuLi (1 mmol, 625 µl 1,6 M in hexanes) was added to a solution of freshly distilled diisopropylamine (1 eq, 1 mmol, 141 µl) in anhydrous THF (1 ml, 1.0 M) under nitrogen at 0 °C. The reaction mixture was then cooled to -78 °C and ester **1** (0.9 eq, 0.9 mmol, 228 µl) was carefully added dropwise. The reaction was stirred at the same temperature for 30 min. and then bromide **6c** (1 eq, 227 mg) was added dropwise. The mixture is stirred overnight slowly reaching RT.

The reaction was quenched adding one volume of a saturated solution of ammonium chloride in water. The organic phase was separated and the aqueous phase was extracted with ethyl acetate three times. Organic phases were reunited and washed 2 times with HCl 2 M and one time with brine. The organic phase was collected and dried over sodium sulphate then the solvent was evaporated under vacuum.

The crude mixture was used for the step 4 without further purification.

Synthesis of **6e** *-Step 4*

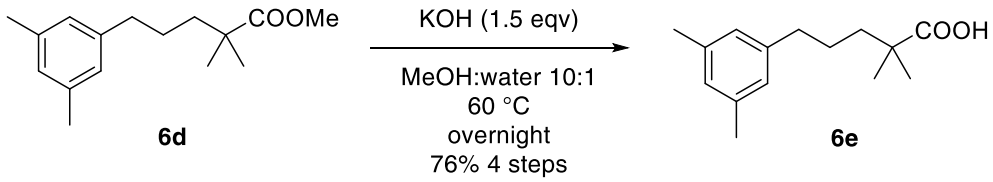

Figure S 14: Synthesis of 5-(3,5-dimethylphenyl)-2,2-dimethylpentanoic acid

The crude ester **6d** (485 mg) was dissolved in methanol:water 8:2 (10 ml, 0.1 M). KOH (2 eq, 27.5 mg) was slowly added and the reaction was brought to reflux overnight under magnetic stirring.

The mixture was cooled to RT and the methanol was evaporated under vacuum. The residue was dissolved in water and the aqueous phase was extracted three times with diethyl ether. Aqueous phase was then acidified with HCl 1 M until the pH was 3, then the same phase was extracted three times with ethyl acetate. The organic phase collected after the extraction of the acid phase was dried over sodium sulphate and the solvent was removed under vacuum.

6e was a yellow oil that does not need further purification. Y% = 79% (185 mg) over 4 steps.

^{1}H NMR (400 MHz, Chloroform-*d*) δ 6.85 (d, *J* = 9.4 Hz, 3H), 2.56 (dq, *J* = 4.2, 2.4 Hz, 2H), 2.33 (s, 6H), 1.65 (d, *J* = 3.9 Hz, 4H), 1.24 (s, 6H).

^{13}C NMR (101 MHz, Chloroform-*d*) δ 184.91, 142.16, 137.78, 127.45, 126.21, 42.13, 40.25, 36.20, 26.84, 24.95, 21.29.

HRMS (ESI-): m/z $[M-H]^-$, calculated for $C_{15}H_{21}O_2^-$: 233.1547; found: 233.1542.

Synthesis of **7e** *-Step 1*

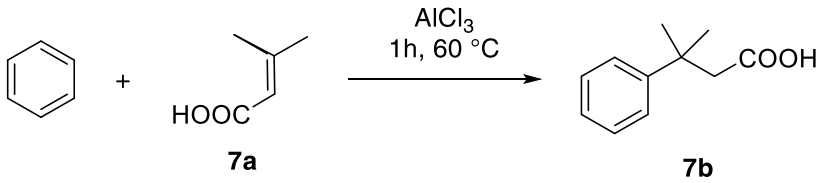

Figure S 15: Synthesis of 3-methyl-3-phenylbutanoic acid

The carboxylic acid **7a** was synthesized following the procedure by Nieman, James A.; et al.[69]

The crude was used without further purification for step 2.

^{1}H-NMR analysis matches with the one reported by Nieman, James A.; et al.[69]

Synthesis of **7e***-Step 2*

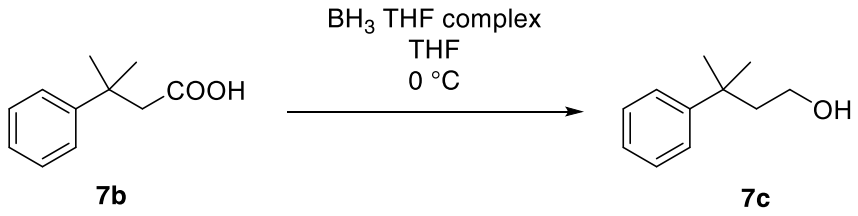

Figure S 16: Synthesis of 3-methyl-3-phenylbutan-1-ol

The alcohol **7b** was synthesized following the procedure by Bartkovitz, David Joseph; et al.[70]

The crude was used without further purification for step 2.

^{1}H-NMR analysis matches with the one reported by Bartkovitz, David Joseph; et. al. [70]

Synthesis of **7e**-*Step 3*

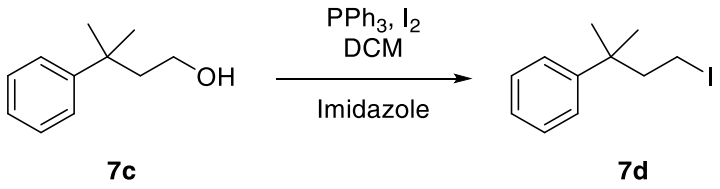

Figure S 17: Synthesis of (4-iodo-2-methylbutan-2-yl)benzene

The alcohol **7c** was iodinated following the procedure of Chen, Weiqiang; et al. [71] obtaining the iodide **7d**.

Molecular iodine (1.3 eq, 6.5 mmol, 1,6 g) was added portionwise to a solution of PPh_3 (1.3 eq, 6.5 mmol, 1.7 g) in CH_2Cl_2 (32 ml, 0.2 M) at 0 °C. The resulting suspension was stirred for 2 hours at 0 °C. A solution of alcohol **7c** (1.0 eq, 5 mmol, 822 mg) and imidazole (1.3 eq, 6.5 mmol, 446 mg) in CH_2Cl_2 (3 ml, 1.7 M) was added dropwise to the reaction mixture. The reaction was stirred overnight until RT. The reaction was the quenched adding $Na_2S_2O_3$ (1.0 M, aq.) and the aqueous phase was extracted three times with MTBE (3 x 2 volumes). The collected organic

phases were washed with 2 volumes of brine and the residue was dried over sodium sulphate, then the solvent was evaporated under reduced pressure.

The crude resulting mixture was filtered over a silica pad with hexane as mobile phase, then the solvent was evaporated under vacuum. The product was obtained as a clear oil. Y% = 78% (1.07 g)

^{1}H NMR (400 MHz, Chloroform-*d*) δ 7.34 (d, *J* = 5.3 Hz, 4H), 7.26 – 7.20 (m, 1H), 2.98 – 2.83 (m, 2H), 2.40 – 2.27 (m, 2H), 1.36 (s, 6H).

^{13}C NMR (101 MHz, Chloroform-*d*) δ 146.26, 127.44, 125.00, 124.69, 48.62, 39.38, 27.52.

Synthesis of **7e**-*Step 4*

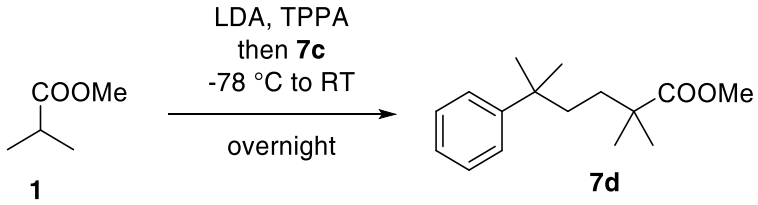

Figure S 18: Synthesis of methyl 2,2,5-trimethyl-5-phenylhexanoate

1.1 eq. of *n*-BuLi (3.3 mmol, 1.88 ml 1,6 M in hexanes) was added to a solution of freshly distilled diisopropylamine (1 eq, 3 mmol, 423 µl) in anhydrous THF (3 ml, 1.0 M) under nitrogen at 0 °C. The reaction mixture was then cooled to -78 °C and a solution of ester **1** (0.9 eq, 2.7 mmol, 431.4 µl) and TPPA (1.05 eq, 3.15 mmol, 783 µl) in dry THF (3 ml, 1.1 M) was carefully added dropwise. The reaction was stirred at the same temperature for 30 min. and then iodide **7c** (1 eq, 3 mmol, 822 mg)

was added dropwise. The mixture is stirred overnight slowly reaching RT.

The reaction was quenched adding one volume of a saturated solution of ammonium chloride in water. The organic phase was separated and the aqueous phase was extracted with ethyl acetate three times. Organic phases were reunited and washed 2 times with HCl 2 M and one time with brine. The organic phase was collected and dried over sodium sulphate then the solvent was evaporated under vacuum.

The crude was purified on silica gel using 98:2 Hexane/EtOAc as mobile phase obtaining ester **7d**. The resulting yellow oil was used for the step 5. Y% : 77% (573 mg).

^{1}H NMR (400 MHz, Chloroform-*d*) δ 7.32 (d, *J* = 4.3 Hz, 4H), 7.20 (q, *J* = 4.3 Hz, 1H), 3.64 (d, *J* = 0.9 Hz, 3H), 1.62 – 1.52 (m, 4H), 1.31 (m, 8H), 1.11 (s, 6H).

^{13}C NMR (101 MHz, Chloroform-*d*) δ 178.40, 149.06, 128.02, 125.79, 125.42, 51.51, 42.09, 39.15, 37.38, 35.56, 28.95, 25.08.

Synthesis of **7e**-*Step 5*

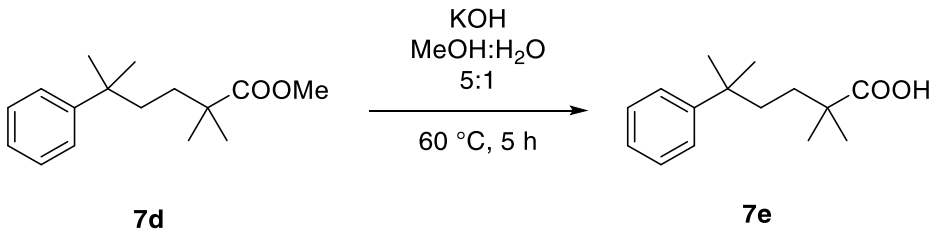

Figure S 19: Synthesis of 2,2,5-trimethyl-5-phenylhexanoic acid

The ester **7d** (500 mg) was dissolved in methanol:water 8:2 (30 ml, 0.1 M). KOH (2 eq, 259.1 mg) was slowly added and the reaction was brought to reflux overnight under magnetic stirring.

The mixture was cooled to RT and the methanol was evaporated under vacuum. The residue was dissolved in water and the aqueous phase was extracted three times with diethyl ether. Aqueous phase was then acidified with HCl 1 M until the pH was 3, then the same phase was extracted three times with ethyl acetate. The organic phase collected after the extraction of the acid phase was dried over sodium sulphate and the solvent was removed under vacuum.

The resulting white powder was obtained in a quantitative yield as **7e** and it does not need further purification.

^{1}H NMR (400 MHz, Chloroform-*d*) δ 7.39 – 7.30 (m, 4H), 7.21 (td, *J* = 5.9, 2.8 Hz, 1H), 1.73 – 1.60 (m, 2H), 1.34 (m, 8H), 1.16 (s, 6H).

^{13}C NMR (101 MHz, Chloroform-*d*) δ 184.62, 149.02, 128.09, 125.80, 125.49, 41.90, 38.94, 37.40, 35.32, 28.97, 24.86.

HRMS (ESI-): m/z $[M-H]^-$, calculated for $C_{15}H_{21}O_2^-$: 233.1547; found: 233.1542.

Synthesis of **8g** *– step 1*

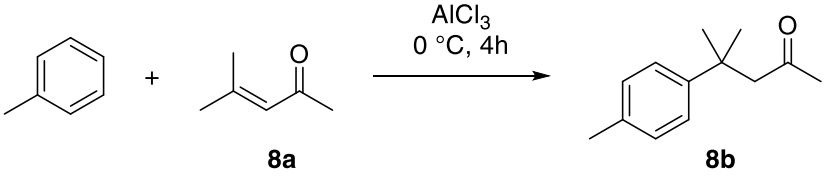

Figure S 20: Synthesis of 4-methyl-4-(p-tolyl)pentan-2-one

Ketone **8b** has been synthesized and purified following the procedure by Hao, Hong-Yan et al. [72]

1H NMR analysis was consistent to the one reported by Hao, Hong-Yan et al. [72]

MW = 190.29 g/mol

Synthesis of **8g** *– step 2*

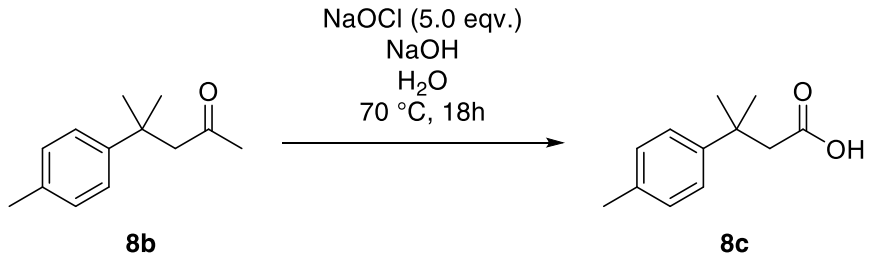

Figure S 21: Synthesis of 3-methyl-3-(p-tolyl)butanoic acid

Carboxylic acid **8c** has been synthesized and purified following the procedure by Dabrowski, J. A. et al. [73]

A flask equipped with stirring bar was charged with ketone **8b** (200 mg, 1.05 mmol, 1 eq). NaOCl 4-6% (aq.) (5.0 eq, 8 mL), NaOH (aq.) (1.1 eq, 2M, 500 µl) and water (50 ml) were added at RT. The resulting solution was warmed up to 70 °C (oil bath) and stirred for 18 hours. The reaction was allowed to cool to RT and acetone was added until the reaction tested negative for peroxides by starch paper. The reaction was then allowed to cool to 0 °C and concentrated HCl was added dropwise until the solution reached pH 3. The aqueous layer was extracted three times with ethyl acetate. Organic layers was washed with water and brine The

organic phase was collected and dried over sodium sulphate, then the solvent was evaporated under vacuum to yield a yellow oil which was purified by crystallization in n-hexane to afford carboxylic acid **8c** as a white solid. Y% = 60 %

^{1}H NMR analysis was consistent to the one reported by Yu, Xiao-Ye; et al. [74]

MW = 192.26 g/mol

Synthesis of **8g** *– step 3*

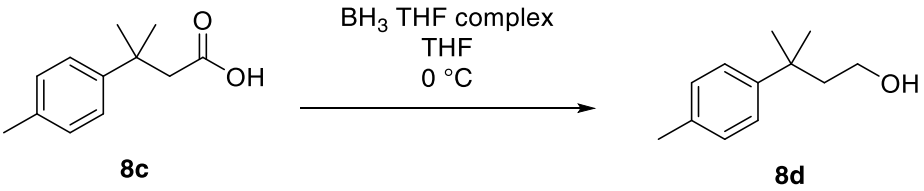

Figure S 22: Synthesis of 3-methyl-3-(p-tolyl)butan-1-ol

The alcohol **8d** was synthesized following the procedure by Bartkovitz, David Joseph; et al. [70]

To a solution of carboxylic acid **8c** (100 mg, 0.52 mmol, 1 eq) in anhydrous tetrahydrofuran (5 ml, 0.02 M) at 0°C was added dropwise a tetrahydrofuran solution of BH_3·THF (2 eq, 1.04 mmol, 1.04 ml, 1 M) under nitrogen. The reaction mixture was stirred at room temperature for 3 h. The mixture was cooled to 0°C and satured bicarbonate was added. The residue was partitioned between ethyl acetate and water. The organic layer were separated, washed with water, aqueous HCl solution (1 M),

brine. The organic phase was dried over sodium sulphate, then the solvent was evaporated under vacuum.

Alcohol **8d** was obtained as colorless oil in a quantitative yield. No further purification was required.

MW = 178.28 g/mol

^{1}H NMR (400 MHz, Chloroform-*d*) δ 7.27 (d, *J* = 8.3 Hz, 2H), 7.15 (dt, *J* = 8.0, 0.7 Hz, 2H), 3.58 – 3.46 (m, 2H), 2.34 (s, 3H), 1.96 (dd, *J* = 7.7, 6.9 Hz, 2H), 1.36 (s, 6H).

^{13}C NMR (101 MHz, Chloroform-*d*) δ 145.67, 135.24, 128.99, 125.55, 60.24, 46.90, 36.30, 29.37, 20.86.

Synthesis of **8g** *– step 4*

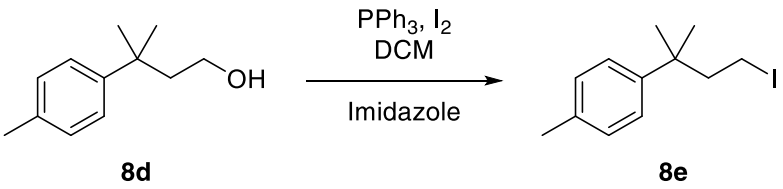

Figure S 23: Synthesis of 1-(4-iodo-2-methylbutan-2-yl)-4-methylbenzene

The alcohol **8d** was iodinated following the procedure of Chen, Weiqiang; et al. [71] obtaining the iodide **8e**.

Molecular iodine (1.3 eq, 4.87 mmol, 1.23 g) was added portionwise to a solution of PPh_3 (1.3 eq, 4.87 mmol, 1.27 g) in CH_2Cl_2 (30 ml, 0.2 M) at 0 °C. The resulting suspension was stirred for 2 hours at 0 °C. A solution of alcohol **8d** (1.0 eq, 3.7 mmol, 668 mg) and imidazole (1.3 eq, 4.87

mmol, 331 mg) in CH_2Cl_2 (2 ml, 1.7 M) was added dropwise to the reaction mixture. The reaction was stirred overnight until RT. The reaction was the quenched adding $Na_2S_2O_3$ (1.0 M, aq.) and the aqueous phase was extracted three times with ethyl acetate (3 x 2 volumes). The collected organic phases were washed with 2 volumes of brine and the residue was dried over sodium sulphate, then the solvent was evaporated under reduced pressure.

The crude resulting mixture was filtered over a silica pad with hexane as mobile phase, then the solvent was evaporated under vacuum. The product was obtained as a clear oil in quantitative yield.

MW = 288.17 g/mol

^{1}H NMR (400 MHz, Chloroform-*d*) δ 7.25 – 7.11 (m, 4H), 2.97 – 2.85 (m, 2H), 2.37 – 2.25 (m, 5H), 1.33 (s, 6H).

^{13}C NMR (101 MHz, Chloroform-*d*) δ 142.90, 134.14, 127.80, 124.27, 48.30, 38.73, 27.28, 19.57.

Synthesis of **8g** *– step 5*

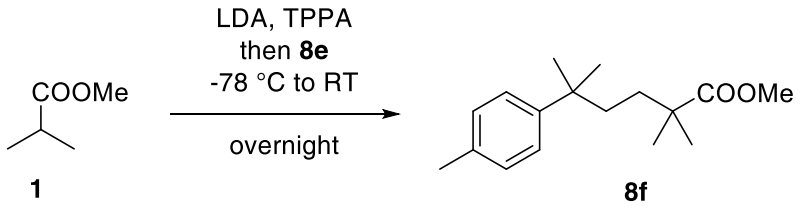

Figure S 24: Synthesis of methyl 2,2,5-trimethyl-5-(p-tolyl)hexanoate

1.1 eq. of *n*-BuLi (2.58 mmol, 1.61 ml 1,6 M in hexanes) was added to a solution of freshly distilled diisopropylamine (1 eq, 1.91 mmol, 270 µl) in anhydrous THF (2 ml, 1.0 M) under nitrogen at 0 °C. The reaction mixture was then cooled to -78 °C and a solution of ester **1** (0.9 eq, 1.7 mmol, 270 µl) and TPPA (1.05 eq, 2.0 mmol, 460 µl) in dry THF (2 ml, 1.1 M) was carefully added dropwise. The reaction was stirred at the same temperature for 30 min. and then iodide **8e** (1 eq, 1.9 mmol, 550 mg) was added dropwise. The mixture is stirred overnight slowly reaching RT.

The reaction was quenched adding one volume of a saturated solution of ammonium chloride in water. The organic phase was separated and the aqueous phase was extracted with ethyl acetate three times. Organic phases were reunited and washed 2 times with HCl 2 M and one time with brine. The organic phase was collected and dried over sodium sulphate then the solvent was evaporated under vacuum.

The crude was purified on silica gel using 98:2 Hexane/EtOAc as mobile phase obtaining ester **8f**. The resulting yellow oil was used for the step 6. Y% = 80%.

MW = 262.39 g/mol

^{1}H NMR (400 MHz, Chloroform-*d*) δ 7.21 (d, *J* = 8.3 Hz, 2H), 7.14 (d, *J* = 0.8 Hz, 2H), 3.65 (s, 3H), 2.35 (s, 3H), 1.57 – 1.51 (m, 2H), 1.34 – 1.25 (m, 8H), 1.11 (s, 6H).

^{13}C NMR (101 MHz, Chloroform-*d*) δ 178.47, 146.06, 134.80, 128.74, 125.68, 51.55, 42.11, 39.09, 37.03, 35.58, 29.07, 25.10, 20.87.

Synthesis of **8g** *– step 6*

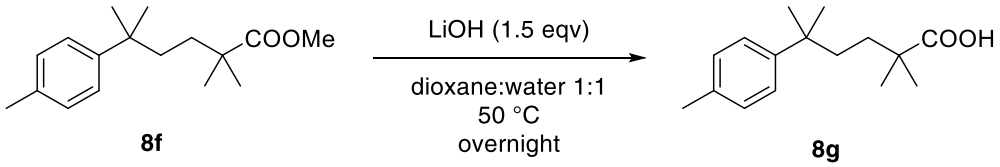

Figure S 25: Synthesis of 2,2,5-trimethyl-5-(p-tolyl)hexanoic acid

Ester **8f** (1 eq, 1 mmol, 255 mg) was dissolved in a 1:1 mixture water:1,4 dioxane (10 ml, 0.1 M). LiOH (1.5 eq, 200 mg) was added to the reaction mixture and the temperature was brought to 50 °C under magnetic stirring for one night.

After the mixture was cooled to RT, 1,4 dioxane was removed under vacuum. The residue was washed three times with diethyl ether. Aqueous phase was then acidified with HCl 1 M (aq) until the pH was 3, then the same phase was extracted three times with ethyl acetate. The organic phase collected after the extraction of the acid phase was dried over sodium sulphate and the solvent was removed under vacuum.

The product **8g** results as white crystals in quantitative yield and no further purification was required.

MW = 248.37 g/mol

^{1}H NMR (400 MHz, Chloroform-*d*) δ 7.20 (d, *J* = 8.2 Hz, 2H), 7.11 (d, *J* = 8.0 Hz, 2H), 2.32 (s, 3H), 1.66 – 1.53 (m, 2H), 1.36 – 1.29 (m, 2H), 1.27 (s, 7H), 1.12 (s, 6H).

^{13}C NMR (101 MHz, Chloroform-*d*) δ 183.06, 146.01, 134.85, 128.79, 125.68, 41.80, 38.91, 37.03, 35.36, 29.05, 24.89, 20.87.

HRMS (ESI-): m/z [M-H]$^-$, calculated for $C_{16}H_{23}O_2^-$: 247.1704; found: 247.1708.

Synthesis of **9e** *– step 1*

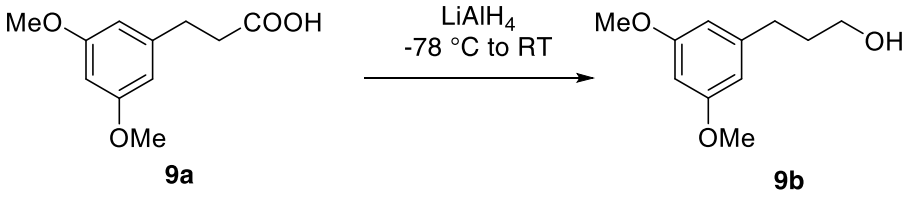

Figure S 26: Synthesis of 3-(3,5-dimethoxyphenyl)propan-1-ol

The carboxylic acid **9a** was reduced to its corrispective alcohol **9b** following the procedure of Plamondon et al. [75] obtaining the product in quantitative yield.

The crude resulting mixture was used without further purification for the following step.

^{1}H-NMR analysis matches with the one reported in literature by Plamondon et al. [75]

Synthesis of **9e** *– step 2*

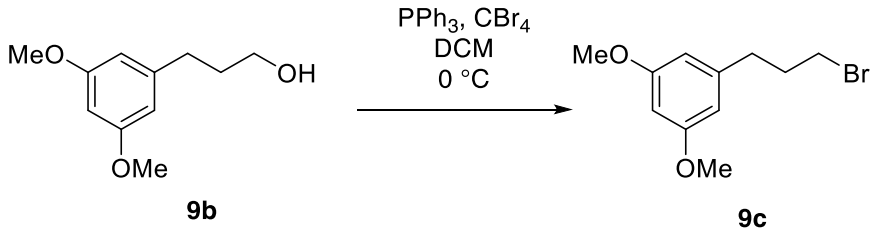

Figure S 27: Synthesis of 1-(3-bromopropyl)-3,5-dimethoxybenzene

The alcohol **9b** was brominated following the procedure of Informa et al. [76] obtaining the bromide **9c**.

The crude resulting mixture was filtered over a silica pad with hexane as mobile phase, then the solvent was evaporated under vacuum. The product was obtained as a clear oil in quantitative yield.

^{1}H-NMR analysis matches with the one reported in literature by Informa et al. [76]

Synthesis of **9e** *– step 3*

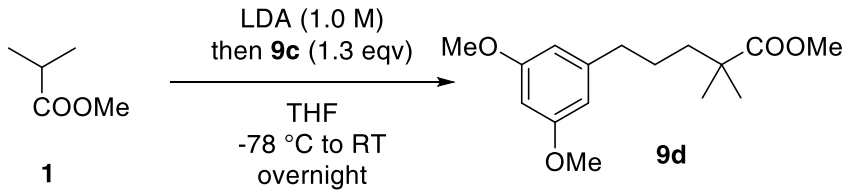

Figure S 28: Synthesis of methyl 5-(3,5-dimethoxyphenyl)-2,2-dimethylpentanoate

1.1 eq. of *n*-BuLi (1 mmol, 625 µl 1,6 M in hexanes) was added to a solution of freshly distilled diisopropylamine (1 eq, 1 mmol, 141 µl) in

anhydrous THF (1 ml, 1.0 M) under nitrogen at 0 °C. The reaction mixture was then cooled to -78 °C and ester **1** (0.9 eq, 0.9 mmol, 228 µl) was carefully added dropwise. The reaction was stirred at the same temperature for 30 min. and then bromide **9c** (1 eq, 257 mg) was added dropwise. The mixture is stirred overnight slowly reaching RT.

The reaction was quenched adding one volume of a saturated solution of ammonium chloride in water. The organic phase was separated and the aqueous phase was extracted with ethyl acetate three times. Organic phases were reunited and washed 2 times with HCl 2 M and one time with brine. The organic phase was collected and dried over sodium sulphate then the solvent was evaporated under vacuum.

The crude mixture was used for the step 4 without further purification.

Synthesis of **9e** *– step 4*

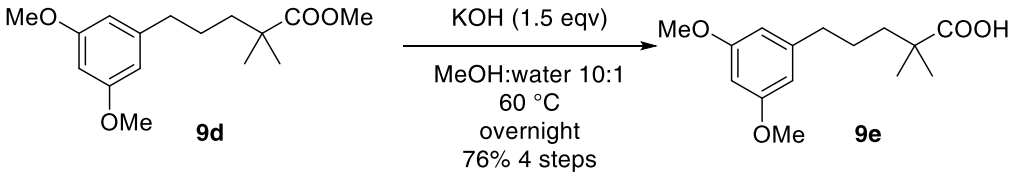

Figure S 29: Synthesis of 5-(3,5-dimethoxyphenyl)-2,2-dimethylpentanoic acid

The crude ester **9d** (471 mg) was dissolved in methanol:water 10:1 (10 ml, 0.1 M). KOH (2 eq, 27.5 mg) was slowly added and the reaction was brought to reflux overnight under magnetic stirring.

The mixture was cooled to RT and the methanol was evaporated under vacuum. The residue was dissolved in water and the aqueous phase was extracted three times with diethyl ether. Aqueous phase was then acidified with HCl 1 M until the pH was 3, then the same phase was extracted three times with ethyl acetate. The organic phase collected after the extraction of the acid phase was dried over sodium sulphate and the solvent was removed under vacuum.

9e was a brown oil that does not need further purification. Y% = 71% (215 mg) over 4 steps.

^{1}H NMR (400 MHz, Chloroform-*d*) δ 6.38 (d, *J* = 2.3 Hz, 2H), 6.34 (d, *J* = 2.3 Hz, 1H), 3.81 (s, 6H), 2.59 (d, *J* = 2.3 Hz, 2H), 1.72 – 1.55 (m, 4H), 1.23 (s, 6H).

^{13}C NMR (101 MHz, Chloroform-*d*) δ 184.95, 160.75, 144.62, 106.46, 97.76, 55.26, 42.09, 40.03, 36.56, 26.43, 24.95.

HRMS (ESI-): m/z $[M-H]^-$, calculated for $C_{15}H_{21}O_4^-$: 265.1445; found: 265.1445.

Synthesis of **10e** *– step 1*

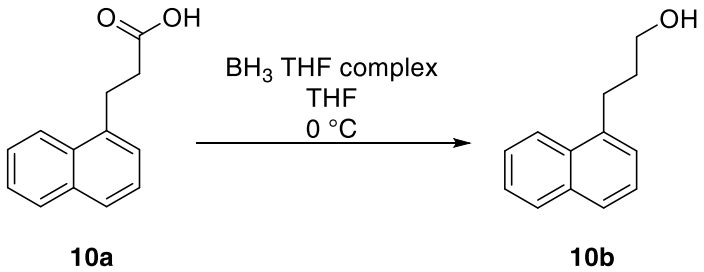

Figure S 30: Synthesis of 3-(naphthalen-1-yl)propan-1-ol

The alcohol **10b** was synthesized following the procedure by Bartkovitz, David Joseph; et al.[70]

To a solution of carboxylic acid **10a** (1 g, 5 mmol, 1 eq) in anhydrous tetrahydrofuran (50 ml, 0.1 M) at 0°C was added dropwise a tetrahydrofuran solution of $BH_3 \cdot THF$ (2 eq, 10 mmol, 10 ml, 1 M) under nitrogen. The reaction mixture was stirred at room temperature for 3 h. The mixture was cooled to 0°C and satured bicarbonate was added. The residue was partitioned between ethyl acetate and water. The organic layer were separated, washed with water, aqueous HCl solution (1 M), brine. The organic phase was dried over sodium sulphate, then the solvent was evaporated under vacuum.

Alcohol **10b** was obtained as colorless oil in a quantitative yield. No further purification was required.

^{1}H-NMR analysis matches with the one reported in literature by Yao, Yi-Xuan et al.[77]

MW = 186.25 g/mol

^{1}H NMR (400 MHz, Chloroform-*d*) δ = 7.99 (d, J = 8.2 Hz, 1 H), 7.84-7.58 (m, 2 H), 7.50-7.12 (m, 4 H), 3.67 (t, J = 6.3 Hz, 2 H), 3.10 (dd, J = 8.6, 6.8 Hz, 2 H), 2.04-1.87 (m, 2 H), 1.24 (d, J = 54.2 Hz, 1 H).

Synthesis of **10e** *– step 2*

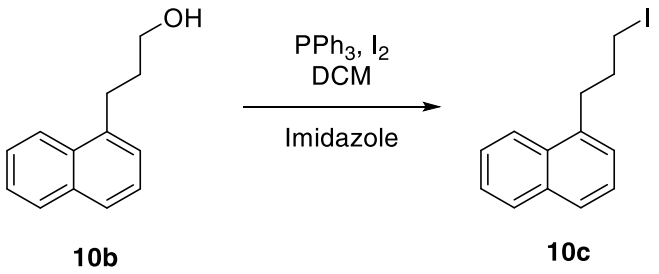

Figure S 31: Synthesis of 1-(3-iodopropyl)naphthalene

The alcohol **10b** was iodinated following the procedure of Chen, Weiqiang; et al. [71] obtaining the iodide **10c**.

Molecular iodine (1.3 eq, 6.5 mmol, 1.65 g) was added portionwise to a solution of PPh_3 (1.3 eq, 6.5 mmol, 1.7 g) in CH_2Cl_2 (32 ml, 0.2 M) at 0 °C. The resulting suspension was stirred for 2 hours at 0 °C. A solution of alcohol **10b** (1.0 eq, 5 mmol, 930 mg) and imidazole (1.3 eq, 6.5 mmol, 440 mg) in CH_2Cl_2 (3 ml, 1.7 M) was added dropwise to the reaction mixture. The reaction was stirred overnight until RT. The reaction was the quenched adding $Na_2S_2O_3$ (1.0 M, aq.) and the aqueous phase was extracted three times with ethyl acetate (3 x 2 volumes). The collected organic phases were washed with 2 volumes of brine and the residue was dried over sodium sulphate, then the solvent was evaporated under reduced pressure.

The crude resulting mixture was filtered over a silica pad with hexane as mobile phase, then the solvent was evaporated under vacuum. The product was obtained as a clear oil in quantitative yield.

MW = 296.15 g/mol

^{1}H NMR (400 MHz, Chloroform-*d*) δ 8.07 (dd, *J* = 8.3, 1.4 Hz, 1H), 7.93 – 7.85 (m, 1H), 7.77 (dt, *J* = 7.8, 1.1 Hz, 1H), 7.54 (dddd, *J* = 17.8, 8.1, 6.8, 1.4 Hz, 2H), 7.48 – 7.36 (m, 2H), 3.41 – 3.05 (m, 4H), 2.54 – 2.16 (m, 2H).

^{13}C NMR (101 MHz, Chloroform-*d*) δ 136.50, 133.98, 131.74, 128.88, 127.06, 126.40, 125.98, 125.56 (d, *J* = 7.2 Hz), 123.63, 34.13, 33.48, 6.78.

Synthesis of **10e** *– step 3*

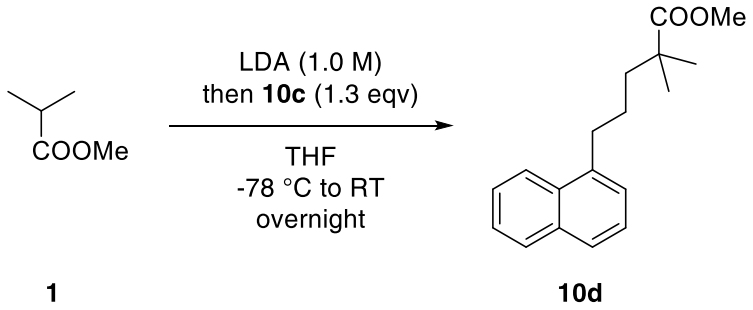

Figure S 32: Synthesis of methyl 2,2-dimethyl-5-(naphthalen-1-yl)pentanoate

1.1 eq. of *n*-BuLi (5.5 mmol, 3.4 ml 1,6 M in hexanes) was added to a solution of freshly distilled diisopropylamine (1 eq, 5 mmol, 722 µl) in anhydrous THF (5 ml, 1.0 M) under nitrogen at 0 °C. The reaction mixture was then cooled to -78 °C and ester **1** (0.9 eq, 4.5 mmol, 510 µl) was carefully added dropwise. The reaction was stirred at the same temperature for 30 min. and then iodide **10c** (1 eq, 1.48 g) was added dropwise. The mixture is stirred overnight slowly reaching RT.

The reaction was quenched adding one volume of a saturated solution of ammonium chloride in water. The organic phase was separated and the

aqueous phase was extracted with ethyl acetate three times. Organic phases were reunited and washed 2 times with HCl 2 M and one time with brine. The organic phase was collected and dried over sodium sulphate then the solvent was evaporated under vacuum.

The crude mixture was purified on silica gel using hexane/EtOAc 9:1 obtaining pure ester **10d** with 63% yield (806 mg).

^{1}H NMR (400 MHz, Chloroform-*d*) δ 8.07 – 8.00 (m, 1H), 7.92 – 7.84 (m, 1H), 7.73 (dt, *J* = 8.2, 1.1 Hz, 1H), 7.61 – 7.45 (m, 2H), 7.42 (dd, *J* = 8.2, 7.0 Hz, 1H), 7.34 (dd, *J* = 6.6, 1.1 Hz, 1H), 3.63 (s, 3H), 3.07 (td, *J* = 5.0, 2.5 Hz, 2H), 1.89 – 1.65 (m, 4H), 1.19 (s, 6H).

^{13}C NMR (101 MHz, Chloroform-*d*) δ 178.43, 138.35, 133.89, 131.84, 128.77, 126.58, 125.84, 125.73, 125.51, 125.40, 123.73, 51.64, 42.34, 40.78, 33.41, 26.24, 25.19.

Synthesis of **10e** *– step 4*

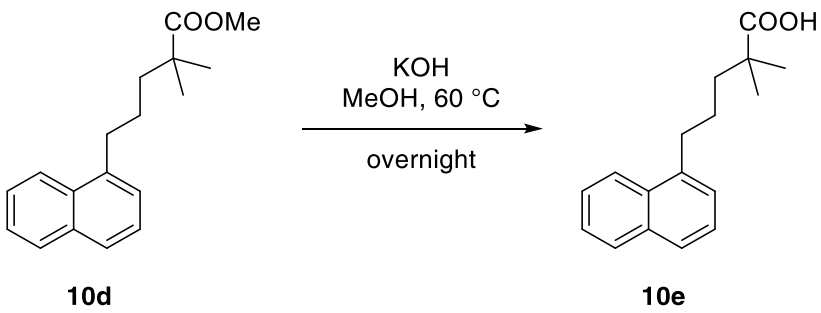

Figure S 33: Synthesis of methyl 2,2-dimethyl-5-(naphthalen-1-yl)pentanoic acid

The ester **10d** (800 mg) was dissolved in methanol:water 10:1 (30 ml, 0.1 M). KOH (2 eq, 170 mg) was slowly added and the reaction was brought to reflux overnight under magnetic stirring.

The mixture was cooled to RT and the methanol was evaporated under vacuum. The residue was dissolved in water and the aqueous phase was extracted three times with diethyl ether. Aqueous phase was then acidified with HCl 1 M until the pH was 3, then the same phase was extracted three times with ethyl acetate. The organic phase collected after the extraction of the acid phase was dried over sodium sulphate and the solvent was removed under vacuum.

10e was obtained as a white solid that does not need further purification in quantitative yield (750 mg).

^{1}H NMR (400 MHz, Chloroform-*d*) δ 7.91 (d, *J* = 8.0 Hz, 1H), 7.80 – 7.69 (m, 1H), 7.61 (d, *J* = 8.1 Hz, 1H), 7.46 – 7.33 (m, 3H), 7.32 – 7.26 (m, 1H), 7.22 (d, *J* = 6.9 Hz, 1H), 2.96 (t, *J* = 6.9 Hz, 2H), 1.72 – 1.59 (m, 4H), 1.10 (d, *J* = 2.0 Hz, 6H).

^{13}C NMR (101 MHz, Chloroform-*d*) δ 184.98, 138.33, 133.93, 131.90, 128.82, 126.66, 125.86, 125.82, 125.57, 125.46, 123.77, 42.21, 40.54, 33.47, 26.17, 24.99.

HRMS (ESI-): m/z $[M-H]^-$, calculated for $C_{15}H_{21}O_4^-$: 242.1307; found: 242.1306.

3.4 Optimization studies on 2b

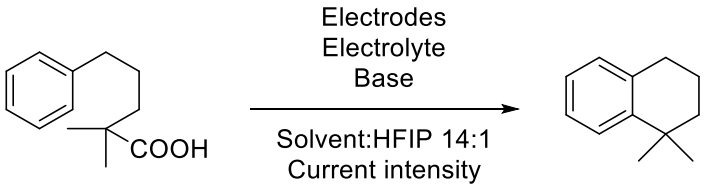

2b **2**

Electrolyte (0.1 M)	Current intensity (mA)	Current quantity (F/mol)	Base (type)	Solvent (X : HFIP 14:1)	Base (eqv)	Substrate concentration (M)	Working electrode	Counter electrode
TBAOAc	1	1.5	Collidine	DCM	1	0.01	GC	C
TBABF4	2.5	2.1	Lutidine	DMSO	2	0.02	C	Pt
TBAClO4	5	2.6	Triethylamine	THF	3	0.04	RVC	Ni
TBAPF6	7.5		DIPEA	DMF	4	0.1	Pt	Zn
TBAOH	10		DBU	Acetone	5			SS
			4-MeO-Py	MeCN				
			Quinuclidine					

Table S 1: Chosen parameters for the optimization.

Yields have been calculated via GC-MS using 1,4-diisopropylbenzene as an internal standard.

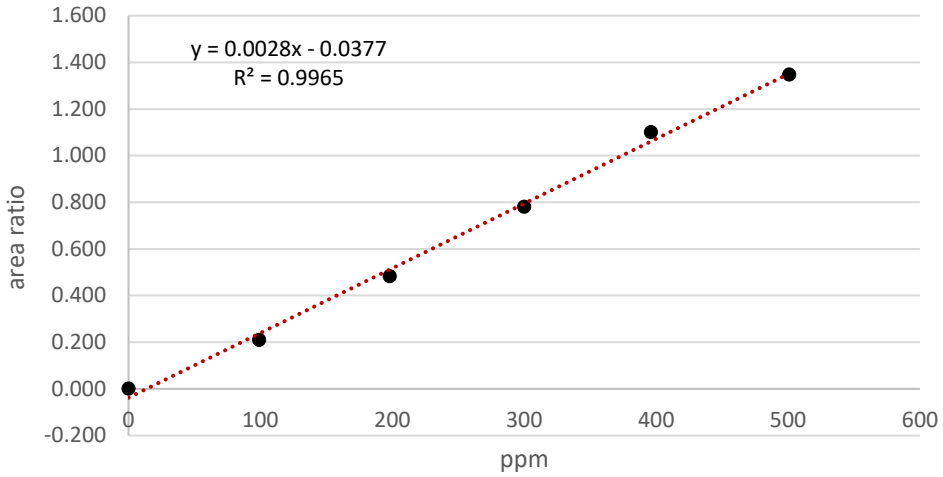

Figure S 34: Calibration line of GC-MS.

General procedure 1 *for batch optimization electrolysis:*

All reactions were performed in an IKA ElectraSyn 2.0 using electrodes purchased from IKA. In a 10 mL IKA ElectraSyn vial, equipped with a stir bar, 1 mmol of electrolyte, 0.2 mmol (1 eqv) of **2b**, 0.7 mL of HFIP, 0.6 mmol of base (3 eqv) were dissolved in 10 mL of dichloromethane and bubbled with Ar while mixed for 5 minutes, than the electrochemical cell was assembled. The instrument was operated under constant current mode at 400 rpm of stirring. After 2.1 F/mol were passed through, the reaction mixture was washed with 1 M HCl (aq.) and the internal standard was added to the organic fraction to measure the yield in GC-MS. All the variations from **General procedure 1** were specified.

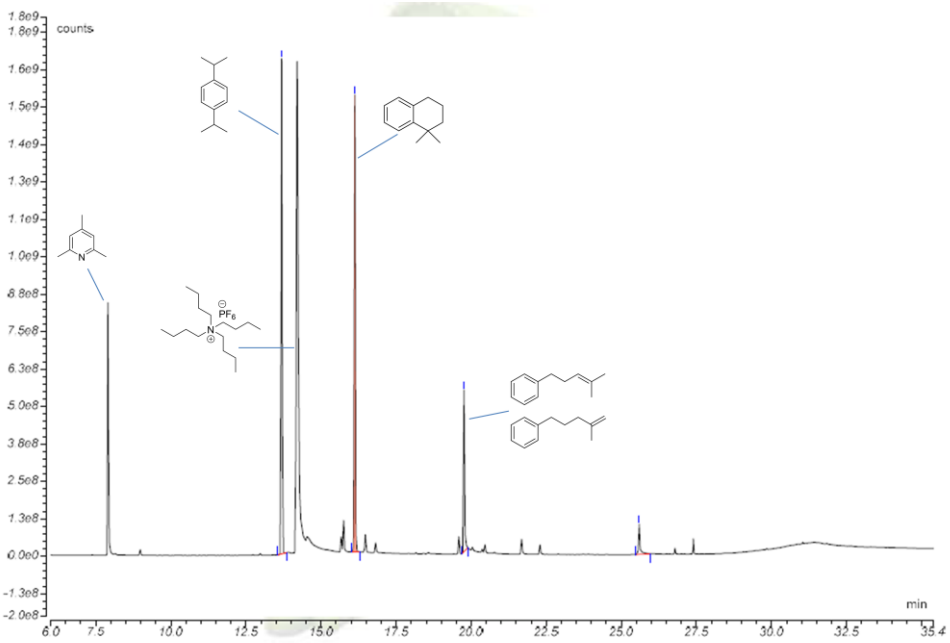

Figure S 35: Typical GC-MS chromatogram of an optimization reaction with the internal standard.

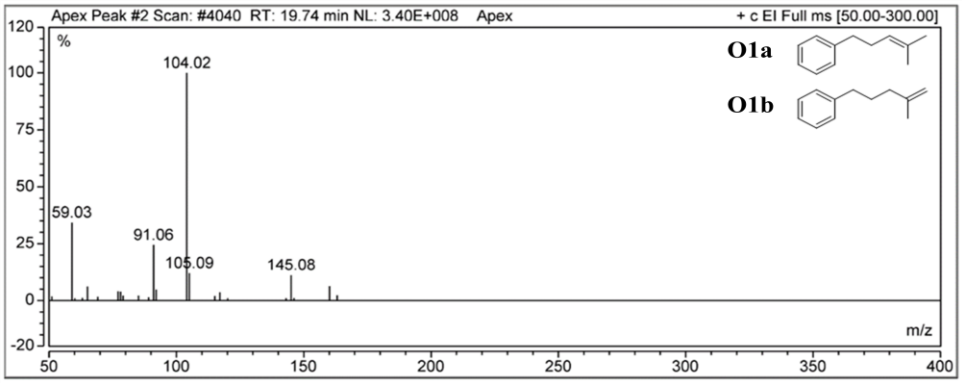

Figure S 36: Mass spectrum of the olefinic byproducts.

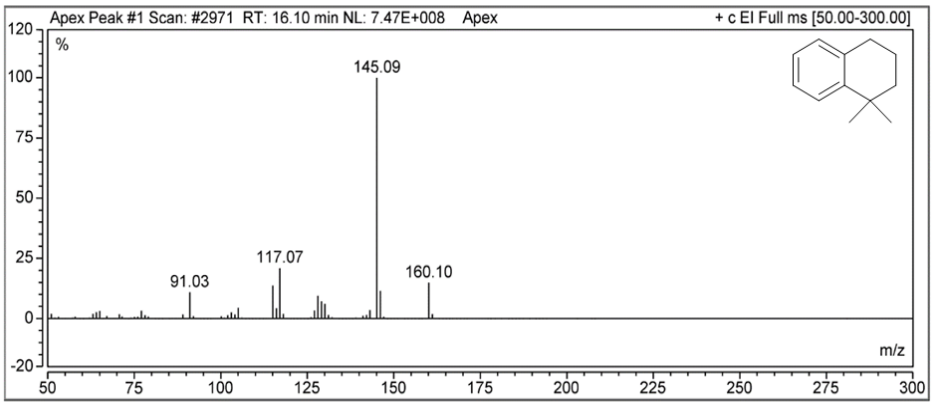

Figure S 37: Mass spectrum of the desired product.

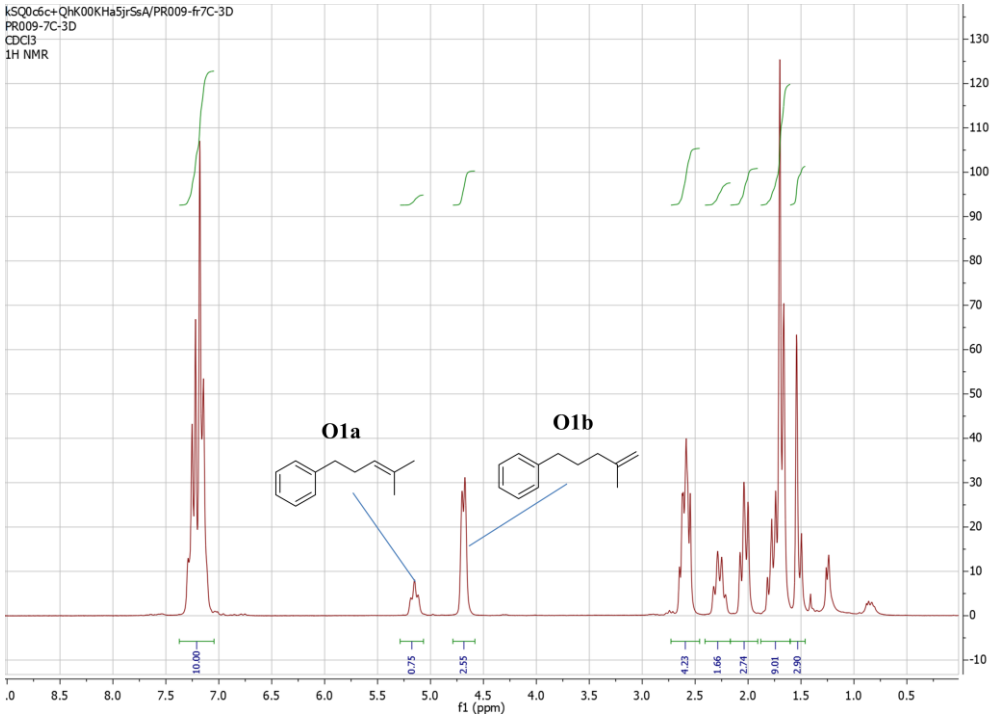

Figure S 38: 1H-NMR spectrum of the olefinic subproducts.

Cyclic voltammetry analysis on **2b**:

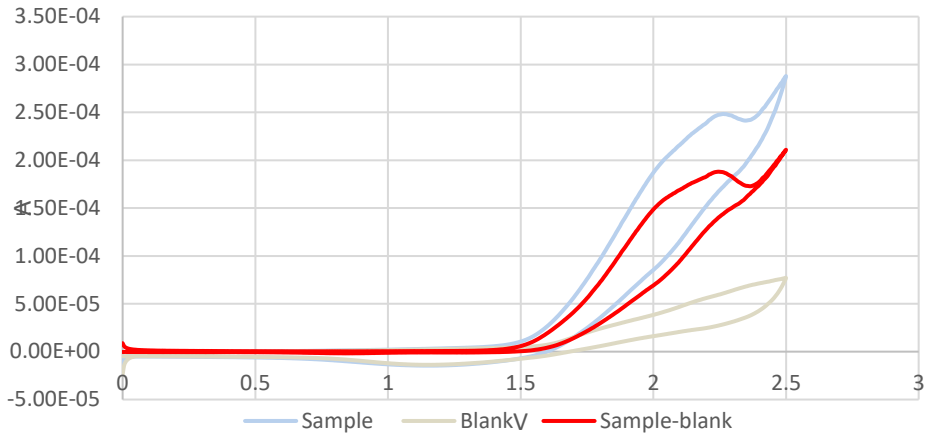

Figure S 39: Cyclic voltammetry analysis of SM. Conditions: 0.1 M n-Bu_4NBF_4, 5 mM 2b, 10 mL DCM:HFIP 14:1, 3 eq 2,4,6-collidine, 50 mV/s

Optimization of the electrolyte:

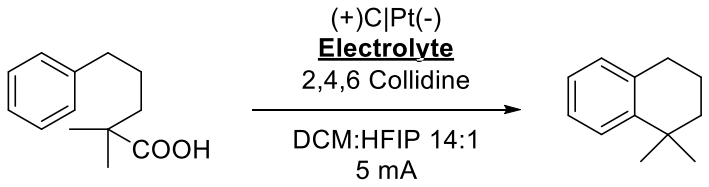

Electrolyte (0.1 M)	Current intensity (mA)	Current quantity (F/mol)	Base (type)	Solvent (X : HFIP 14:1)	Base (eqv)	Substrate concentration (M)	Working electrode	Counter electrode	Yield % (GC/MS)
TBAOAc	5	2	-	DCM	-	0.02	C	Pt	21
TBABF4	5	2	Collidine	DCM	3	0.02	C	Pt	30
TBAClO4	5	2	Collidine	DCM	3	0.02	C	Pt	21
TBAPF6	5	2	Collidine	DCM	3	0.02	C	Pt	51
TBAOH	5	2	-	DCM	-	0.02	C	Pt	10

Table S 2: Optimization of the electrolyte.

Optimization of the current intensity:

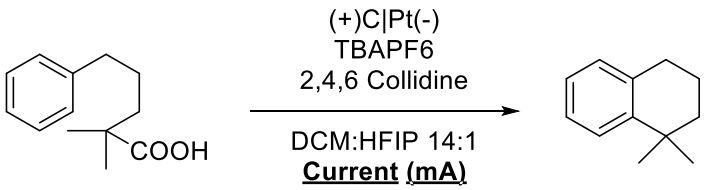

Electrolyte (0.1 M)	Current intensity (mA)	Current quantity (F/mol)	Base (type)	Solvent (X : HFIP 14:1)	Base (eqv)	Substrate concentration (M)	Working electrode	Counter electrode	Yield % (GC/MS)
TBAPF6	1	2	Collidine	DCM	3	0.02	C	Pt	31
TBAPF6	2.5	2	Collidine	DCM	3	0.02	C	Pt	49
TBAPF6	5	2	Collidine	DCM	3	0.02	C	Pt	51
TBAPF6	7.5	2	Collidine	DCM	3	0.02	C	Pt	52
TBAPF6	10	2	Collidine	DCM	3	0.02	C	Pt	38

Table S 3: Optimization of the current intensity.

Optimization of current quantity (F/mol)

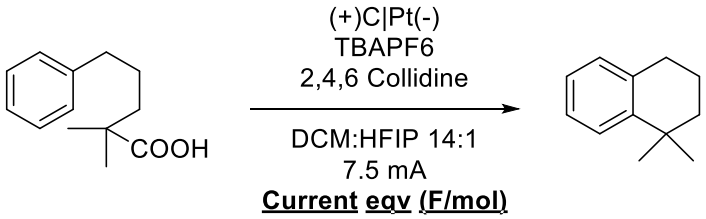

Electrolyte (0.1 M)	Current intensity (mA)	Current quantity (F/mol)	Base (type)	Solvent (X : HFIP 14:1)	Base (eqv)	Substrate concentration (M)	Working electrode	Counter electrode	Yield % (GC/MS)
TBA PF6	7.5	1.5	Collidine	DCM	3	0.02	C	Pt	49
TBA PF6	7.5	2.1	Collidine	DCM	3	0.02	C	Pt	64
TBA PF6	7.5	2.5	Collidine	DCM	3	0.02	C	Pt	48

Table S 4: Optimization of the current quantity.

Optimization of the solvent:

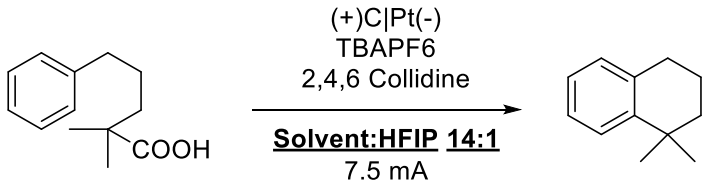

Electrolyte (0.1 M)	Current intensity (mA)	Current quantity (F/mol)	Base (type)	Solvent (X : HFIP 14:1)	Base (eqv)	Substrate concentration (M)	Working electrode	Counter electrode	Yield % (GC/MS)
TBAPF6	7.5	2.1	Collidine	DCM	3	0.02	C	Pt	64
TBAPF6	7.5	2.1	Collidine	DMSO	3	0.02	C	Pt	<5
TBAPF6	7.5	2.1	Collidine	DMF	3	0.02	C	Pt	<5
TBAPF6	7.5	2.1	Collidine	THF	3	0.02	C	Pt	<5
TBAPF6	7.5	2.1	Collidine	ACETONE	3	0.02	C	Pt	<5
TBAPF6	7.5	2.1	Collidine	MeCN	3	0.02	C	Pt	<5

Table S 5: Optimization of the solvent.

Optimization of the base type:

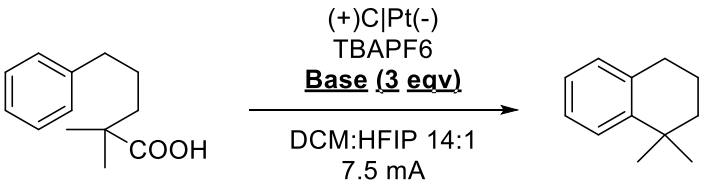

Electrolyte (0.1 M)	Current intensity (mA)	Current quantity (F/mol)	Base (type)	Solvent (X : HFIP 14:1)	Base (eqv)	Substrate concentration (M)	Working electrode	Counter electrode	Yield % (GC/MS)
TBAPF6	7.5	2.1	Collidine	DCM	3	0.02	C	Pt	64
TBAPF6	7.5	2.1	Lutidine	DCM	3	0.02	C	Pt	43
TBAPF6	7.5	2.1	TEA	DCM	3	0.02	C	Pt	<5
TBAPF6	7.5	2.1	DIPEA	DCM	3	0.02	C	Pt	<5
TBAPF6	7.5	2.1	DBU	DCM	3	0.02	C	Pt	46
TBAPF6	7.5	2.1	4-MeO-Py	DCM	3	0.02	C	Pt	53
TBAPF6	7.5	2.1	Quinuclidine	DCM	3	0.02	C	Pt	-

Table S 6: Optimization of the type of base.

Optimization of base equivalents:

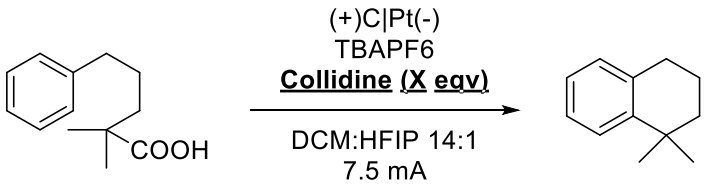

Electrolyte (0.1 M)	Current intensity (mA)	Current quantity (F/mol)	Base (type)	Solvent (X : HFIP 14:1)	Base (eqv)	Substrate concentration (M)	Working electrode	Counter electrode	Yield % (GC/MS)
TBAPF6	7.5	2.1	Collidine	DCM	0.5	0.02	C	Pt	15
TBAPF6	7.5	2.1	Collidine	DCM	1	0.02	C	Pt	40
TBAPF6	7.5	2.1	Collidine	DCM	1.5	0.02	C	Pt	54
TBAPF6	7.5	2.1	Collidine	DCM	2	0.02	C	Pt	64
TBAPF6	7.5	2.1	Collidine	DCM	3	0.02	C	Pt	64
TBAPF6	7.5	2.1	Collidine	DCM	4	0.02	C	Pt	45
TBAPF6	7.5	2.1	Collidine	DCM	5	0.02	C	Pt	45

Table S 7: Optimization of the equivalents of base.

Optimization of the working electrode:

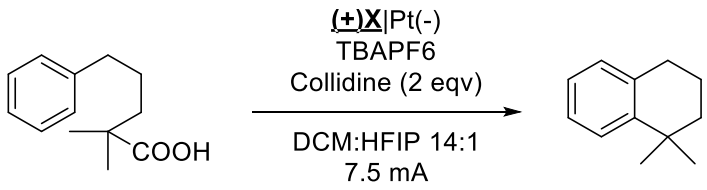

Electrolyte (0.1 M)	Current intensity (mA)	Current quantity (F/mol)	Base (type)	Solvent (X : HFIP 14:1)	Base (eqv)	Substrate concentration (M)	Working electrode	Counter electrode	Yield % (GC/MS)
TBAPF6	7.5	2.1	Collidine	DCM	2	0.02	C	Pt	64
TBAPF6	7.5	2.1	Collidine	DCM	2	0.02	GC	Pt	-
TBAPF6	7.5	2.1	Collidine	DCM	2	0.02	Pt	Pt	-
TBAPF6	7.5	2.1	Collidine	DCM	2	0.02	RVC	Pt	-

Table S 8: Optimization of the working electrode material.

Optimization of counter electrode:

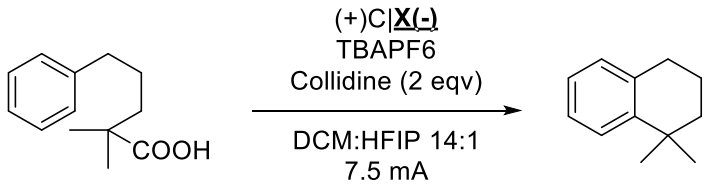

Electrolyte (0.1 M)	Current intensity (mA)	Current quantity (F/mol)	Base (type)	Solvent (X : HFIP 14:1)	Base (eqv)	Substrate concentration (M)	Working electrode	Counter electrode	Yield % (GC/MS)
TBAPF6	7.5	2.1	Collidine	DCM	2	0.02	C	Pt	64
TBAPF6	7.5	2.1	Collidine	DCM	2	0.02	C	Ni	58
TBAPF6	7.5	2.1	Collidine	DCM	2	0.02	C	Zn	60
TBAPF6	7.5	2.1	Collidine	DCM	2	0.02	C	SS	65
TBAPF6	7.5	2.1	Collidine	DCM	2	0.02	C	C	59

Table S 9: Optimization of the counter electrode material.

Optimization of the substrate concentration:

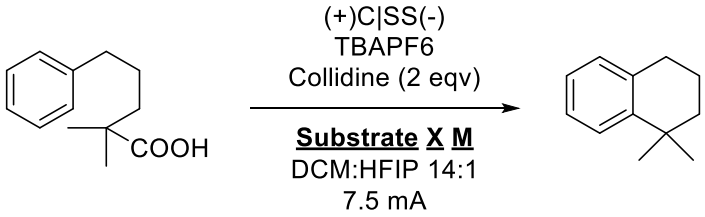

Electrolyte (0.1 M)	Current intensity (mA)	Current quantity (F/mol)	Base (type)	Solvent (X : HFIP 14:1)	Base (eqv)	Substrate concentration (M)	Working electrode	Counter electrode	Yield % (GC/MS)
TBAPF6	7.5	2.1	Collidine	DCM	2	0.01	C	SS	55
TBAPF6	7.5	2.1	Collidine	DCM	2	0.02	C	SS	65
TBAPF6	7.5	2.1	Collidine	DCM	2	0.04	C	SS	65
TBAPF6	7.5	2.1	Collidine	DCM	2	0.1	C	SS	48

Table S 10: Optimization of the substrate concentration.

Final optimized best conditions for batch electrolysis:

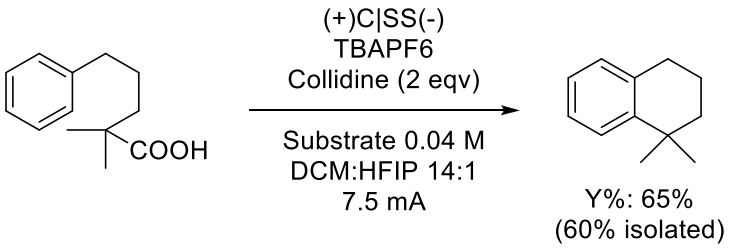

Best electrolyte (0.1 M)	Best current intensity (mA)	Best current quantity (F/mol)	Best base (type)	Best solvent (X : HFIP 14:1)	Bestbase (eqv)	Best substrate concentration (M)	Best working electrode	Best counter electrode	Best yield % (GC/MS)
TBAPF6	7.5	2.1	Collidine	DCM	2	0.02-0.04	C	SS	65 (56% isolated)

Table S 11: Best conditions after the optimization process.

For the isolated yield, the solvent was evaporated under reduced pressure after the reaction was complete and the residue was passed over a silica plug eluted with n-Pentane.

MW: 160.26 g/mol

^{1}H NMR (400 MHz, Chloroform-*d*) δ 7.59 – 7.25 (m, 2H), 7.33 – 7.16 (m, 2H), 2.96 (t, *J* = 6.3 Hz, 2H), 2.11 – 1.89 (m, 2H), 1.86 (dt, *J* = 9.5, 2.6 Hz, 2H), 1.48 (s, 6H).

^{13}C NMR (101 MHz, Chloroform-*d*) δ 145.84, 136.16, 129.10, 126.67, 125.85, 125.29, 39.39, 33.88, 31.93, 30.82, 29.79, 19.79.

General procedure 2 *optimized conditions for batch electrolysis of* **2-10(b or e or g)**

All reactions were performed in an IKA ElectraSyn 2.0 using Graphite SK-50 as working electrode and stainless steel as counter electrode. Electrodes were purchased from IKA. In a 10 mL IKA ElectraSyn vial, equipped with a stir bar, 1 mmol of $TBAPF_6$, 0.4 mmol (1 eqv) of carboxylic acid **2-10(b or e or g)**, 0.7 mL of HFIP, 0.4 mmol of base (2 eqv) were dissolved in 10 mL of dichloromethane and bubbled with Ar while mixed for 5 minutes, then the electrochemical cell was assembled. The instrument was operated under constant current mode at 7.5 mA, at 400 rpm of stirring. After 2.1 F/mol were passed through, the solvent was removed under reduced pressure and the residue was purified over a silica pad, using n-Pentane as mobile phase.

3b *batch electrolysis*

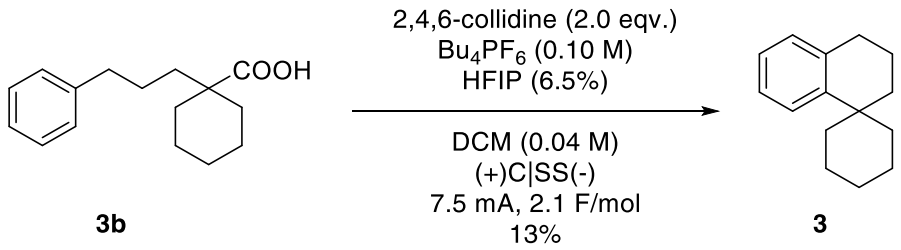

Figure S 40: Electrolysis of 1-(3-phenylpropyl)cyclohexane-1-carboxylic acid in optimal conditions.

3b was electrolyzed following **General procedure 2**. **3** was obtained as a clear oil in 13% isolated yield.

MW: 200.32 g/mol

^{1}H NMR (400 MHz, Chloroform-*d*) δ 7.14 – 7.06 (m, 2H), 7.02 – 6.95 (m, 2H), 2.68 (t, *J* = 6.2 Hz, 2H), 1.75 (dt, *J* = 5.8, 3.5 Hz, 2H), 1.72 – 1.60 (m, 6H), 1.48 (dddd, *J* = 25.2, 12.9, 5.5, 2.7 Hz, 6H)

^{13}C NMR (101 MHz, Chloroform-*d*) δ 146.74, 137.22, 129.13, 126.91, 125.87, 125.24, 38.90, 37.16, 31.15, 31.13, 26.34, 22.15, 19.31.

4b *batch electrolysis*

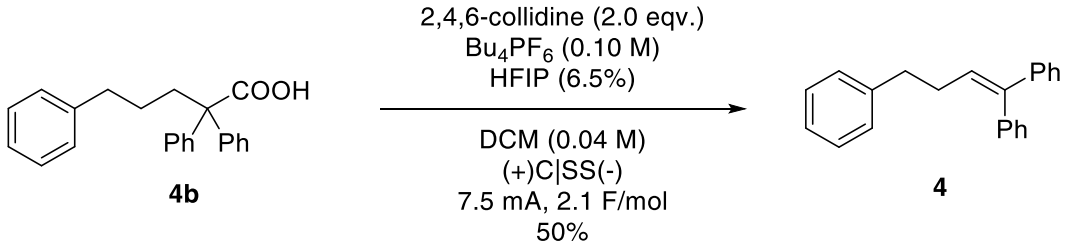

Figure S 41: Electrolysis of 2,2,5-triphenylpentanoic acid in optimal conditions.

4b has been electrolyzed following **General procedure 2**. **4** was obtained as a clear oil in 50% isolated yield. ^{1}H NMR analysis was consistent with results reported by Huang, Hanchu; et al.[78]

^{1}H NMR (400 MHz, Chloroform-*d*) δ 7.28 – 7.02 (m, 15H), 6.03 (t, *J* = 7.4 Hz, 1H), 2.66 (dd, *J* = 8.6, 6.7 Hz, 2H), 2.39 – 2.33 (m, 2H).

5e *batch electrolysis*

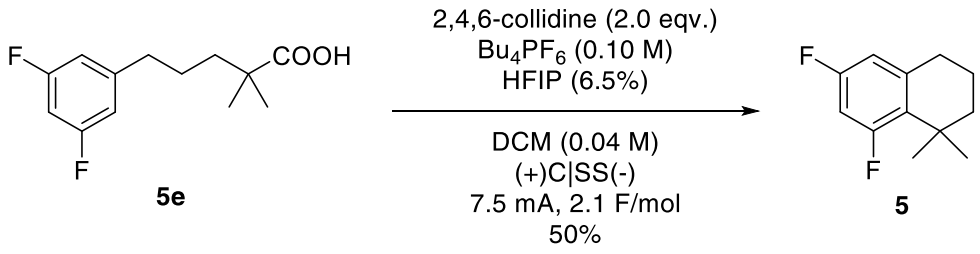

Figure S 42: Electrolysis of 5-(3,5-difluorophenyl)-2,2-dimethylpentanoic acid in optimal conditions.

5e has been electrolyzed following **General procedure 2**. **5** was obtained as a clear oil in 50% isolated yield

^{1}H NMR (400 MHz, Chloroform-*d*) δ 6.56 – 6.44 (m, 2H), 2.64 (t, *J* = 6.2 Hz, 2H), 1.66 (dtd, *J* = 8.9, 5.2, 4.4, 2.6 Hz, 2H), 1.57 (dt, *J* = 8.9, 2.6 Hz, 2H), 1.27 (d, *J* = 1.7 Hz, 6H).

^{13}C NMR (101 MHz, Chloroform-*d*) δ 163.72, 161.60, 161.46, 161.24, 159.02, 142.70 – 139.85 (m), 128.30 (d, *J* = 8.5 Hz), 111.05 (dd, *J* = 19.7, 3.1 Hz), 102.00 (dd, *J* = 28.7, 24.7 Hz), 41.21, 33.12 (d, *J* = 2.3 Hz), 32.34 – 30.60 (m), 29.08 (d, *J* = 5.1 Hz), 19.46.

Su questo composto dovresti anche riportare 19F NMR

6e *batch electrolysis*

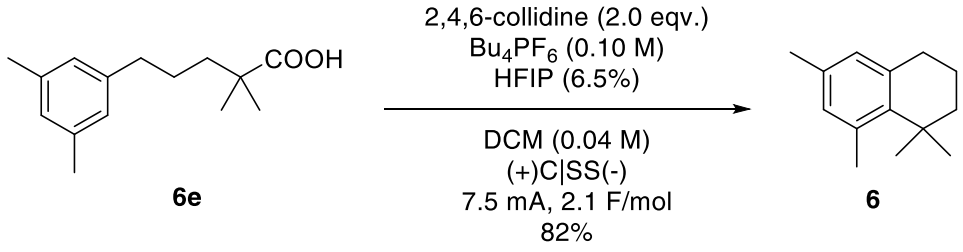

Figure S 43: Electrolysis of 5-(3,5-dimethylphenyl)-2,2-dimethylpentanoic acid in optimal conditions.

6e has been electrolyzed following **General procedure 2**. **6** was obtained as a clear oil in 82% isolated yield

^{1}H NMR (400 MHz, Chloroform-*d*) δ 6.84 – 6.75 (m, 2H), 2.79 (q, *J* = 6.3 Hz, 2H), 2.51 (s, 3H), 2.26 (s, 3H), 1.42 (s, 6H).

^{13}C NMR (101 MHz, Chloroform-*d*) δ 140.49, 137.35, 137.01, 134.58, 131.50, 128.40, 43.99, 34.53, 32.46, 29.33, 29.21, 23.47, 20.46, 19.63.

7e *batch electrolysis*

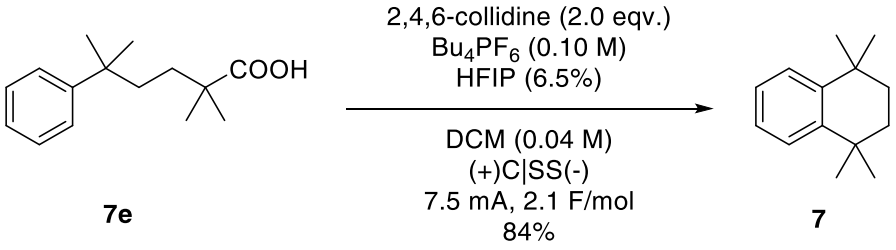

Figure S 44: Electrolysis of 2,2,5-trimethyl-5-phenylhexanoic acid in optimal conditions.

7e has been electrolyzed following **General procedure 2**. **7** was obtained as a clear oil in 84% isolated yield

^{1}H NMR (400 MHz, Chloroform-*d*) δ 7.23 (dq, *J* = 7.0, 3.5 Hz, 2H), 7.04 (dd, *J* = 5.9, 3.4 Hz, 2H), 1.21 (s, 12H).

^{13}C NMR (101 MHz, Chloroform-*d*) δ 144.80, 126.48, 125.53, 35.18, 34.23, 31.91.

8g *batch electrolysis*

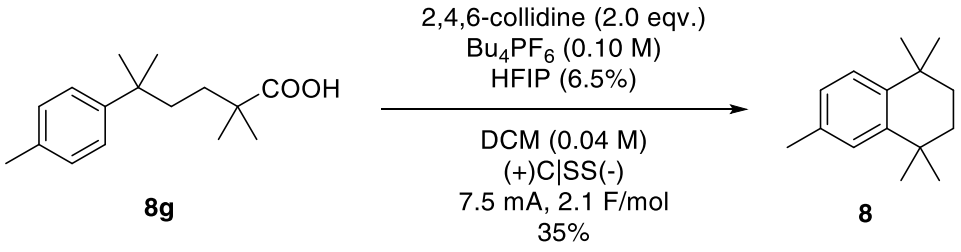

Figure S 45: Electrolysis of 2,2,5-trimethyl-5-phenylhexanoic acid in optimal conditions.

8g has been electrolyzed following **General procedure 2**. **8** was obtained as a clear oil in 35% isolated yield

^{1}H NMR analysis was consistent to the one reported by Ledneczki, Istvan; et al.[79]

9e *batch electrolysis*

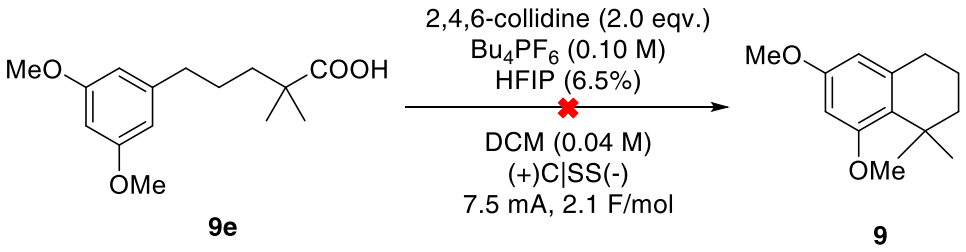

Figure S 46: Batch electrolysis of 5-(3,5-dimethoxyphenyl)-2,2-dimethylpentanoic acid

9e has been electrolyzed following **General procedure 2**. **9** was not found in the reaction mixture.

10e *batch electrolysis*

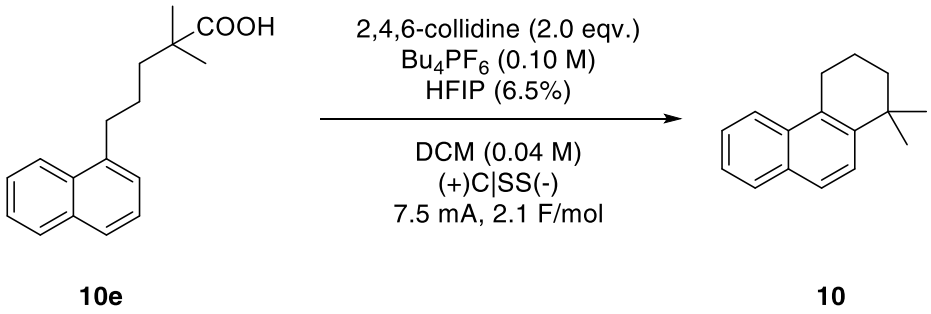

Figure S 47: Batch electrolysis of methyl 2,2-dimethyl-5-(naphthalen-1-yl)pentanoic acid

10e has been electrolyzed following **General procedure 2**. **10** was obtained as a clear oil in 40% isolated yield.

^{1}H NMR (400 MHz, Chloroform-*d*) δ 7.92 (dq, *J* = 8.4, 0.9 Hz, 1H), 7.70 (dd, *J* = 8.4, 1.3 Hz, 1H), 7.59 (d, *J* = 8.7 Hz, 1H), 7.48 – 7.32 (m, 3H), 3.06 (t, *J* = 6.4 Hz, 2H), 1.96 – 1.85 (m, 2H), 1.72 – 1.65 (m, 2H), 1.29 (s, 6H).

3.6 Flow experiments

Every flow experiment has been performed using a hand-made electrochemical flow cell.

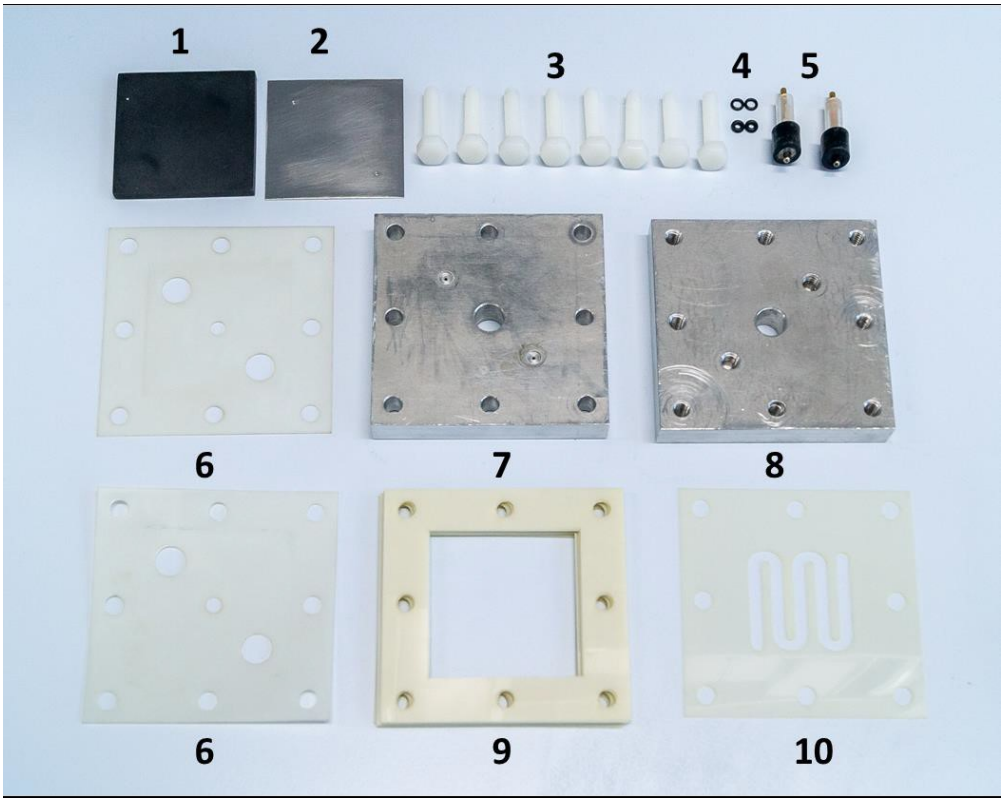

Figure S 48: Components of the flow cell utilized in this work[57]

Components of the flow electrolysis cell utilized in this work. **1**: Graphite anode (IG-63, GTD Graphit Technologie GmbH, 50 × 50 × 3 mm). **2**: Stainless steel cathode (Stainless Steel - AISI 316L, Fe/Cr 18%/Ni 10%/Mo 3%, foil, 50 × 50 × 0.1 mm) incorporating two 1 mm holes. **3**: M6 bolts (polyamide, 30 mm, DIN 933). **4**: O-rings: 5 mm

o.d./2 mm i.d., EPDM (internal); 5 mm o.d., 3 mm i.d., EPDM (external for fitting connections). **5**: current collectors (pogo-pins 2.6 mm diameter, 35 mm length, PTR 1040-D-1.5N-NI-2.4) in a 10 mm o.d. tubing adaptor. **6**: isolation layer (laser-cut Mylar foil, 0.3 mm thickness). **7**: end plate 1 (no M6 threads, inside view). **8**: end plate 2 (with M6 threads, outer view). **9**: alignment gaskets (laser-cut Mylar foil, 0.3 mm thickness). **10**: electrode separator/reaction channel (laser-cut Mylar foil) (11).

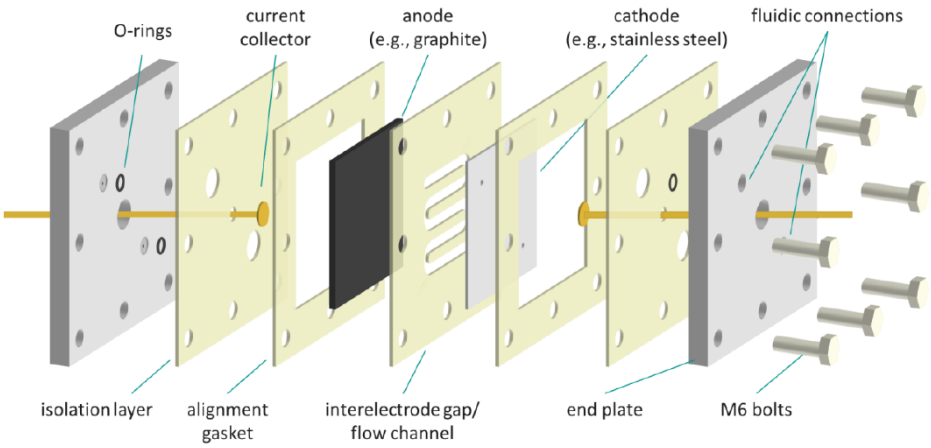

Figure S 49: Scheme of the exploded flow reactor utilized in this work. [57]

3.6.1 Flow recirculation optimization on 2b

General procedure 3 for recirculation flow optimization electrolysis of **2b**:

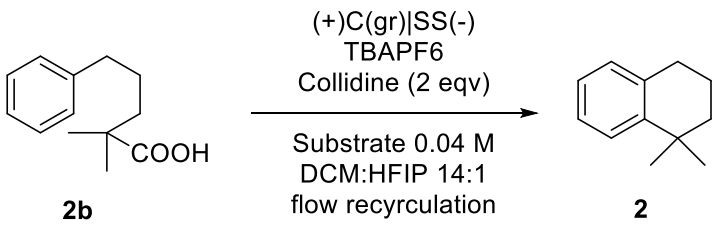

A 20 ml vial equipped with a magnetic stir bar was charged with 0.4 mmol of **2b**, 1 mmol of $TBAPF_6$, 10 ml of DCM, 0.8 mmol of 2,4,6-collidine and 0.7 mL of HFIP. For this purpose, a peristaltic pump was utilized (5 mL/min flow rate). The reactor was operated under constant current mode using a PeakTech 6225 A power supply until the desired amount of charge was passed to the reagent solution. Then, the reactor inlet was removed from the reaction mixture reservoir allowing air to enter the channel and flush all the remaining reaction mixture to the vessel. Parameters like current (mA) and charge (F/mol) have been changed for the optimization of the process. Aliquots (100 µL) of the reaction mixture were collected from the reservoir during cell operation to monitor the reaction progress by HPLC.

HPLC has been calibrated using anisole as an internal standard.

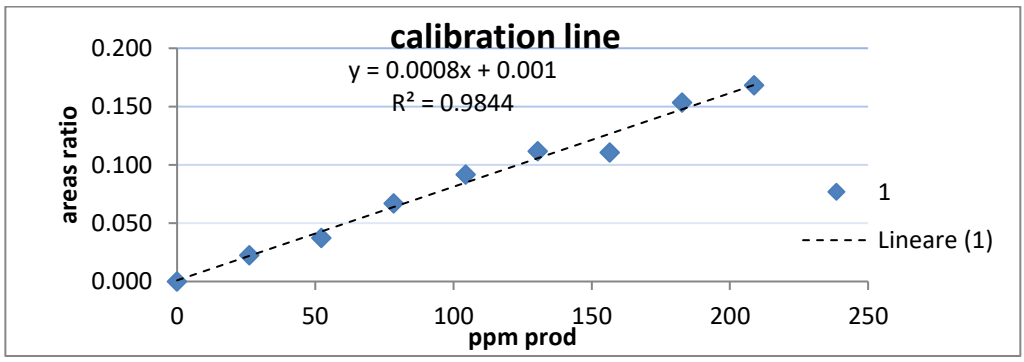

Figure S 50: Calibration line of HPLC

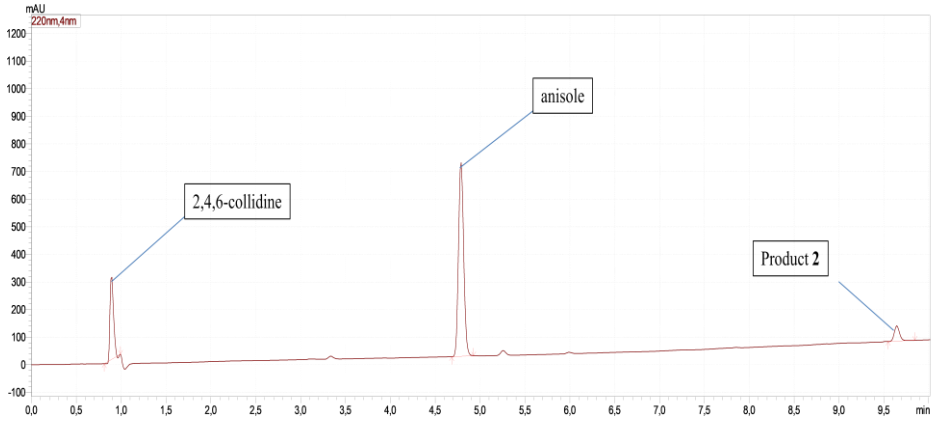

Figure S 51: Typical HPLC chromatogram of an optimization reaction with the internal standard.

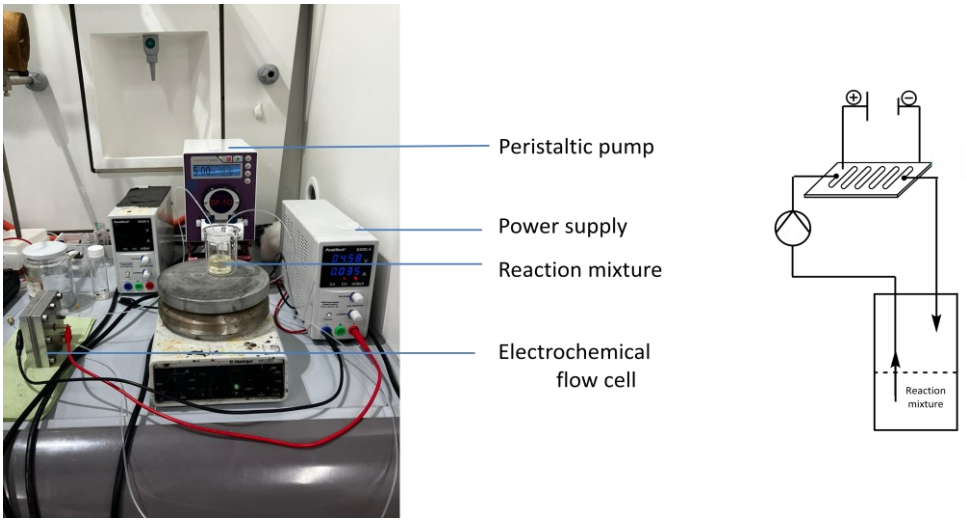

Figure S 52: Real image of the recirculation setup (left); schematic image of the recirculation setup (right).

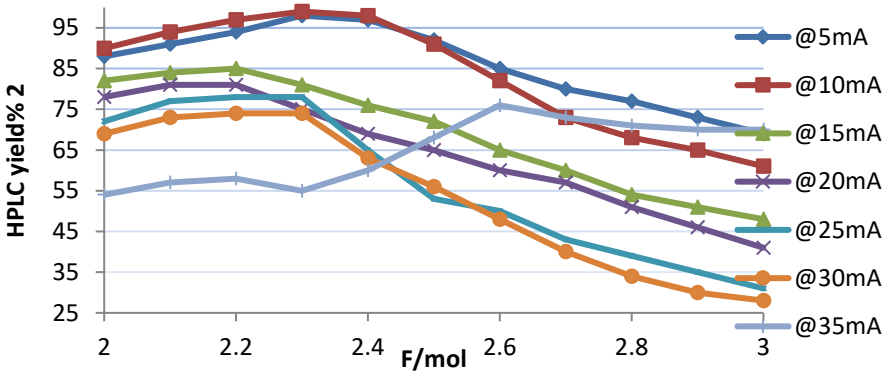

Figure S 53: Trend of the HPLC yields against F/mol applied for each current.

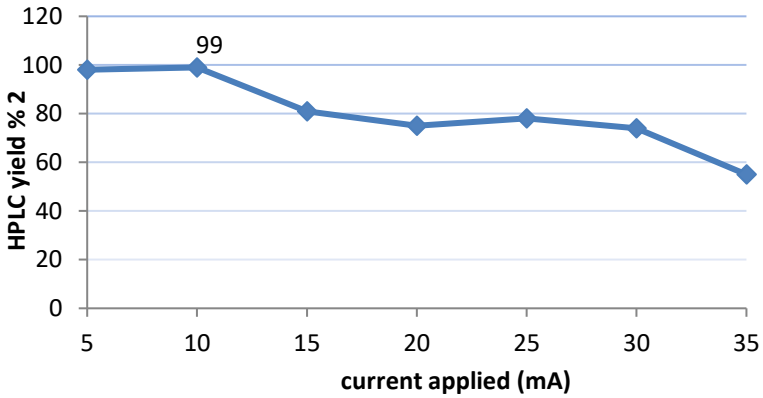

Figure S 54: Trend of the yields against currents applied at 2.3 F/mol

3.6.2 Flow recirculation electrolysis of 2-10 (b or e or g)

General procedure 4 for flow recirculation electrolysis of **2-10 (b or e or g):**

A 20 ml vial equipped with a magnetic stir bar was charged with 0.4 mmol of carboxylic acid, 1 mmol of $TBAPF_6$, 10 ml of DCM, 0.8 mmol of 2,4,6-collidine and 0.7 mL of HFIP. For this purpose, a peristaltic pump was utilized (5 mL/min flow rate). The reactor was operated under

constant current mode using a PeakTech 6225 A power supply at 10 mA until 2.3 F/mol were passed to the reagent solution. Then, the reactor inlet was removed from the reaction mixture reservoir allowing air to enter the channel and flush all the remaining reaction mixture to the vessel. After 2.3 F/mol were passed, the solvent was removed under vacuum and the residue was filtered over a silica pad eluted with n-pentane to afford the product.

Flow recirculation electrolysis of **3b**:

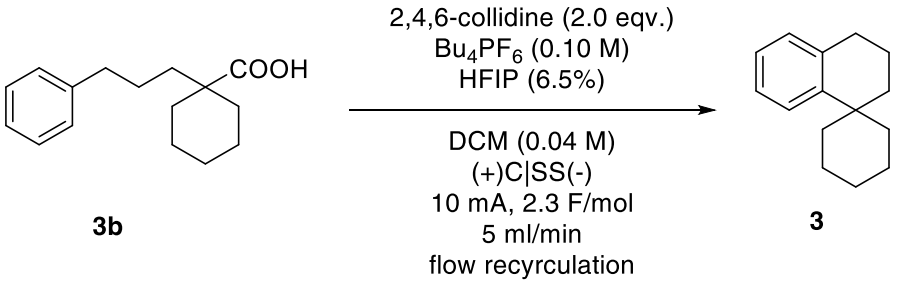

Figure S 55: Flow recirculation electrolysis of 1-(3-phenylpropyl)cyclohexane-1-carboxylic acid in optimized flow conditions

The product **3** has been synthesized and purified according to **General procedure 4**. Y% = 61%

Flow recirculation electrolysis of **4b**:

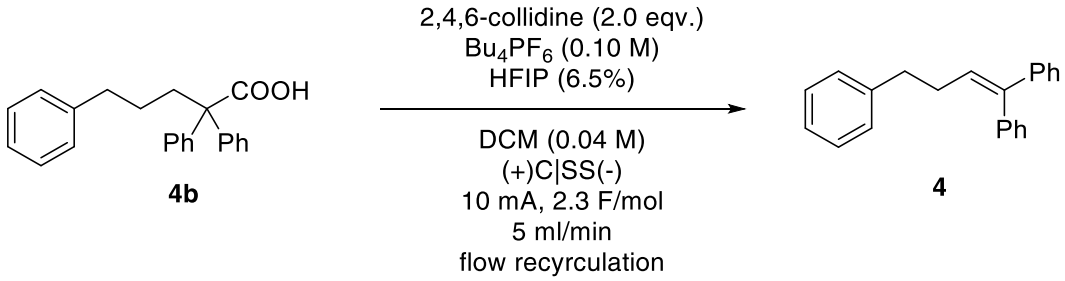

Figure S 56: Flow recirculation electrolysis of 2,2,5-triphenylpentanoic acid in optimized flow conditions.

The product **4** has been synthesized and purified according to **General procedure 4**. Y% = 87%.

Flow recirculation electrolysis of **5e**:

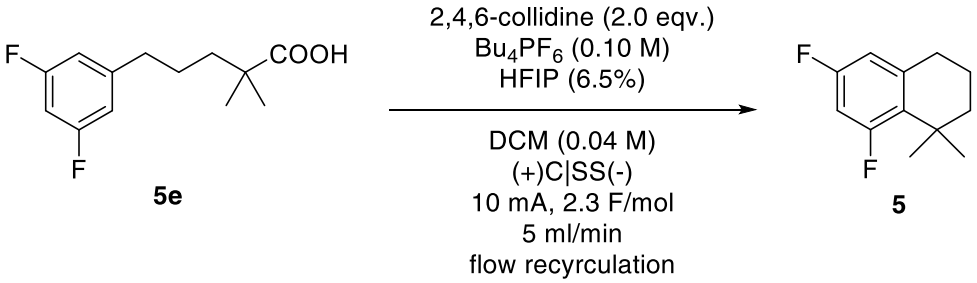

Figure S 57: Flow recirculation electrolysis of 5-(3,5-difluorophenyl)-2,2-dimethylpentanoic acid in optimized flow conditions.

The product **5** has been synthesized and purified according to **General procedure 4**. Y% = 80%

Flow recirculation electrolysis of **6e**:

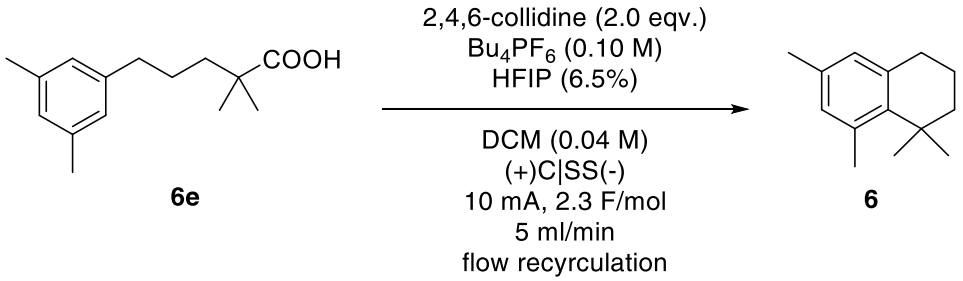

Figure S 58: Flow recirculation electrolysis of 5-(3,5-dimethylphenyl)-2,2-dimethylpentanoic acid in optimized flow conditions.

The product **6** has been synthesized and purified according to **General procedure 4**. Y% = 94%.

Flow recirculation electrolysis of **7e**:

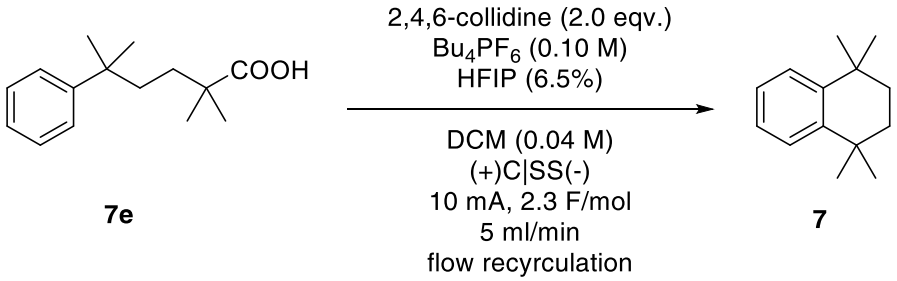

Figure S 59: Flow recirculation electrolysis of 2,2,5-trimethyl-5-phenylhexanoic acid in optimized flow conditions.

The product **7** has been synthesized and purified according to **General procedure 4**. Y% = 98%.

Flow recirculation electrolysis of **8g**:

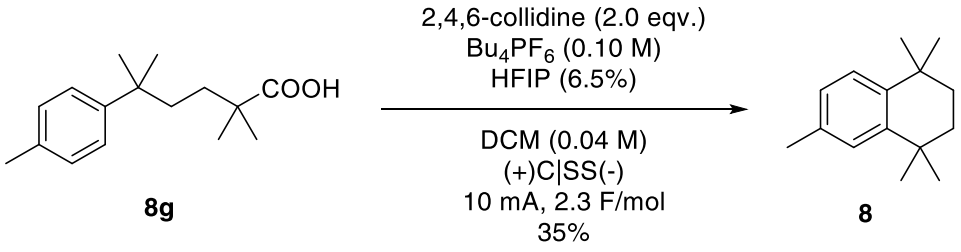

Figure S 60: Flow electrolysis of 2,2,5-trimethyl-5-(p-tolyl)hexanoic acid in optimized flow conditions.

The product **8** has been synthesized and purified according to **General procedure 4**. Y% = 75%.

Flow recirculation electrolysis of **9e**:

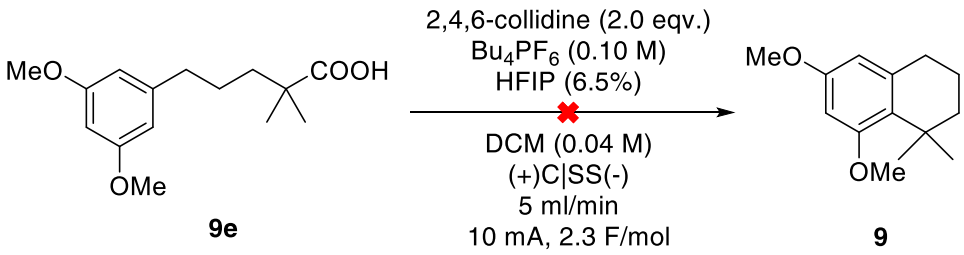

Figure S 61: Flow recirculation electrolysis of 5-(3,5-dimethoxyphenyl)-2,2-dimethylpentanoic acid

The product **P7** has been synthesized and purified according to **General procedure 4**. Product **9** has not been detected.

Flow recirculation electrolysis of **10e**:

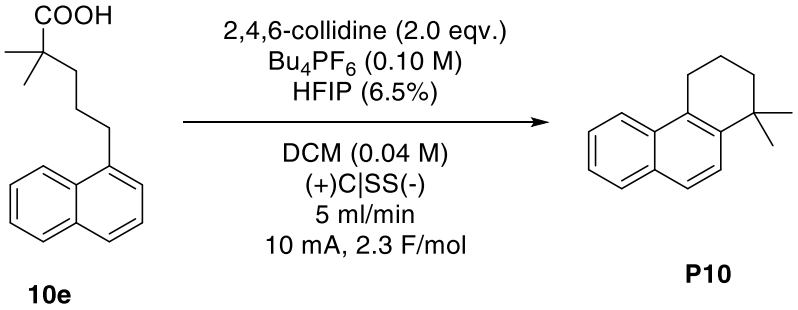

Figure S 62: Flow recirculation electrolysis of 1,1-dimethyl-1,2,3,4-tetrahydrophenanthrene

The product **10** has been synthesized and purified according to **General procedure 4**. Y% = 98%

3.6.3 Flow single pass optimization on 2b

General procedure 6 *for flow single-pass optimization electrolysis of* **2b**

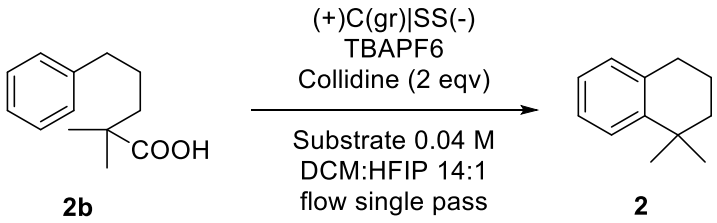

A 250 ml sealed bottle equipped with a magnetic stir bar was charged with 4 mmol of **2b**, 10 mmol of $TBAPF_6$, 100 ml of DCM, 8 mmol of 2,4,6-collidine and 7 mL of HFIP. For this purpose, a peristaltic pump

was utilized. The reactor was operated under constant current mode using a PeakTech 6225 A power supply. The formed solution was pumped through a flow electrolysis cell equipped with a graphite anode and a stainless steel cathode and an interelectrode gap separator of 0.9

mm thickness containing a channel (6.4 cm^2 surface, 570 μL volume). The output tube from the electrochemical cell has been connected into HPLC vials. Parameters like current and flow rate has been changed to optimize the process. 100 uL for each run has been collected to monitor the yield via HPLC.

F/mol	mL/min	Current (mA)	Yield (%)	F/mol	mL/min	Current (mA)	Yield (%)
2.3	0.0541	5	97.29	2.3	0.1622	15	82.42
2.4	0.0518	5	90.15	2.4	0.1555	15	80.86
2.5	0.0497	5	85.78	2.5	0.1492	15	78.68
2.6	0.0478	5	86.60	2.6	0.1435	15	69.64
2.7	0.0461	5	80.12	2.7	0.1382	15	66.07
2.8	0.0444	5	73.29	2.8	0.1333	15	62.65
2.9	0.0429	5	72.80	2.9	0.1287	15	60.45
2.3	0.1081	10	99.57	2.3	0.2163	20	56.45
2.4	0.1036	10	88.00	2.4	0.2073	20	54.15
2.5	0.0995	10	86.02	2.5	0.1990	20	51.31
2.6	0.0957	10	86.06	2.6	0.1913	20	46.82
2.7	0.0921	10	79.65	2.7	0.1843	20	45.91
2.8	0.0888	10	74.60	2.8	0.1777	20	42.35
2.9	0.0858	10	71.56	2.9	0.1715	20	40.32

HPLC has been calibrated using anisole as an internal standard.

F/mol	mL/min	Current (mA)	Yield (%)	F/mol	mL/min	Current (mA)	Yield (%)
2.3	0.2704	25	51.49	2.3	0.3785	35	21.72
2.4	0.2591	25	39.61	2.4	0.3627	35	19.07
2.5	0.2487	25	38.76	2.5	0.3482	35	18.03
2.6	0.2392	25	38.43	2.6	0.3348	35	14.24
2.7	0.2303	25	37.29	2.7	0.3224	35	12.69
2.8	0.2221	25	36.52	2.8	0.3109	35	11.38
2.9	0.2144	25	35.80	2.9	0.3002	35	10.03
2.3	0.3244	30	40.86	2.3	0.4326	40	15.47
2.4	0.3109	30	39.38	2.4	0.4146	40	14.29
2.5	0.2985	30	39.67	2.5	0.3980	40	12.73
2.6	0.2870	30	37.11	2.6	0.3827	40	9.97
2.7	0.2764	30	36.03	2.7	0.3685	40	8.25
2.8	0.2665	30	30.54	2.8	0.3553	40	7.51
2.9	0.2573	30	29.73	2.9	0.3431	40	6.69

Table S 12: Detailed optimization data for the single-pass continuous flow electrolysis of 2b.

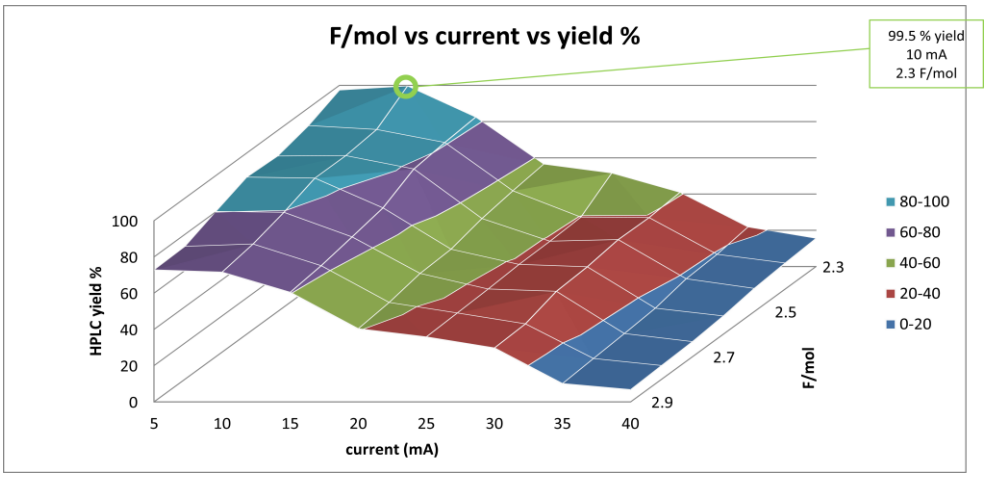

Figure S 63: Trend of HPLC yields against current applied and F/mol.

3.6.4 Flow single pass long run electrolysis of 2b

A 24 hours long run has been performed for yield stability monitoring.

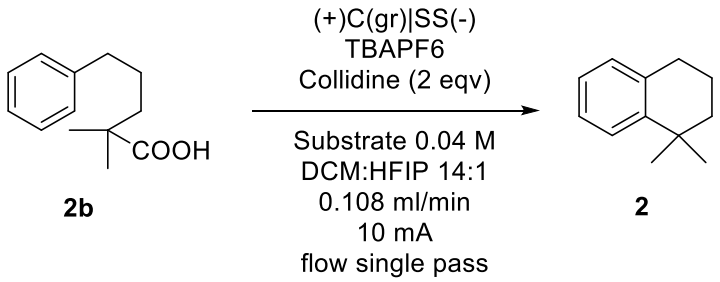

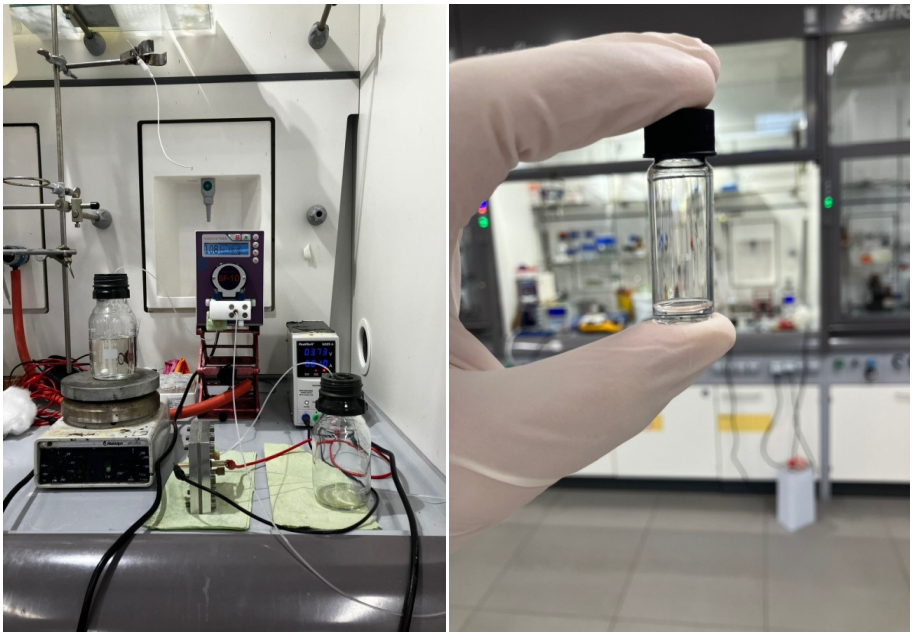

Figure S 64: Picture of the experimental setup of single pass long run (left).

Figure S 65: product obtained from the long run experiment (right).

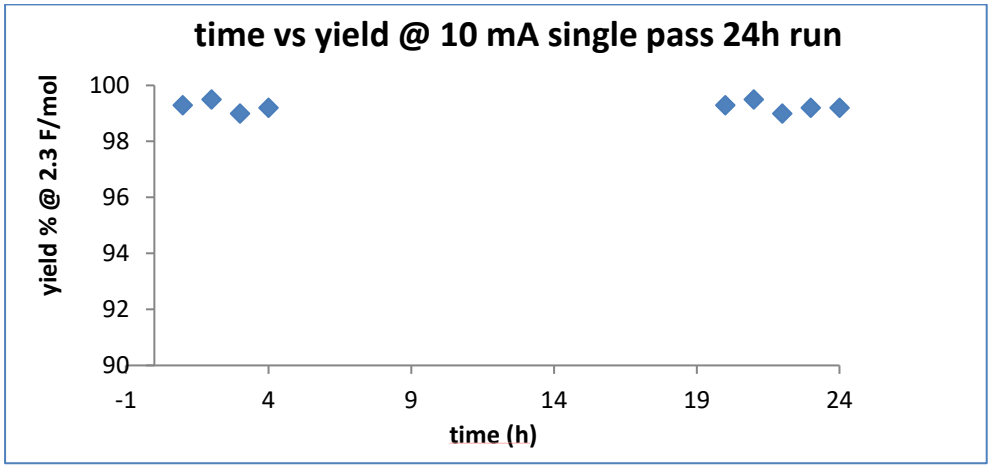

Figure S 66: Trend of the HPLC yields during the long run.

3.7 Mechanistic studies

Procedure for radical trapping with TEMPO

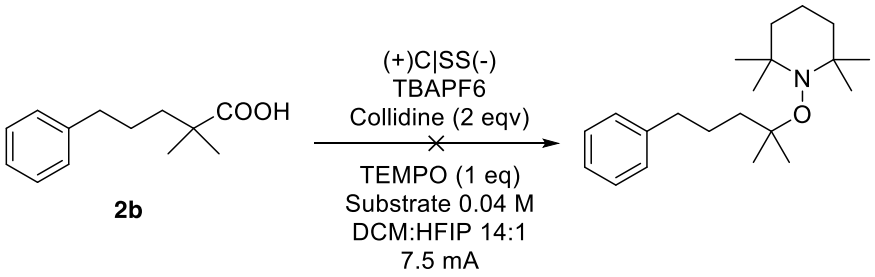

The reaction was performed according to General procedure **2**, adding 1 eq of TEMPO at the reaction. The reaction mixture was then checked via GC-MS and LC-MS and the adduct with TEMPO was not found. The cyclized product **2** has been detected instead.

Procedure for ion trapping with MeOH

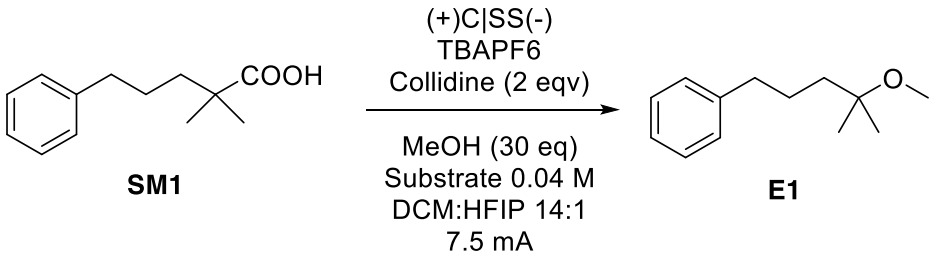

The reaction was performed according to **General procedure 2**, adding 30 eq. of MeOH at the reaction. The reaction mixture was then checked via GC-MS and product **E1** was found as reported in the chromatogram and mass spectra (**Figure S 67-68**).

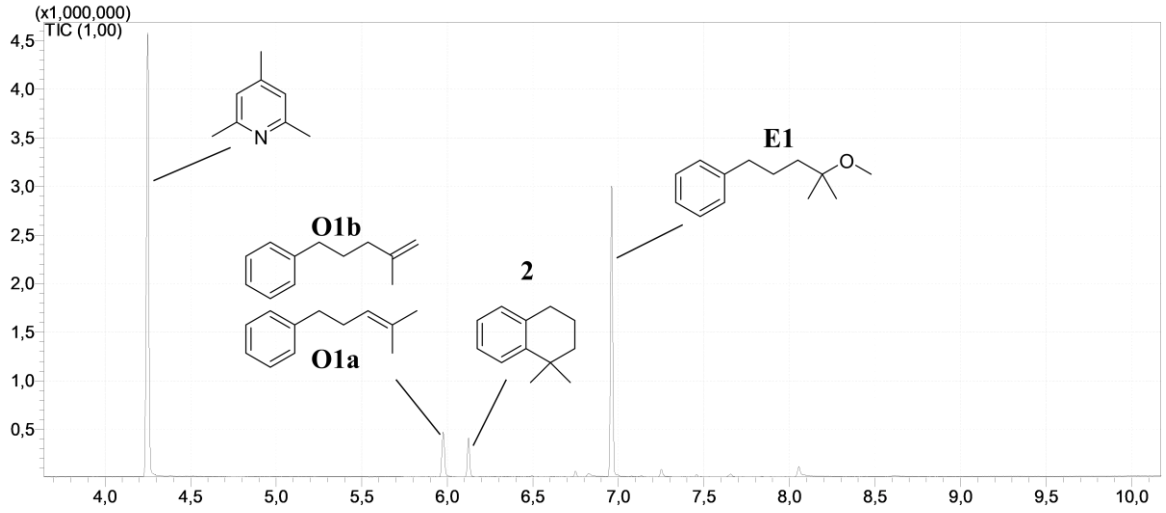

Figure S 67: Gas chromatogram of the ion trapping experiment.

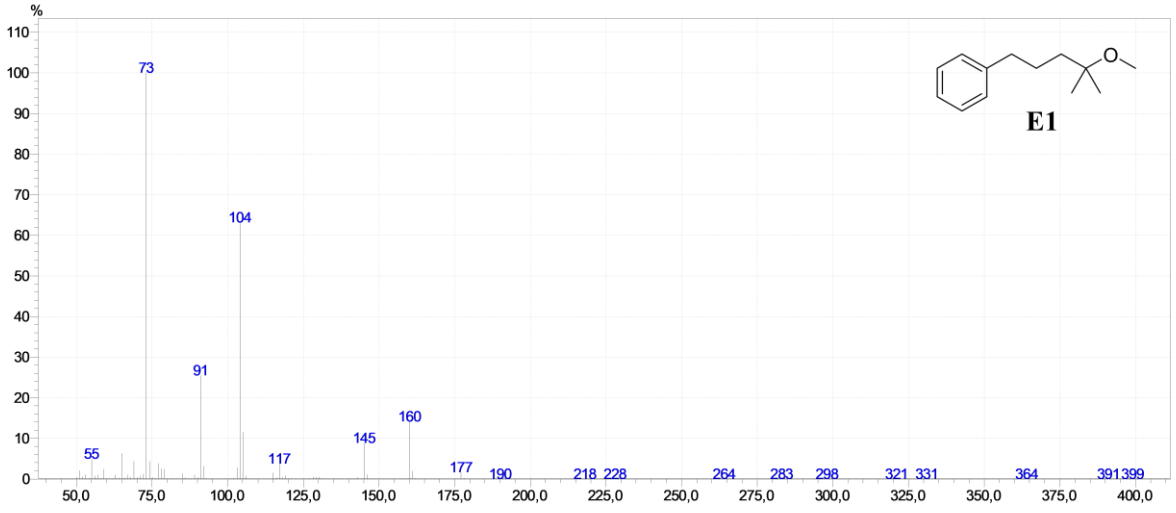

Figure S 68: EI mass spectra of the ether E1 product.

3.8 Computational details

The structure for **A** was prepared and subjected to conformational sampling by using the opensource *CREST* tool associated with the *x*TB software, by specifying the solvents involved in the reaction as well as possible charges already present in the starting materials.[60] This software employs the semiempirical extended tight binding approach known as *x*TB (GFN2-*x*TB) for its theoretical framework, which strikes a balance in sampling a wide range of chemical space. However, its accuracy in calculating thermochemical properties is limited, which necessitates conducting supplementary higher-level calculations.[60] Indeed, with the so obtained conformer structures, we operated a selection by excluding duplicates looking directly at RMSD of the coordinates of the atoms in a spatial region of diameter 1.0Å.

The selected geometries where then subjected to low level of theory calculations using Gaussian 16 software tool and a very simplified level of theory, consisting of B3LYP functional and 6-31g(d,p) as basis set for all the atoms.[59] During these initial calculations the role of dichloromethane solvent was included using the SMD solvation model.[63] The resulting list of optimized conformations of **A** in solvent was then sorted in terms of energies and the most stable one was selected as most preferred conformation.

All structures involved in the next step for the mechanism investigation were optimized using the Gaussian 16 program package.[59] Soon we encountered problems in simulating the elimination step and we decided to use it as a benchmark to identify the best level of theory capable to describe the transition state that links the **A** to the elimination product. In the Table S13 below are reported the level of theory tested and the corresponding descriptive results.

Entry	Functional	Basis set	Result description
1	B3LYP	6-31G(d,p)	Optimizing **A** it spontaneously produces the eliminated product without defining a TS
2	B3LYP	6-31+G(d,p)	Optimizing **A** produces a structure with elimination TS fashion, but the TS optimization failed producing directly the final eliminated product
3	B3LYP-GD3BJ	6-31+G(d,p)	Addition of explicit dispersions during **A** optimization spontaneously produces the eliminated product without defining a TS
4	M06-2X	6-31+G(d,p)	Optimizing **A** produced a stable structure, which was then subjected to TS-search succeding in locating and optimizing it

Table S 13: Benchmark for the elimination reaction step and for the correct combination choice for functional and basis set to describe the reaction profile.

Given the reasonable existence of the elimination transition state, we used the combination of functional and basis set capable in simulating it and which constitutes the best compromise between computational cost and accuracy. We thus selected the M06-2X hybrid functional, which demonstrated to be ideal for thermochemistry and thermochemical kinetics studies, by taking in count also noncovalent interactions.[61] The basis set was set on 6-31+g(d,p) for all the atoms,[62] while the effect of the dichloromethane as a solvent was again simulated by SMD solvation model.[63] Frequency calculations to confirm the effective minimum or transition-state (TS) nature of the optimized system, was performed on each structure, as well as intrinsic reaction coordinate (IRC) calculations

were performed to confirm the continuity of the reaction profile from TSs toward reactants, intermediates, or products.[64]

The final reported energies were then thermally corrected to the free energy using a higher level of theory through single point calculations (SP). With the optimized structures we used the ωB97XD functional, which already includes a version of Grimme's D2 dispersion model,[60] and the valence triple-zeta polarization basis set def2-TZVP for all the atoms, during the SP calculation. Again, we maintained the same SMD model for the dichloromethane solvent.[63]

3.9 ^{1}H and ^{13}C NMR spectra

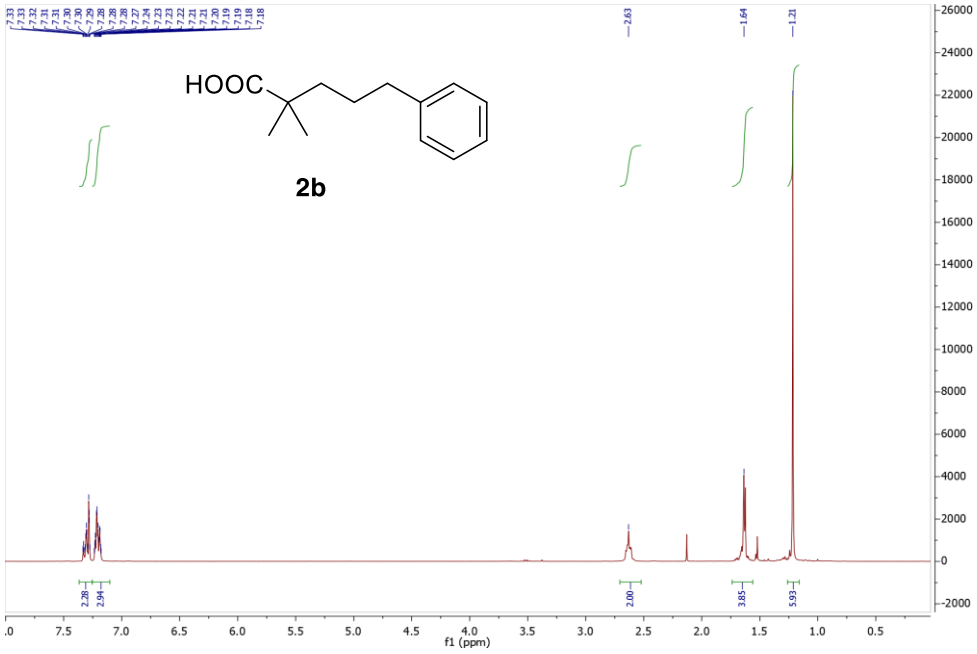

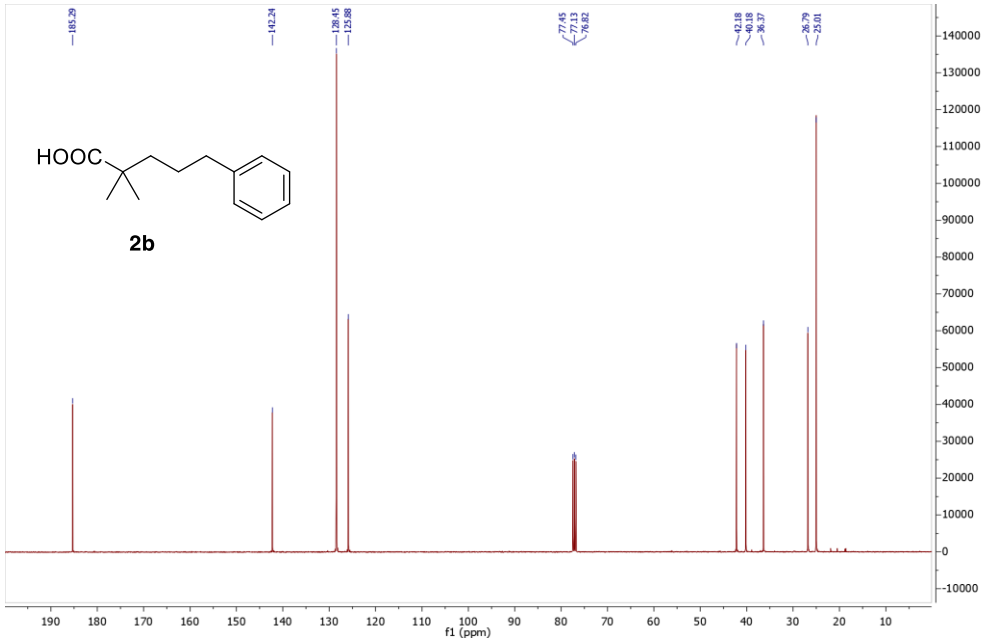
HOOC
2b
185.29
142.24
128.45
125.88
77.45
77.13
76.82
42.18
40.18
36.37
26.79
25.01
f1 (ppm)

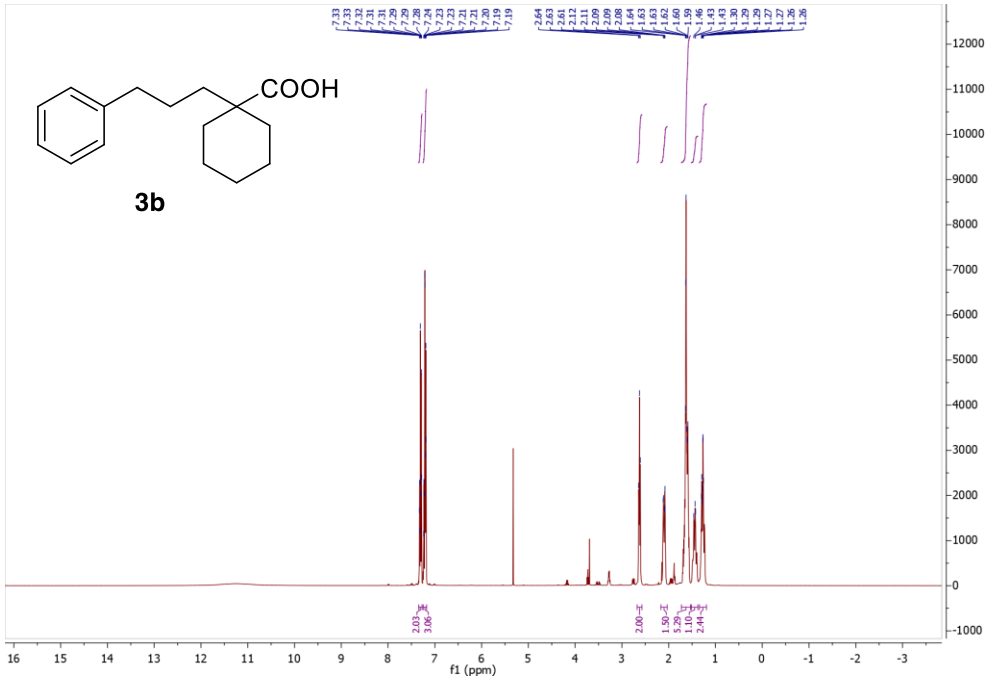
COOH
3b
f1 (ppm)

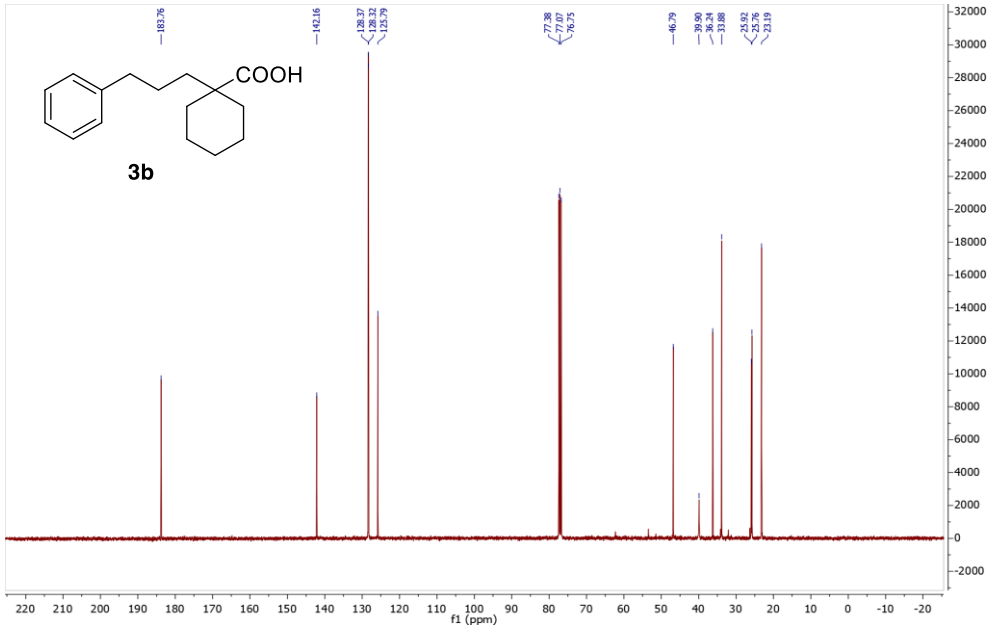
COOH
3b
f1 (ppm)

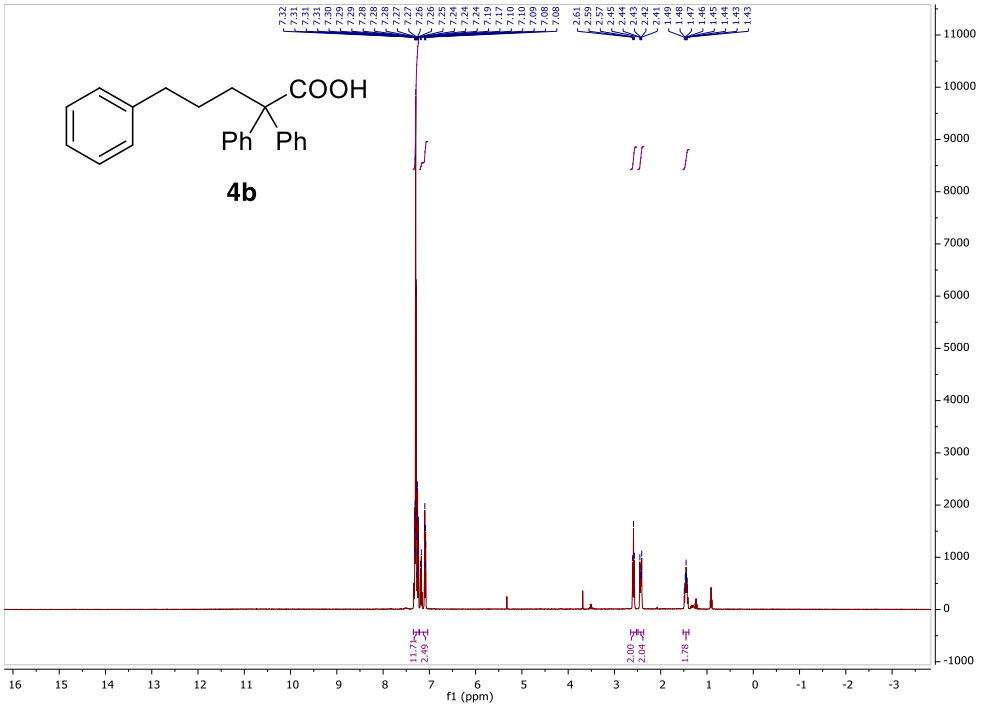
COOH
Ph Ph
4b
f1 (ppm)

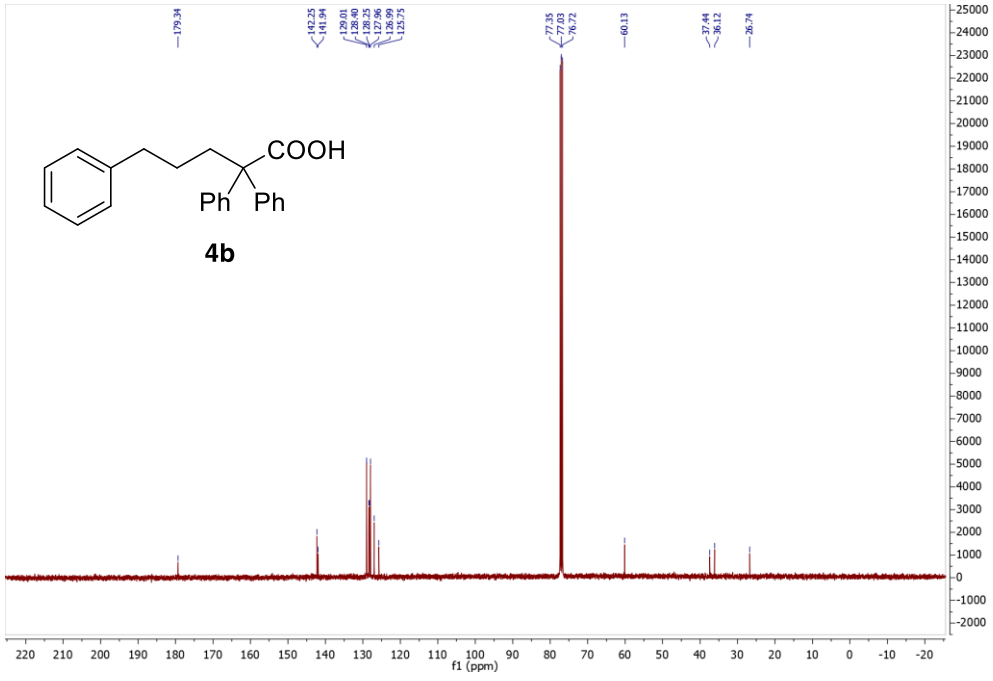
COOH
Ph
Ph
4b
f1 (ppm)

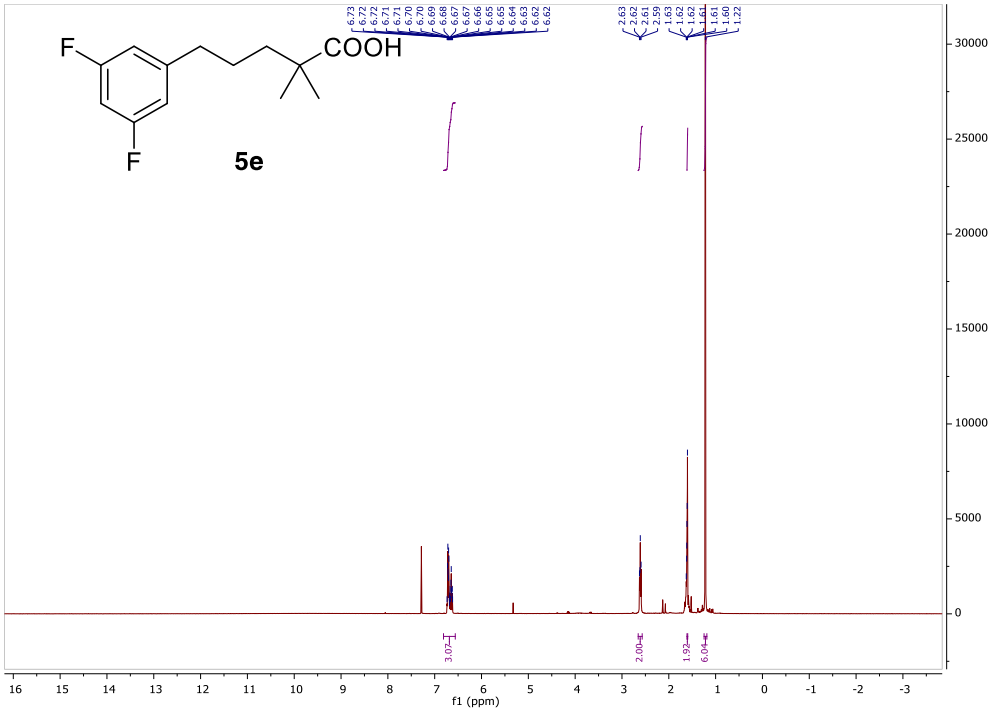
F
COOH
F
5e
f1 (ppm)

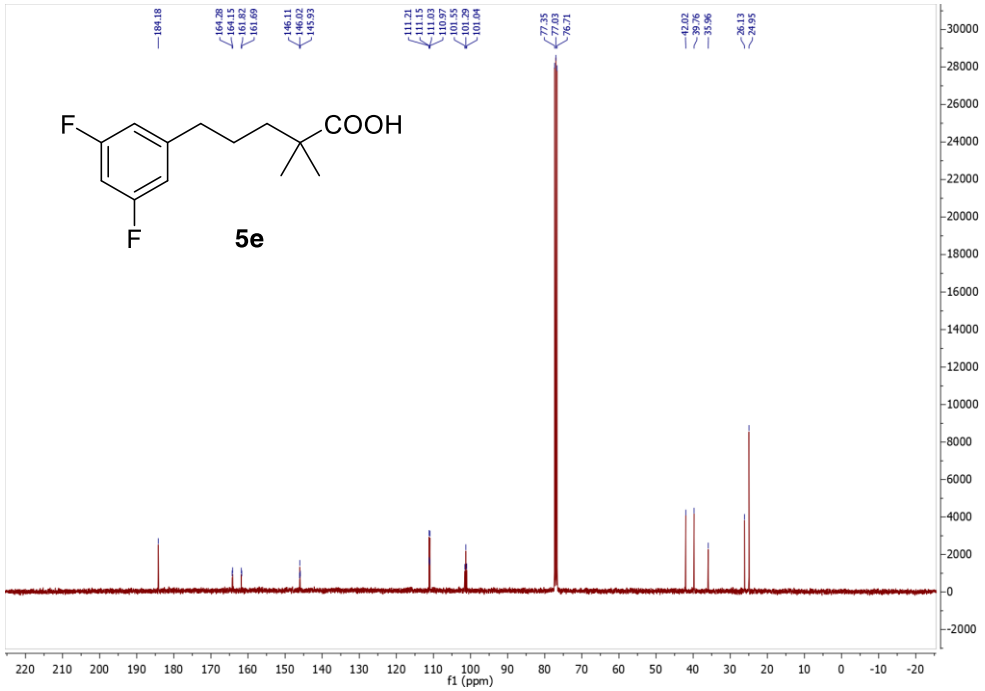
F
COOH
F
5e
f1 (ppm)

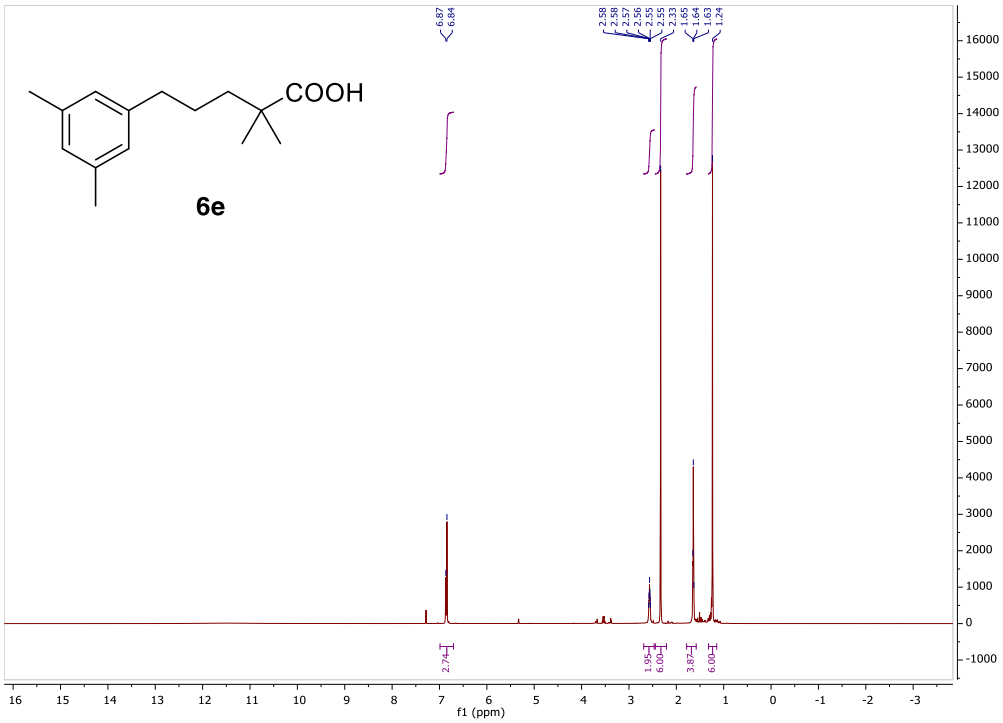
COOH
6e
f1 (ppm)

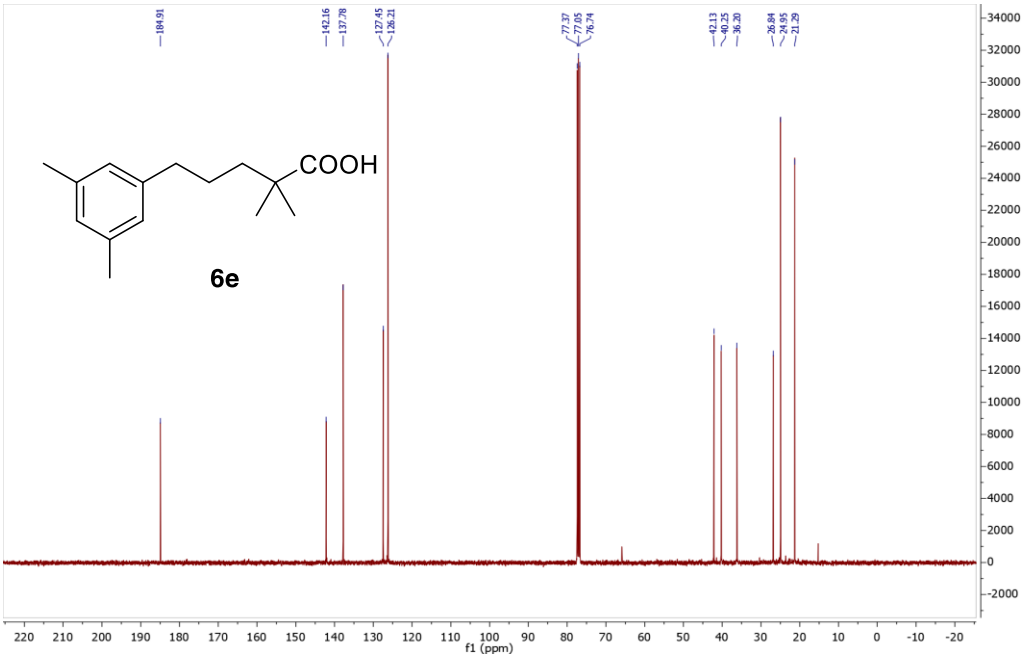
COOH
6e
184.91
142.16
137.78
127.45
126.21
77.37
77.05
76.74
42.13
40.25
30.20
26.84
24.95
21.29
f1 (ppm)

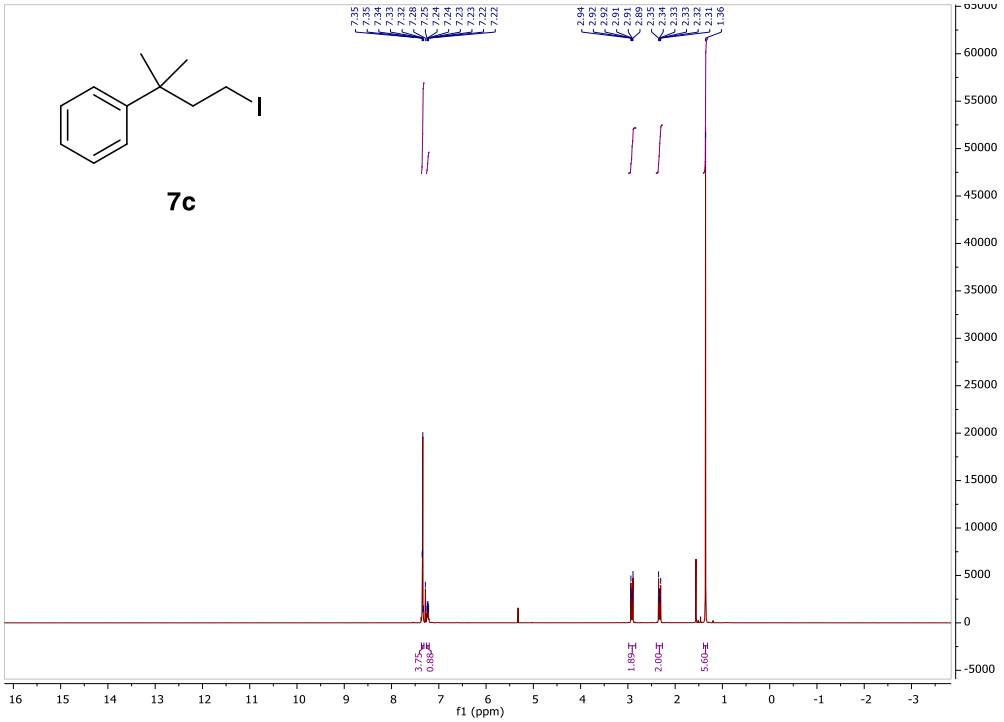
I
7c
7.35
7.34
7.33
7.32
7.28
7.25
7.24
7.24
7.23
7.23
7.22
7.22
2.94
2.92
2.92
2.91
2.91
2.89
2.35
2.34
2.33
2.33
2.32
2.31
1.36
3.75
0.88
1.89
2.00
5.60
f1 (ppm)

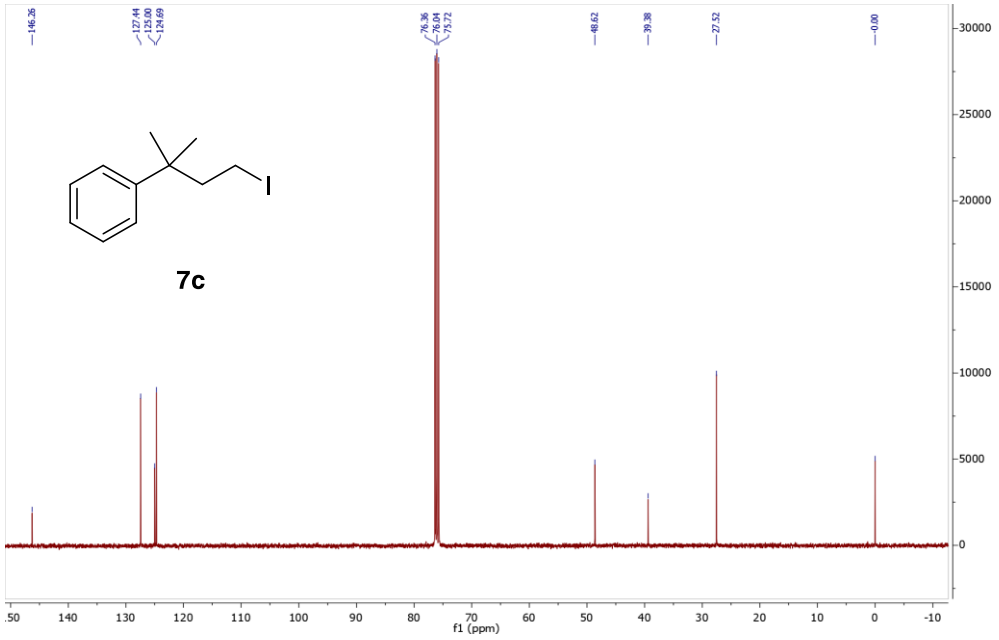
146.26
127.44
125.00
124.69
76.36
76.04
75.72
48.62
39.38
27.52
0.00
I
7c
f1 (ppm)

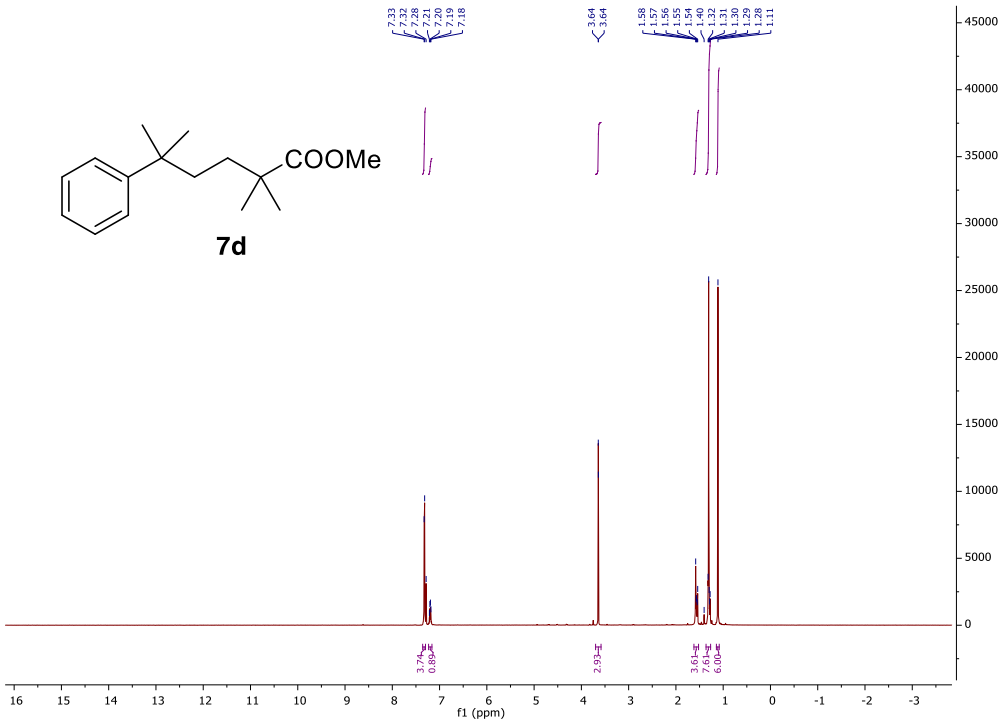
7.33
7.32
7.28
7.21
7.20
7.19
7.18
3.64
3.64
1.58
1.57
1.56
1.55
1.54
1.40
1.32
1.31
1.30
1.29
1.28
1.11
COOMe
7d
3.74
0.89
2.93
3.61
7.61
6.00
f1 (ppm)

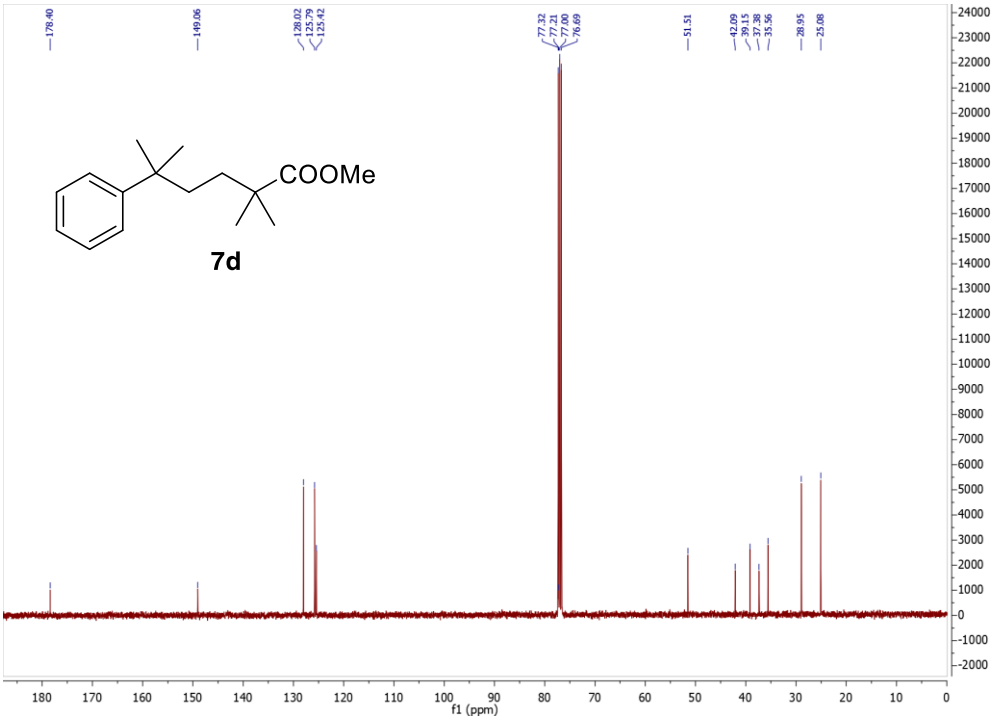
178.40
149.06
128.02
125.79
125.42
77.32
77.21
77.00
76.69
51.51
42.09
39.15
37.38
35.56
28.95
25.08
COOMe
7d
f1 (ppm)

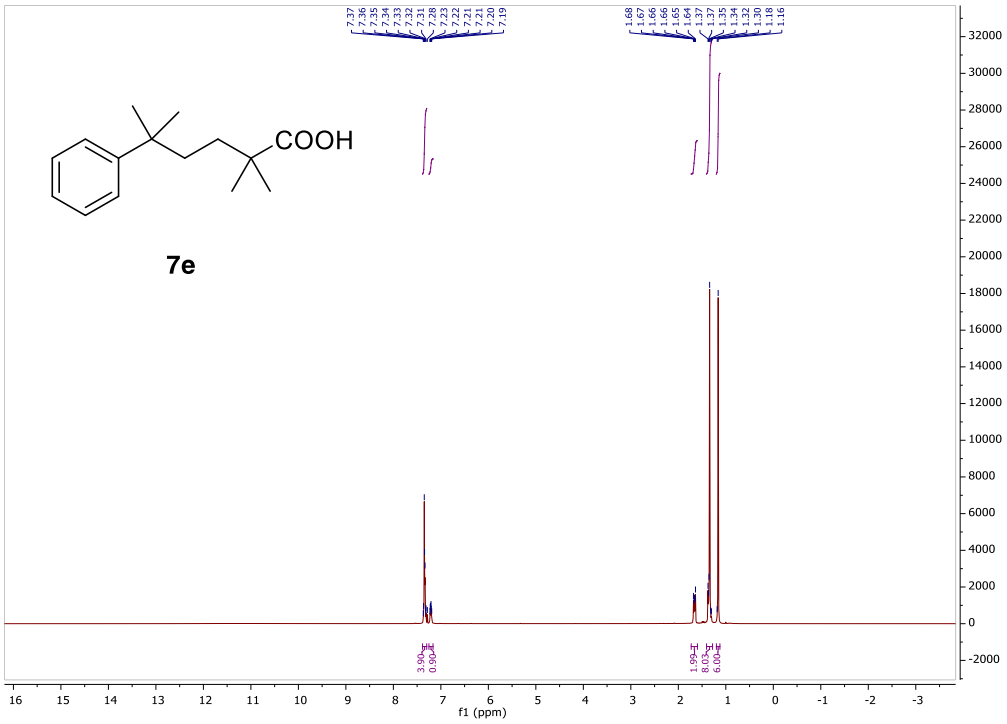
7.37
7.36
7.35
7.34
7.33
7.32
7.31
7.30
7.23
7.22
7.21
7.21
7.20
7.19
1.68
1.67
1.66
1.66
1.65
1.64
1.37
1.37
1.35
1.34
1.32
1.30
1.18
1.16
COOH
7e
3.90
0.96
1.99
8.03
6.00
f1 (ppm)

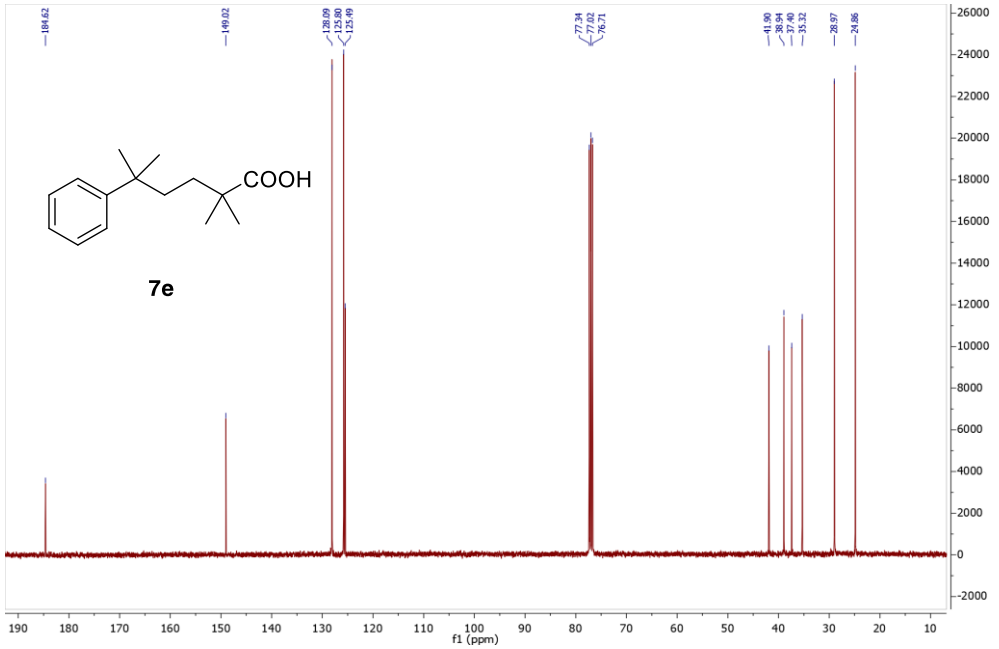
COOH
7e
f1 (ppm)

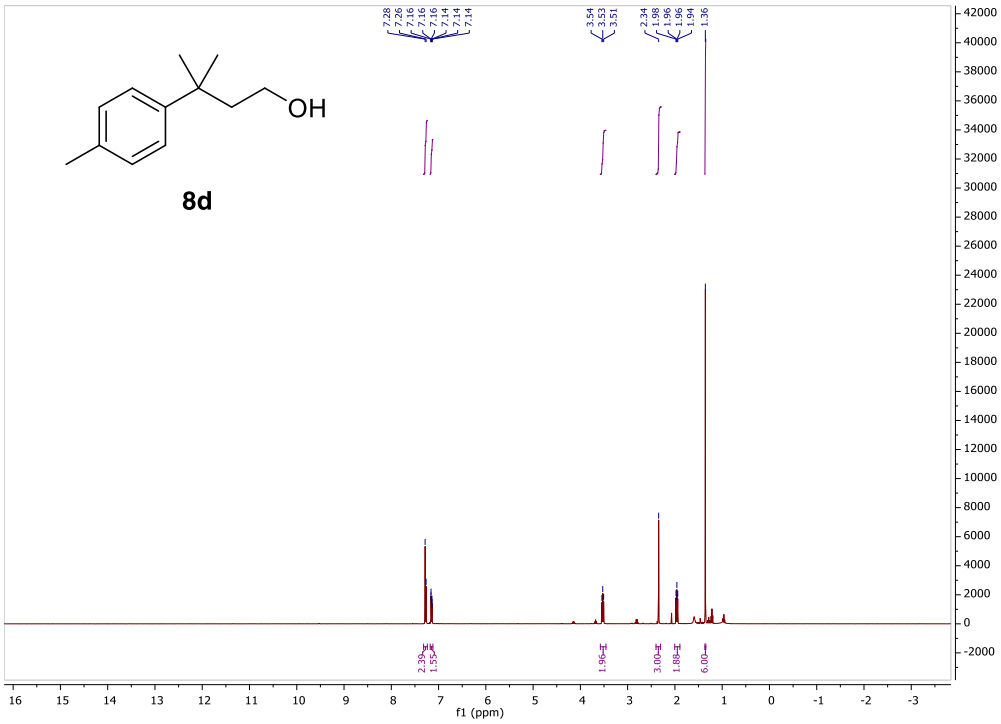
OH
8d
f1 (ppm)

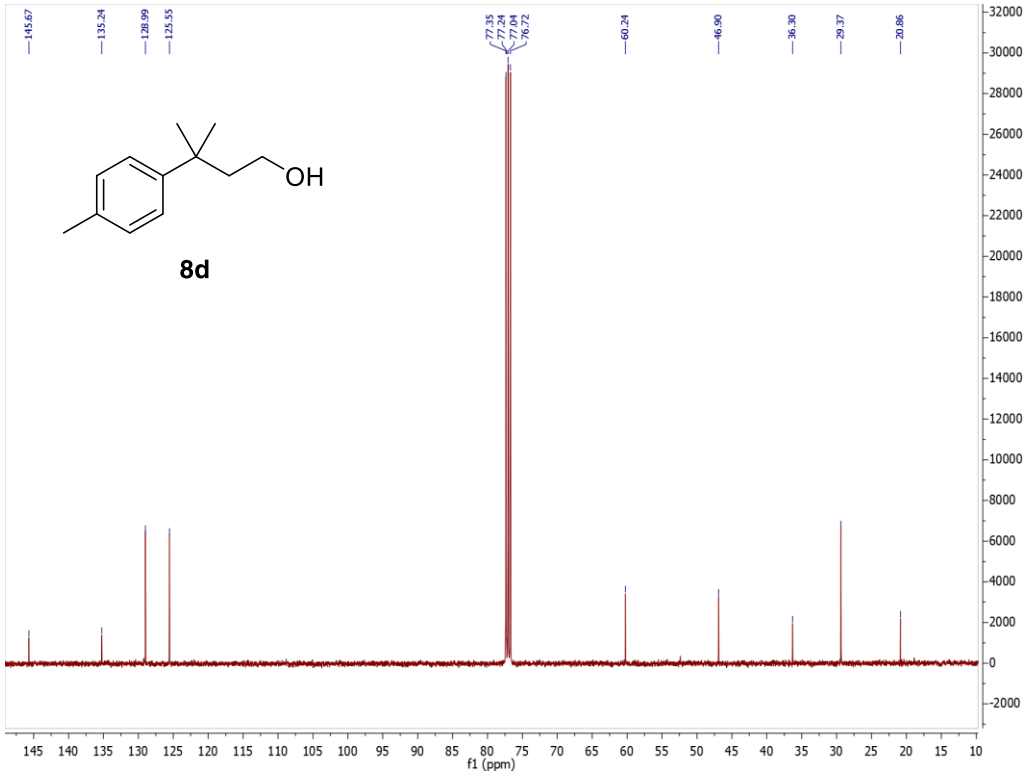
OH
8d
145.67
135.24
128.99
125.55
77.35
77.24
77.04
76.72
60.24
46.90
36.30
29.37
20.86
f1 (ppm)

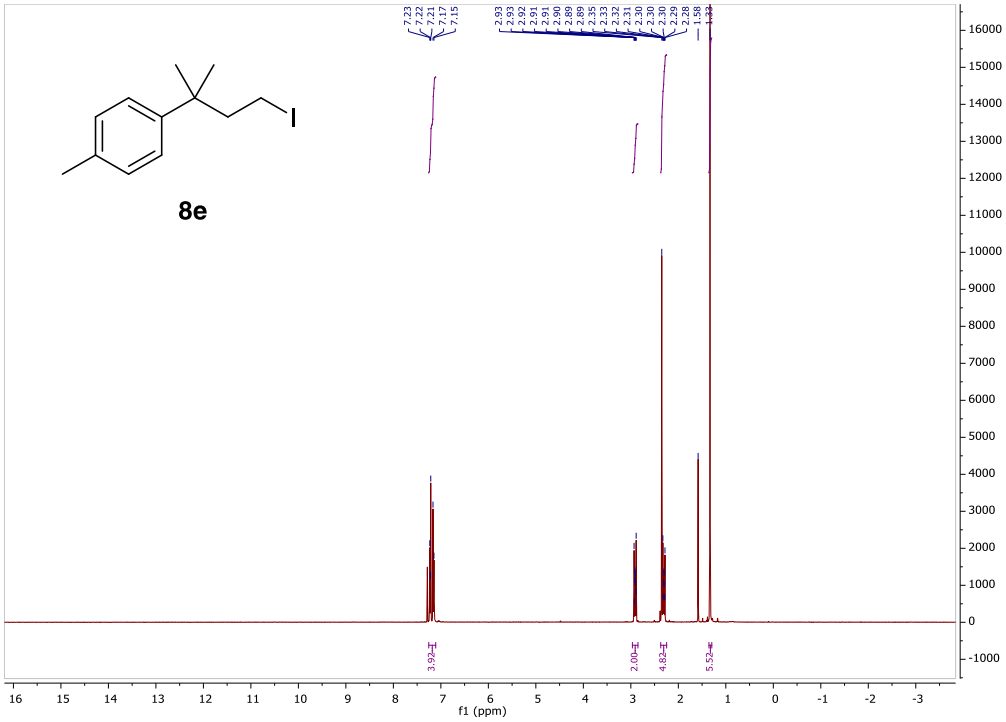
I
8e
7.23
7.22
7.21
7.17
7.15
2.93
2.92
2.91
2.90
2.89
2.35
2.33
2.32
2.31
2.30
2.29
2.28
1.58
3.92
2.00
4.82
5.52
f1 (ppm)

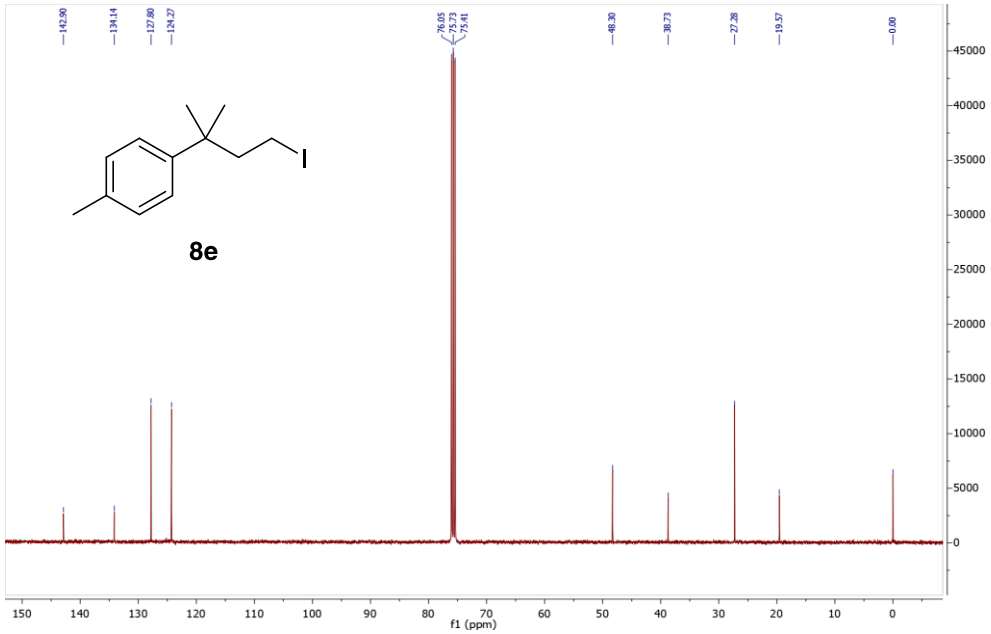
I
8e
f1 (ppm)

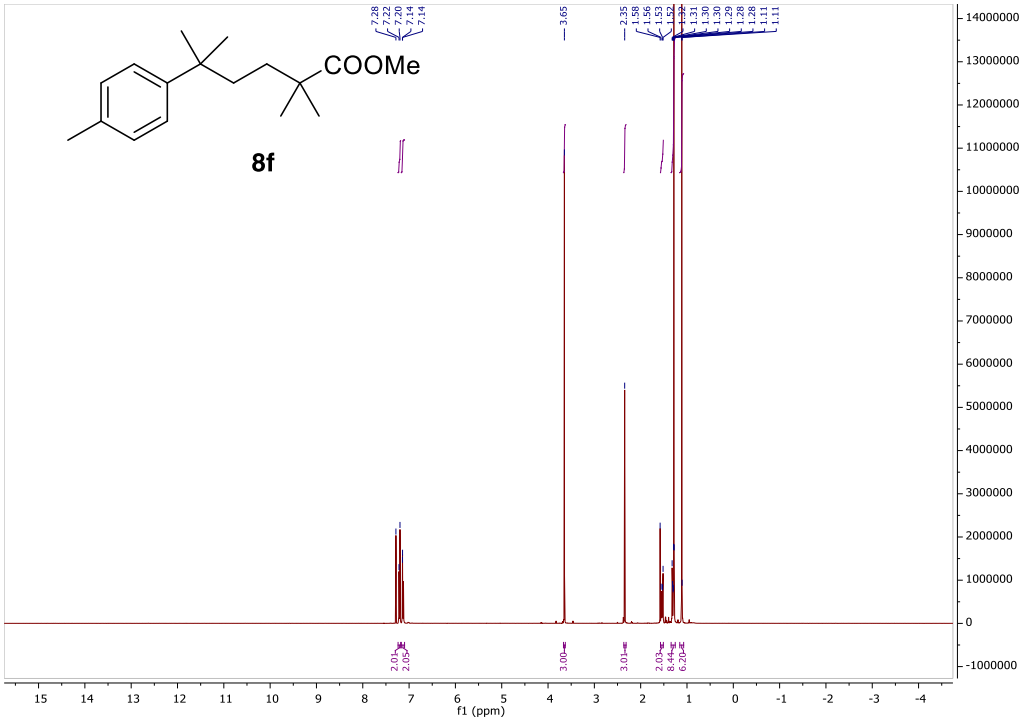
COOMe
8f
f1 (ppm)

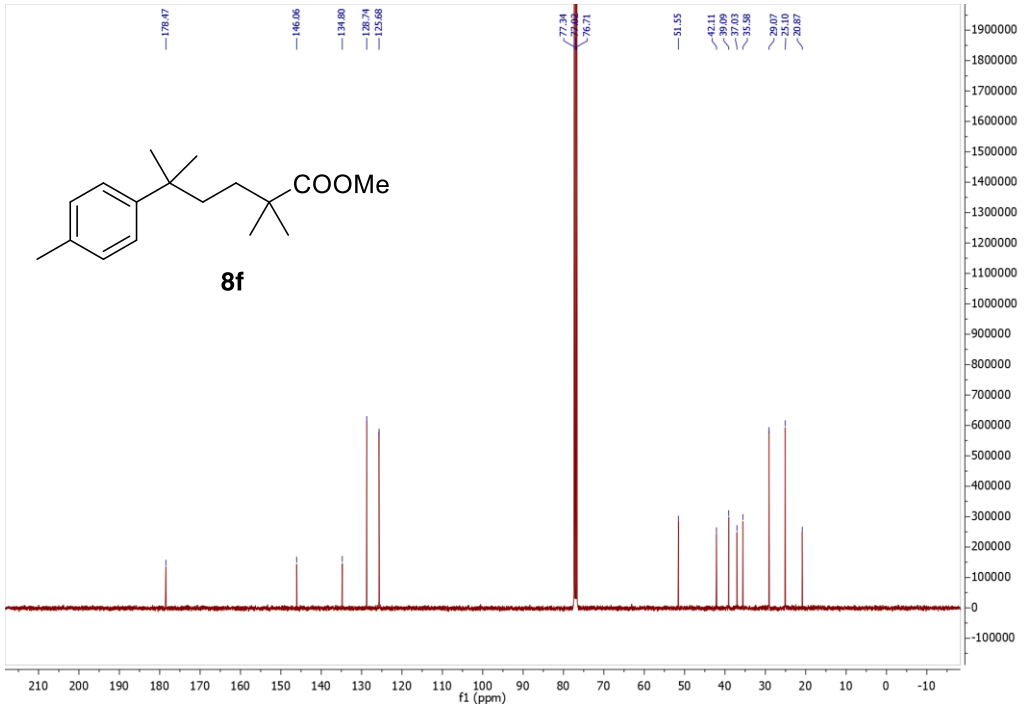
178.47
146.06
134.80
128.74
125.68
77.34
77.03
76.71
51.55
42.11
39.09
37.03
35.58
29.07
25.10
20.87
COOMe
f1 (ppm)

8f

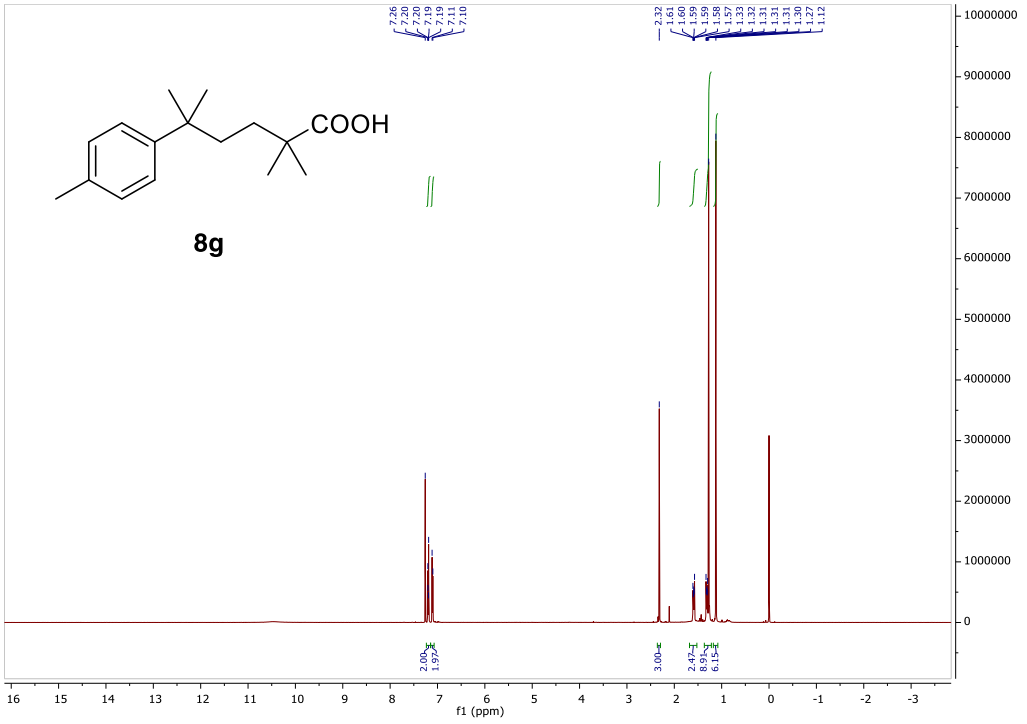
7.26
7.20
7.20
7.19
7.19
7.11
7.10
2.32
1.61
1.60
1.59
1.59
1.58
1.57
1.33
1.32
1.31
1.31
1.31
1.30
1.27
1.12
COOH
2.00
1.97
3.00
2.47
8.91
6.15
f1 (ppm)

8g

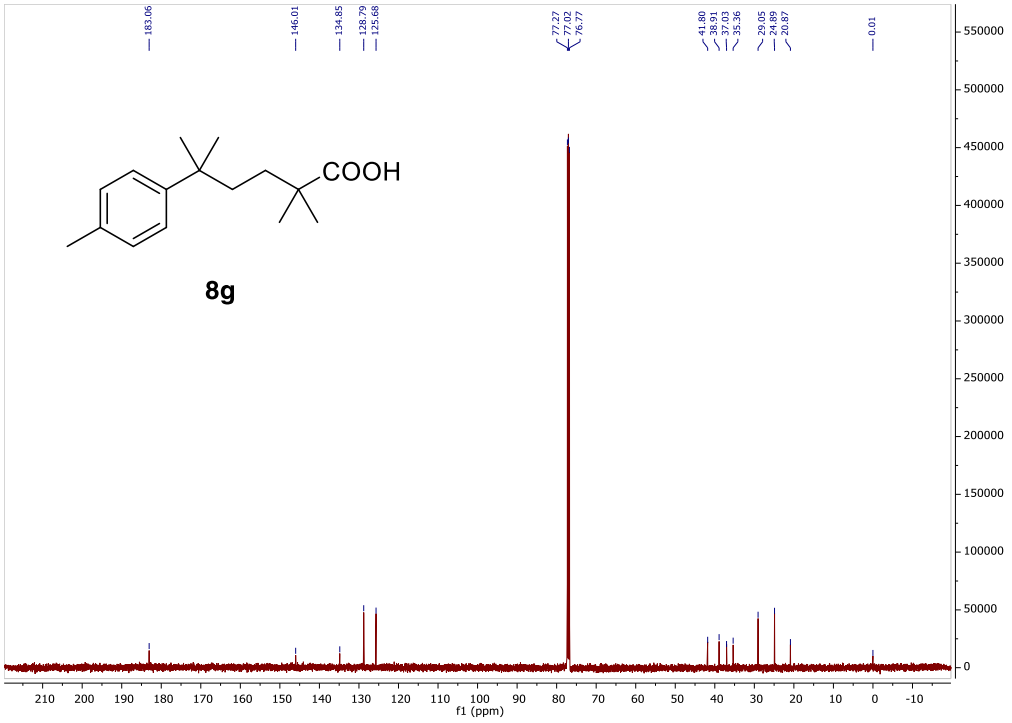
183.06
146.01
134.85
128.79
125.68
77.27
77.02
76.77
41.80
38.91
37.03
35.36
29.05
24.89
20.87
0.01
COOH
8g
f1 (ppm)

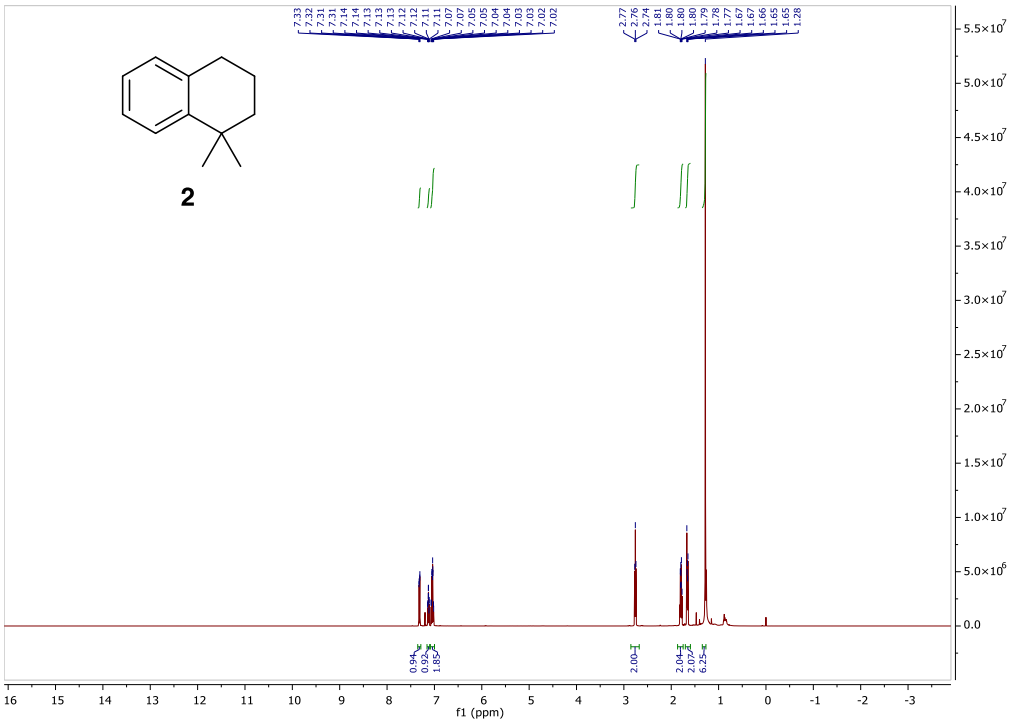
2
f1 (ppm)

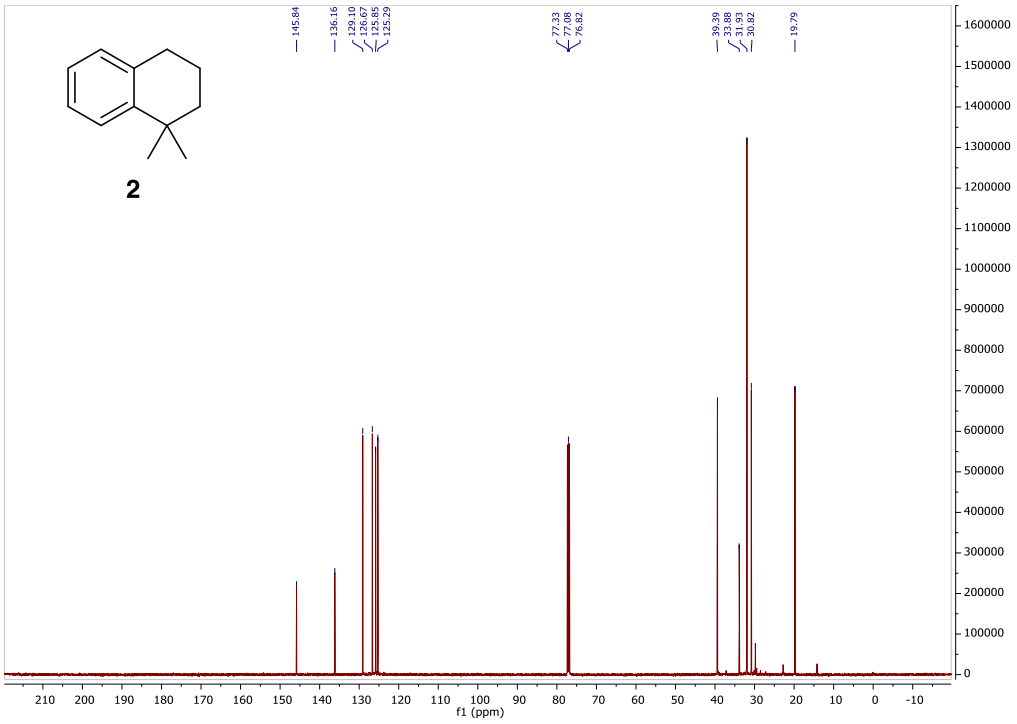
145.84
136.16
129.10
126.77
125.85
125.29
77.33
77.08
76.82
39.39
33.88
31.93
30.82
19.79
2
f1 (ppm)

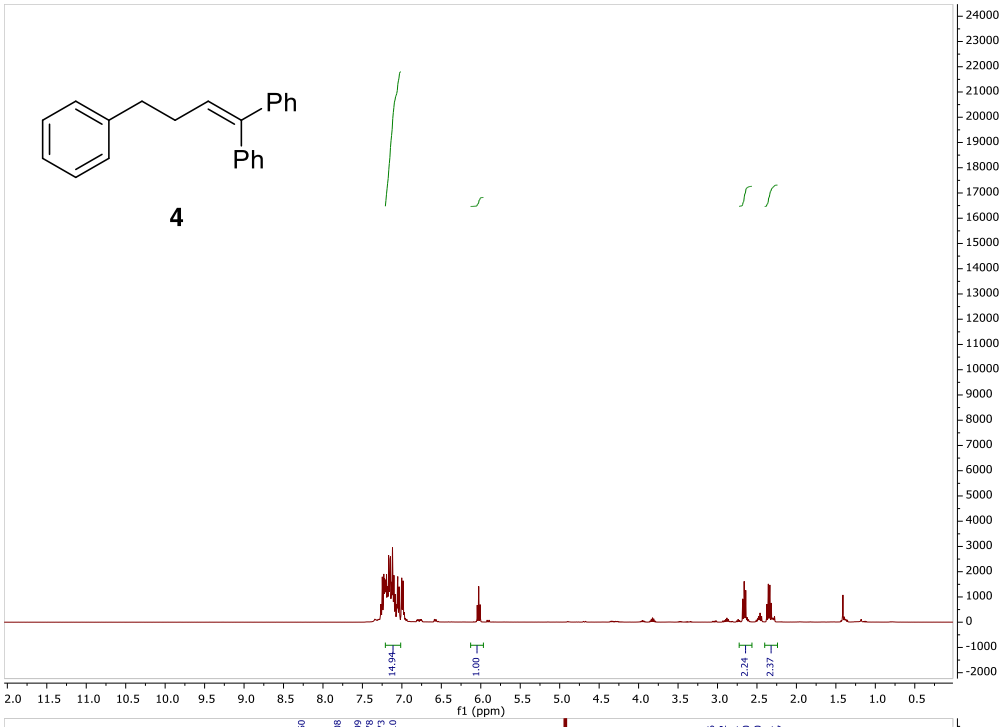
Ph
Ph
4
14.94
1.00
2.24
2.37
f1 (ppm)

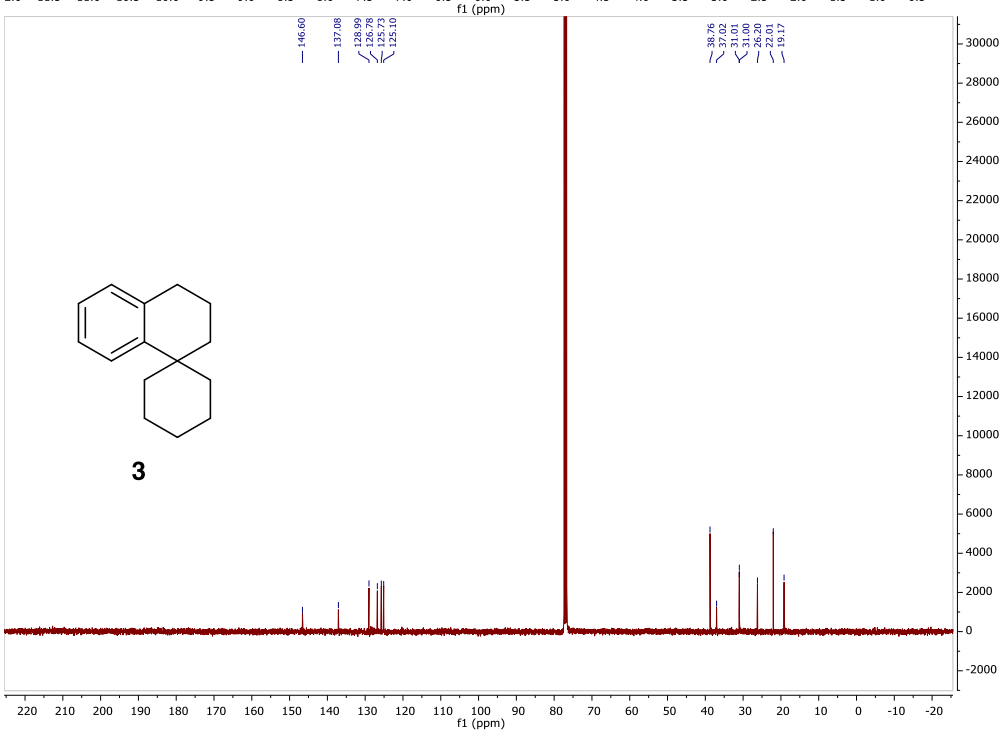
146.60
137.08
128.99
126.78
125.73
125.10
38.76
37.02
31.01
31.00
25.20
22.01
19.17
3
f1 (ppm)

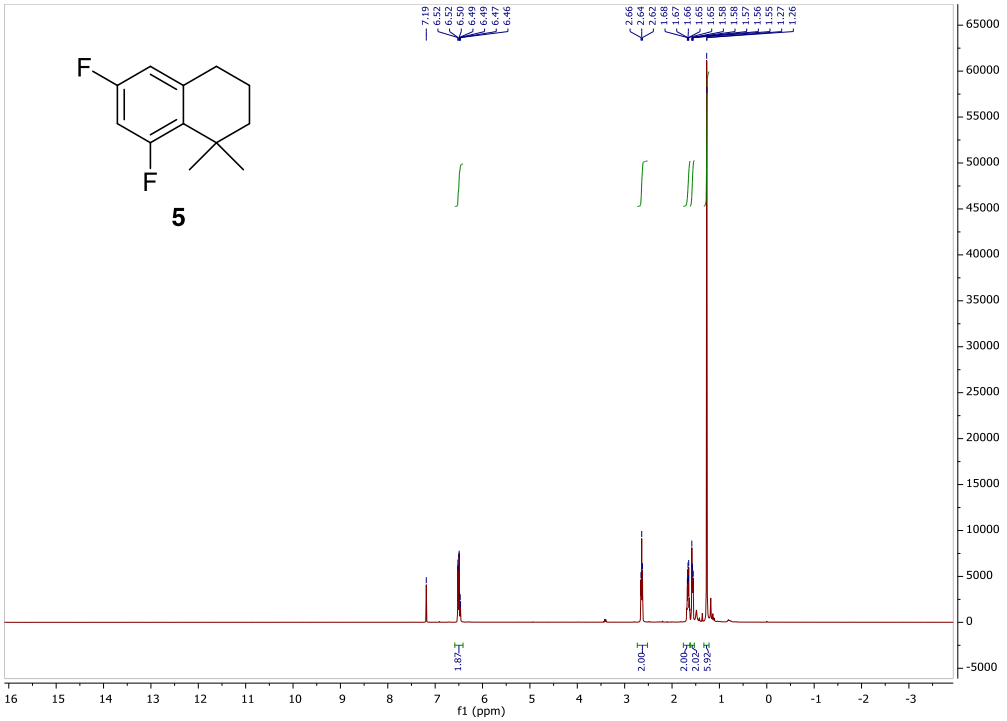
F
F
5
f1 (ppm)

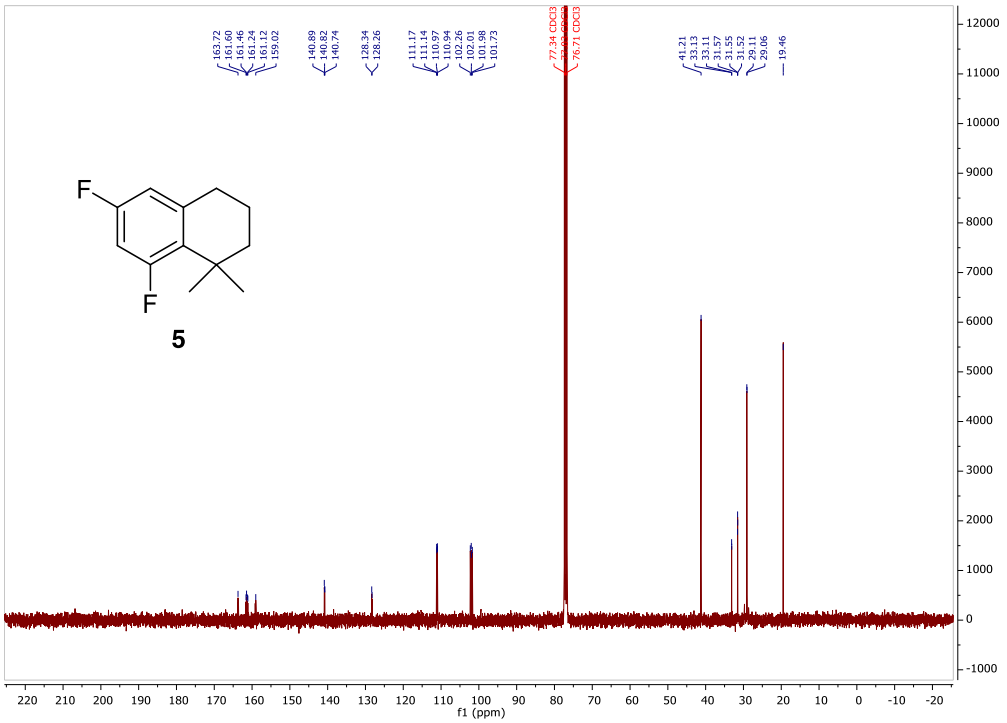
F
F
5
f1 (ppm)

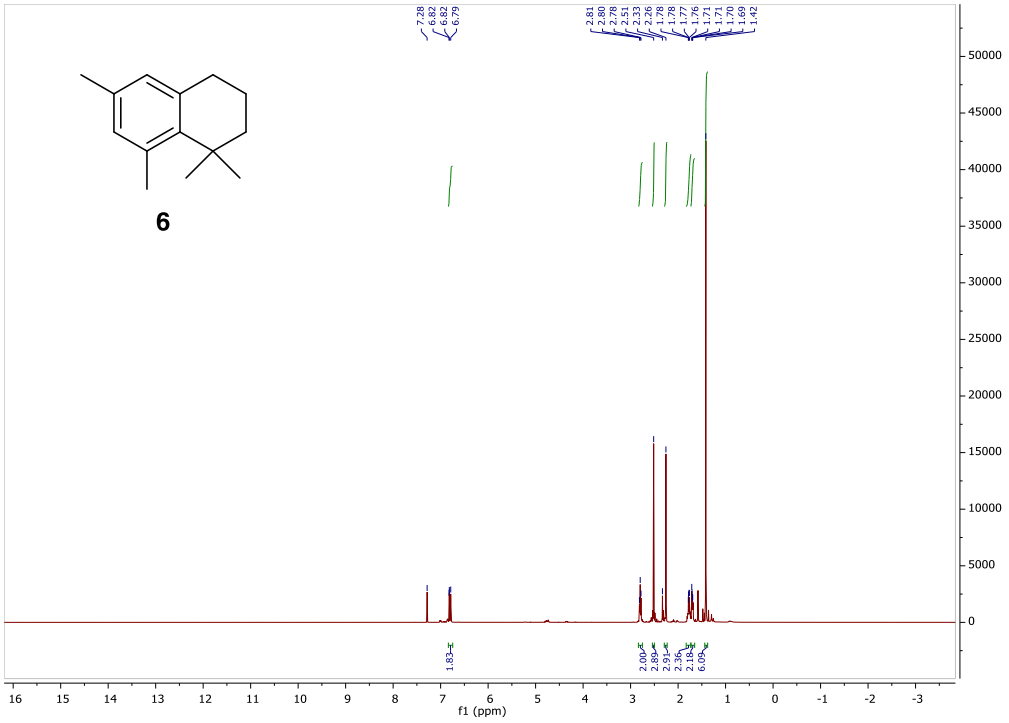
6
f1 (ppm)

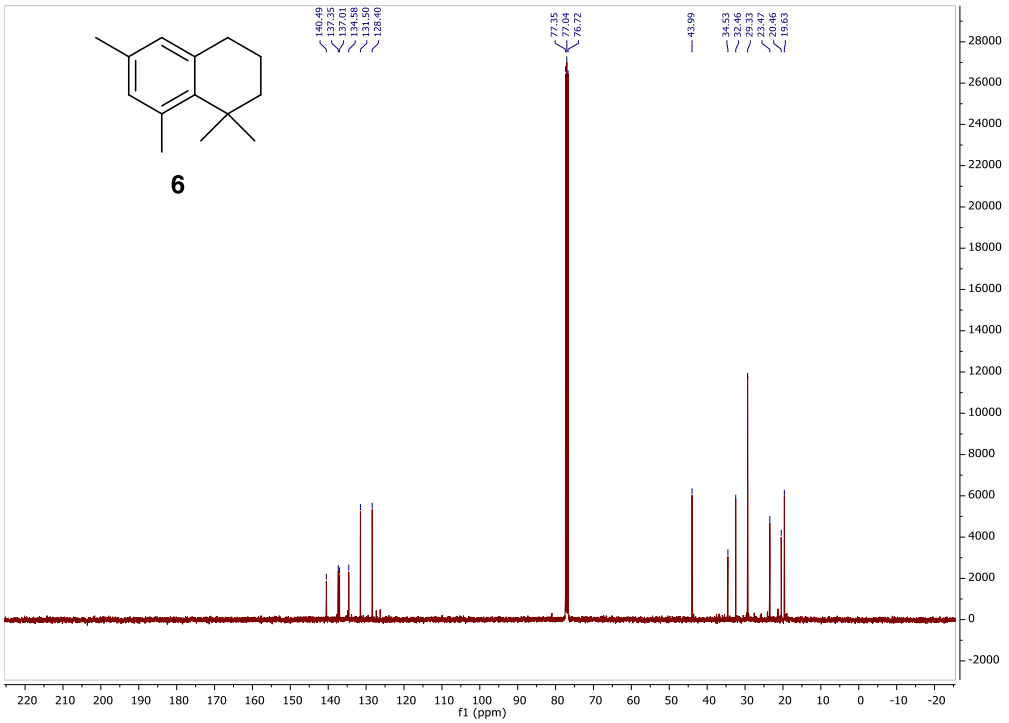
6
f1 (ppm)

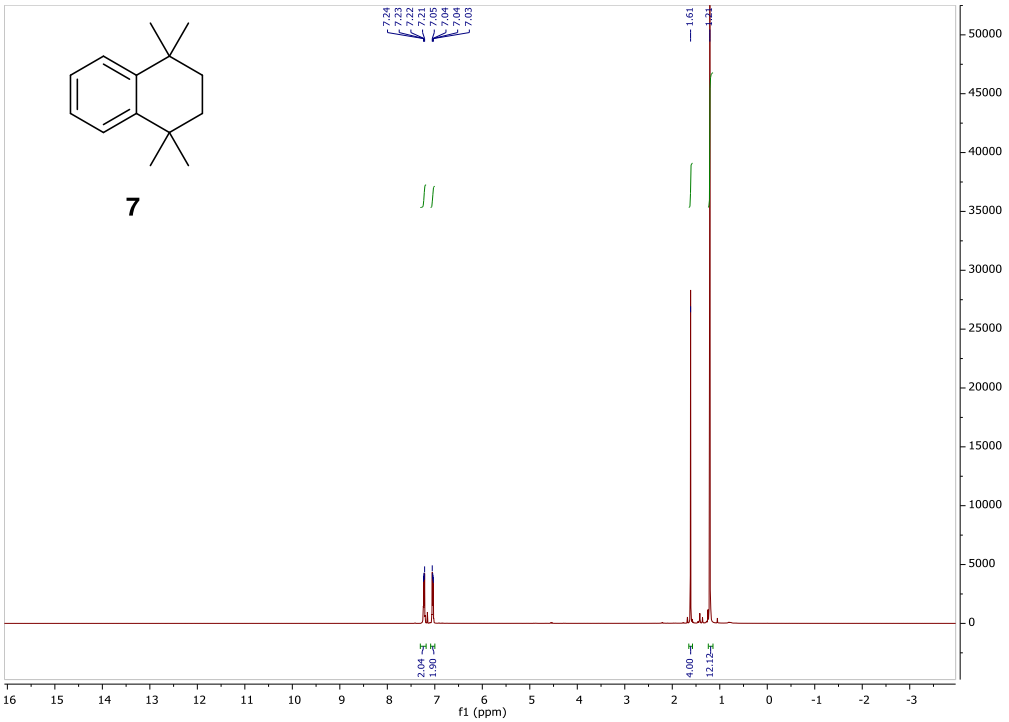
7.24
7.23
7.22
7.21
7.05
7.04
7.04
7.03
1.61
1.31
7
2.04
1.90
4.00
12.12
f1 (ppm)

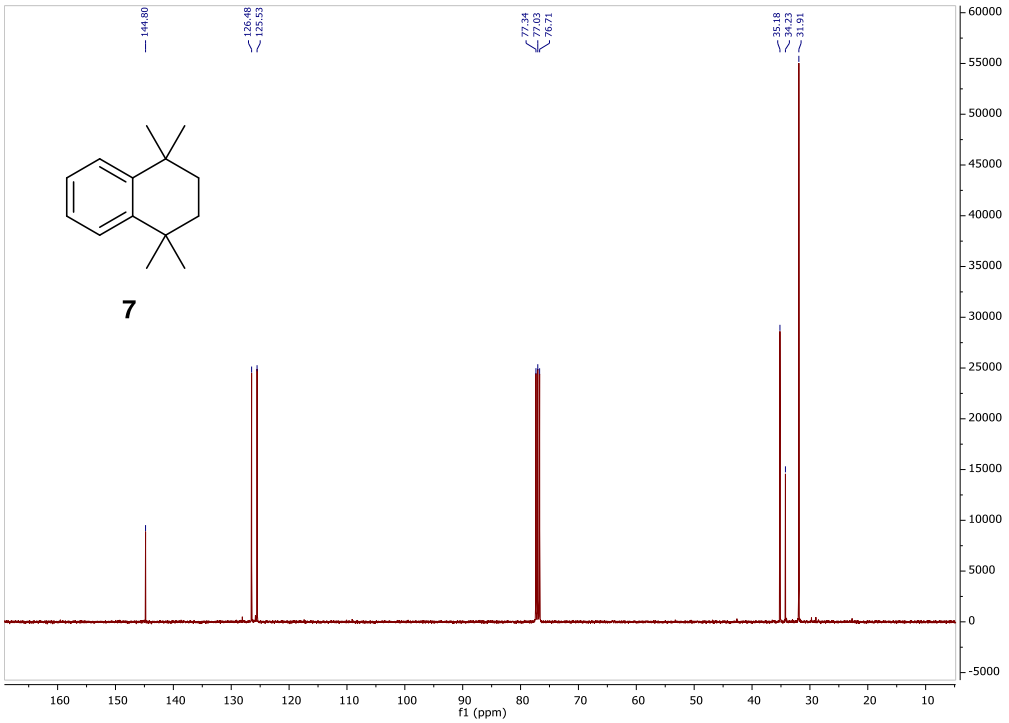
144.80
126.48
125.53
77.34
77.03
76.71
35.18
34.23
31.91
7
f1 (ppm)

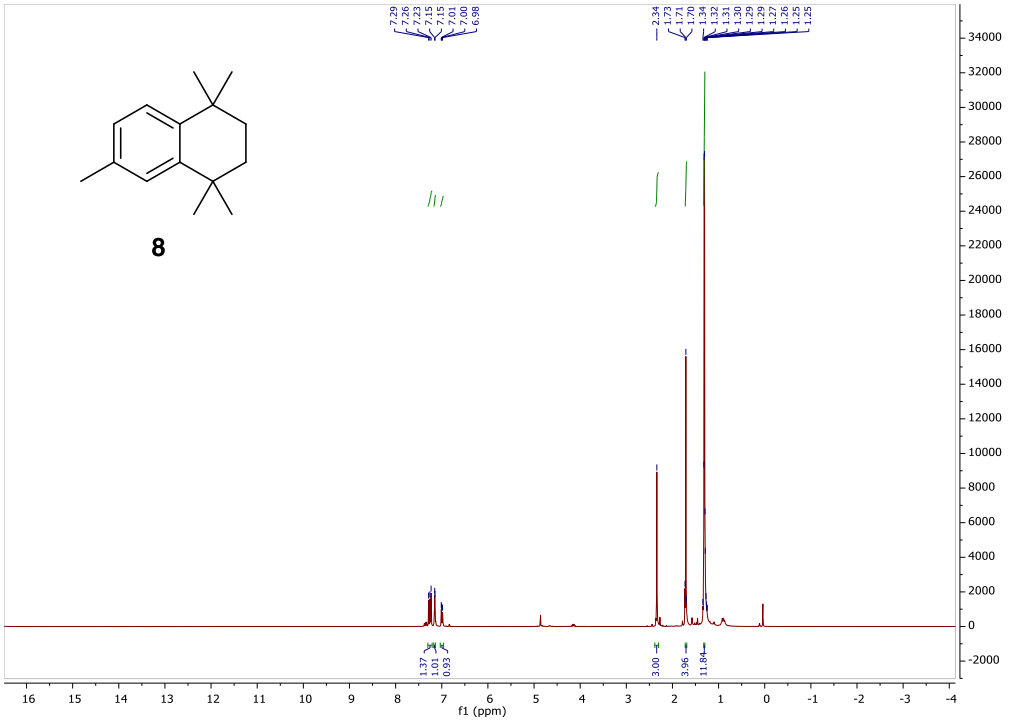
8
f1 (ppm)

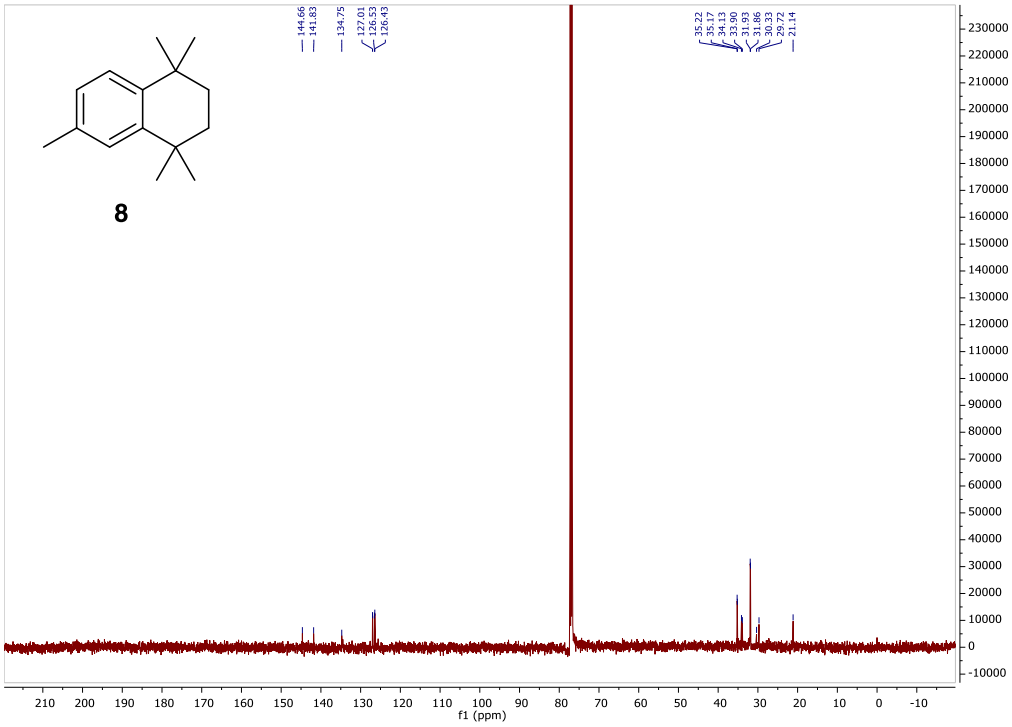
8
f1 (ppm)

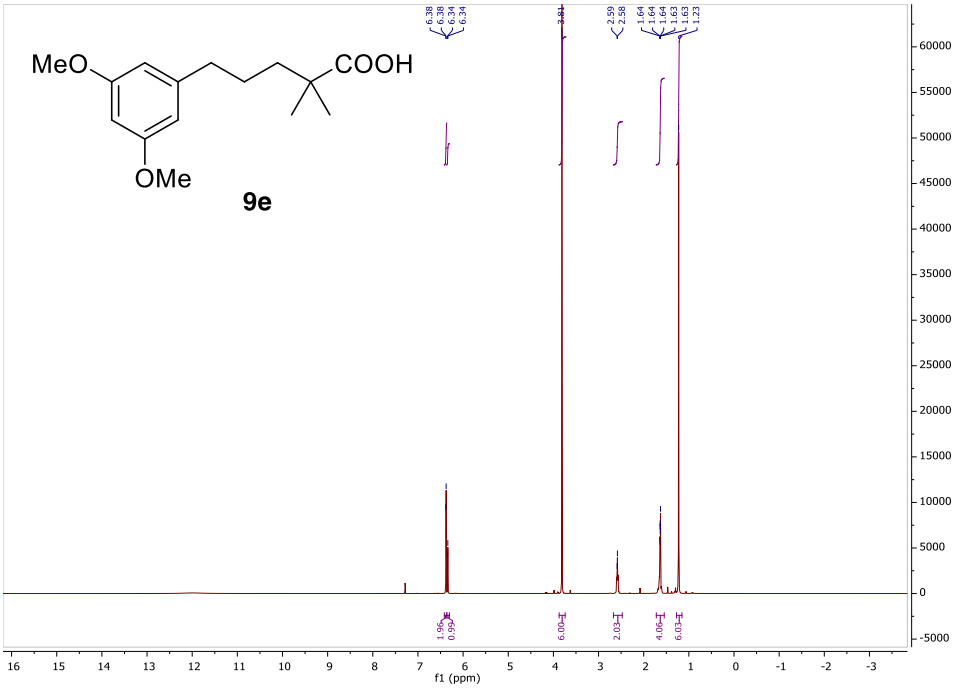
MeO
COOH
OMe
9e
f1 (ppm)

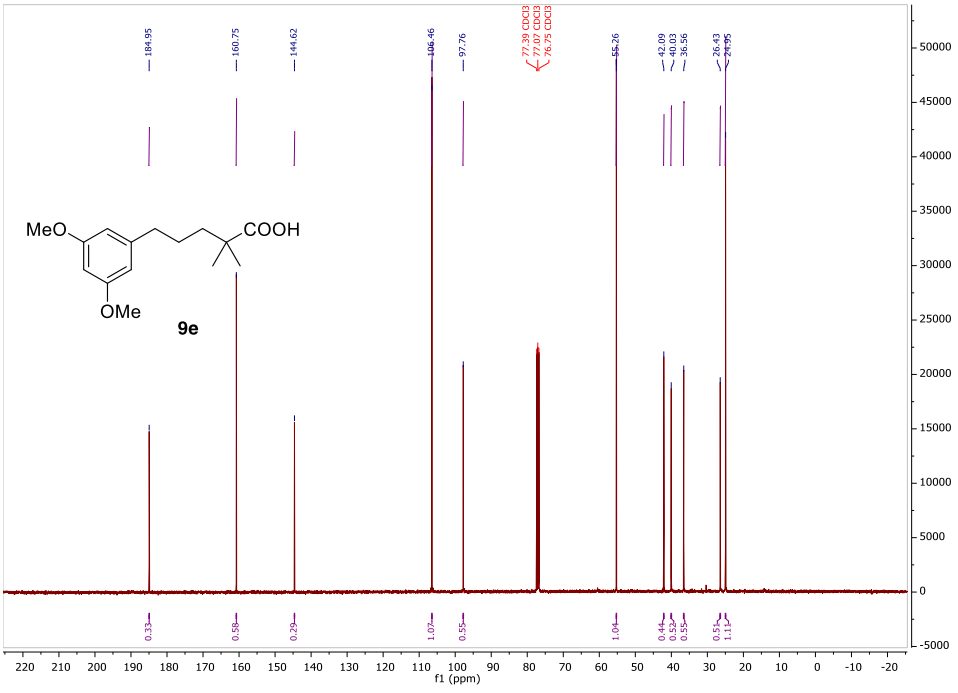
MeO
COOH
OMe
9e
f1 (ppm)

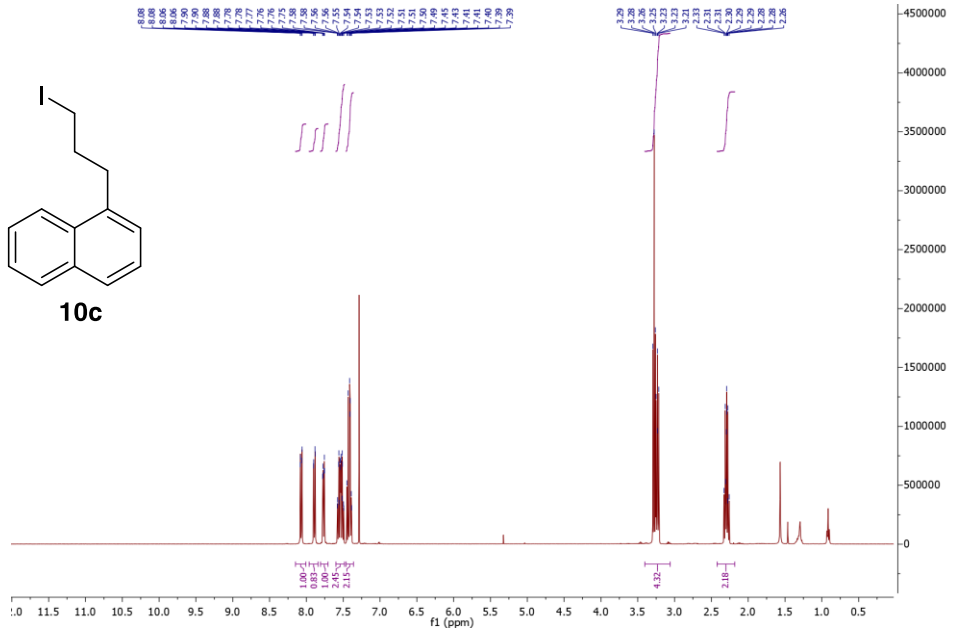
10c
f1 (ppm)

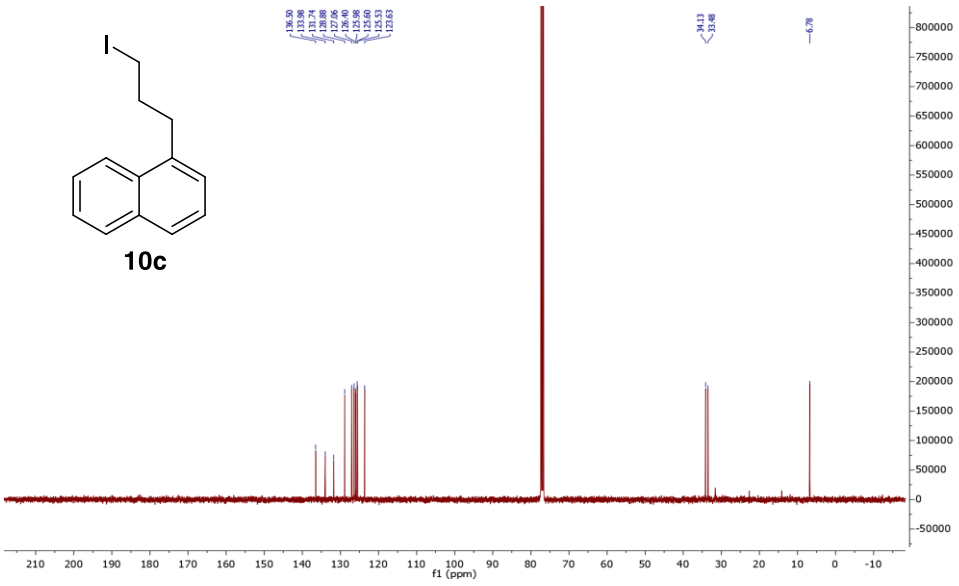
10c
f1 (ppm)

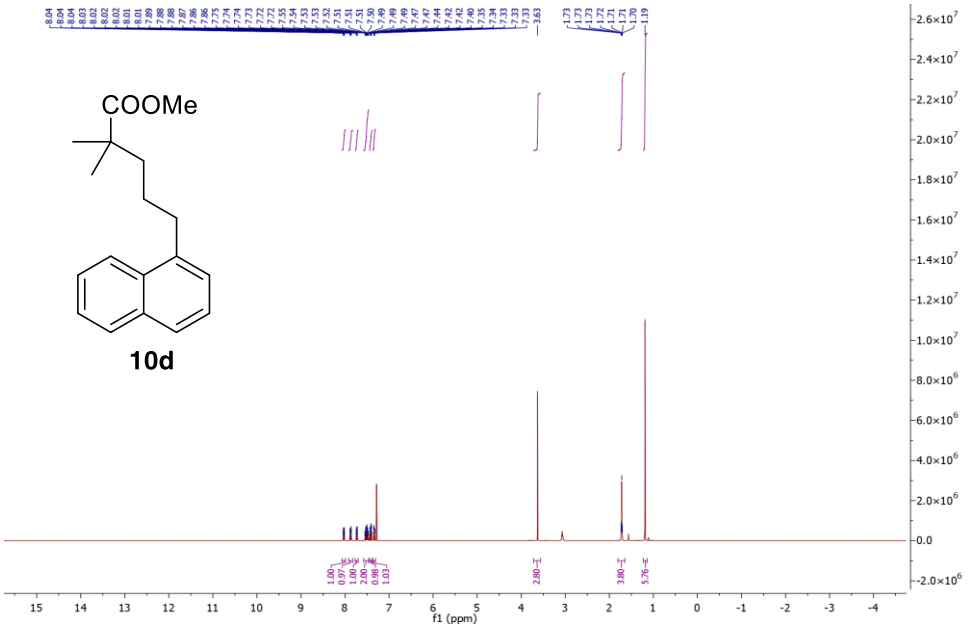
COOMe
10d
f1 (ppm)

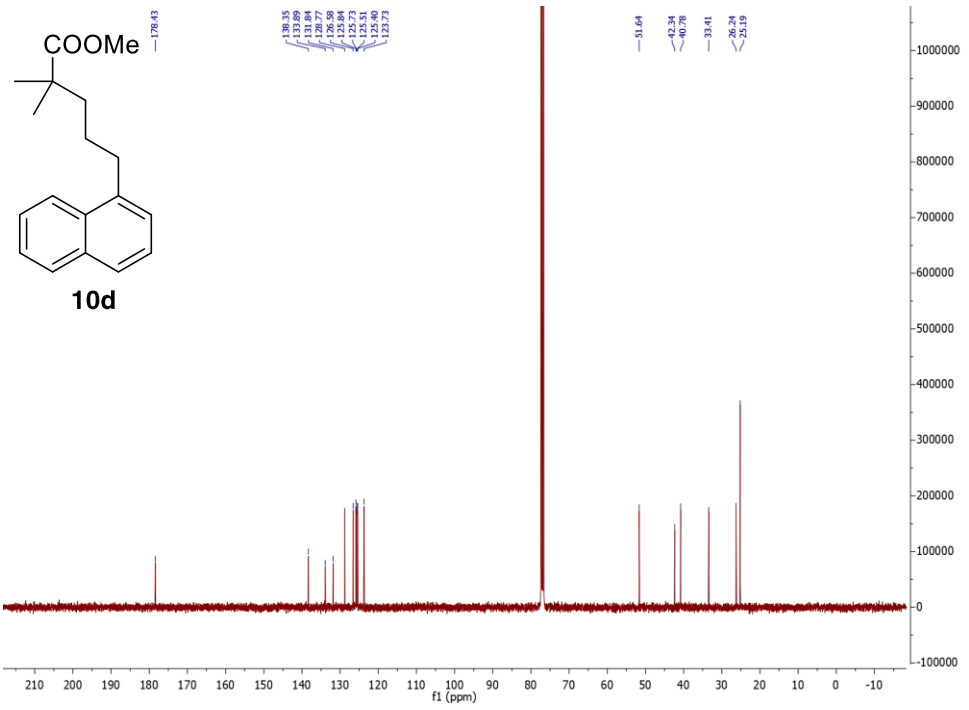
COOMe
10d
f1 (ppm)

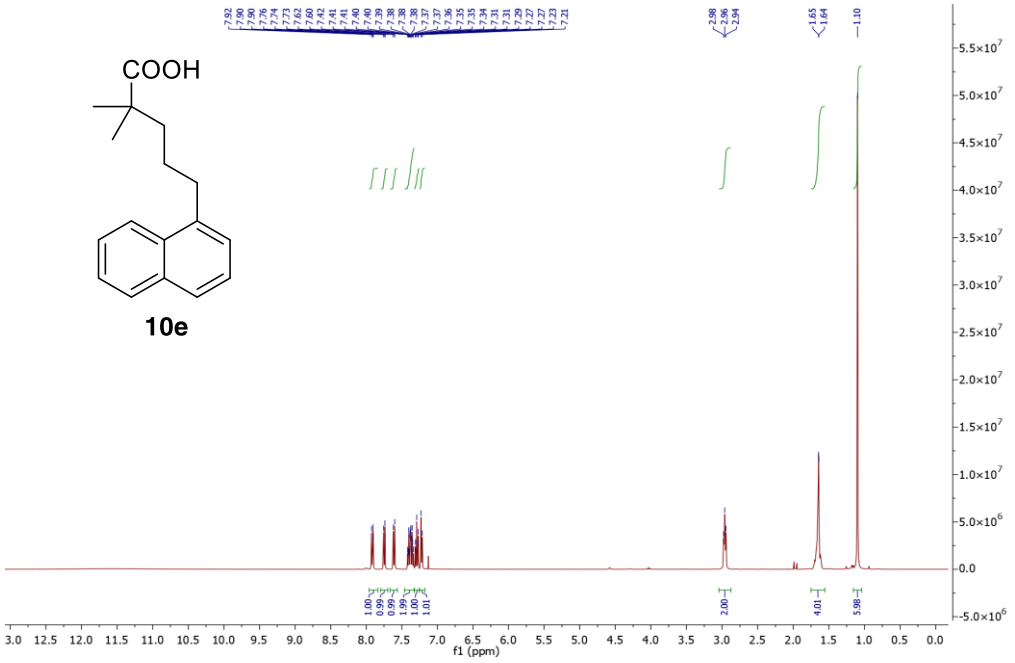
COOH
10e
f1 (ppm)

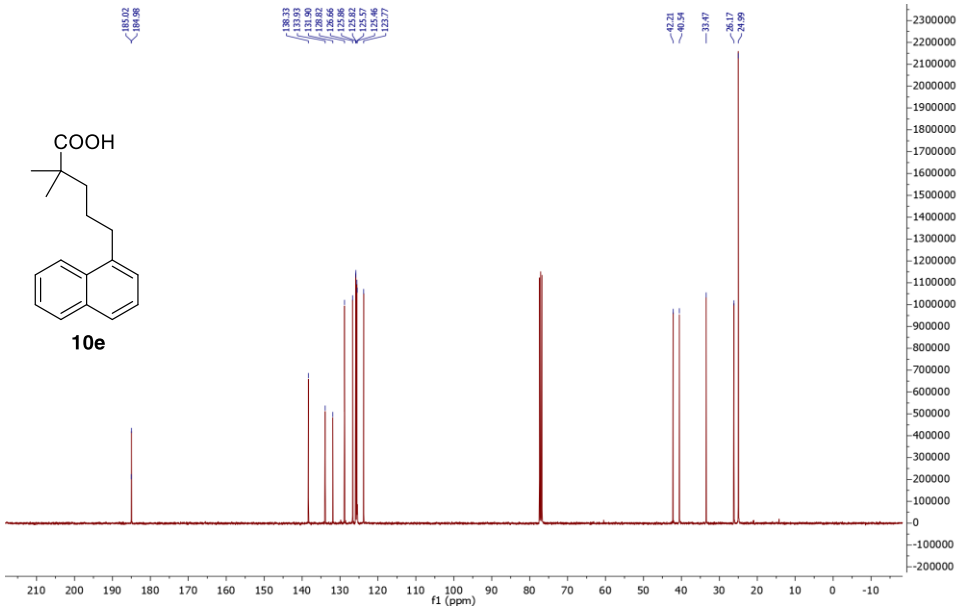
COOH
10e
f1 (ppm)

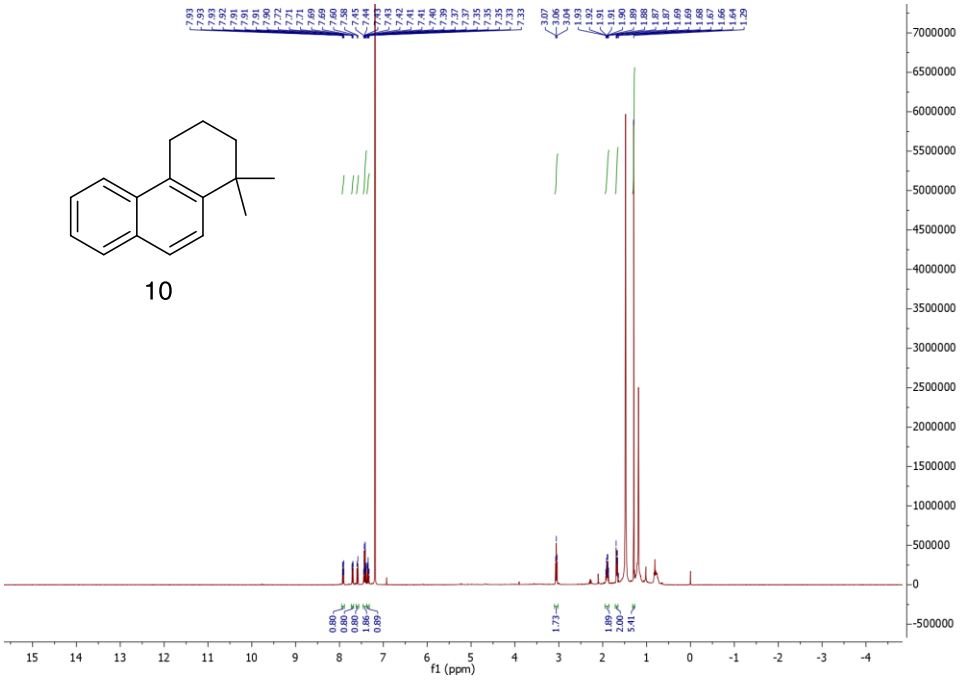
10
f1 (ppm)

3.10 Cartesian coordinates

A

M06-2X/6-31+g(d,p),

el. energy = -467.127663 a.u.

C	3.97729700	-0.01013600	-0.77388500
C	3.38518900	1.19249700	-0.38611500
C	2.15734800	1.18601500	0.27547100
C	1.50580000	-0.01932900	0.56038400
C	2.10763900	-1.21962100	0.16577700
C	3.33528600	-1.21748000	-0.49584300
H	4.93486700	-0.00677100	-1.28576200
H	3.88188900	2.13560000	-0.59454600
H	1.70118500	2.12491300	0.58168800
H	1.61218900	-2.16269000	0.38625400
H	3.79272700	-2.15774600	-0.78950700
C	0.15771200	-0.02581800	1.23904000
H	0.03638100	-0.94703100	1.81833700
H	0.07765600	0.81947100	1.93068800
C	-0.96839600	0.06669300	0.19958500
H	-0.89290600	-0.76734300	-0.50568200
H	-0.88449800	1.00071300	-0.36432000
C	-2.35854800	0.01944400	0.93452000
H	-2.40490300	-0.89823100	1.52578300
H	-2.44458800	0.91349100	1.55690700
C	-3.33320200	0.01707500	-0.14509700
C	-3.86344000	-1.25106300	-0.63479800
H	-3.16089800	-2.07494200	-0.48713000
H	-4.71549400	-1.44852600	0.04391500
H	-4.25289000	-1.19494700	-1.65172200
C	-3.73347200	1.26334000	-0.79319500
H	-3.44164700	2.15693400	-0.24370100
H	-3.24679300	1.25569200	-1.78371700
H	-4.80756000	1.24171100	-1.01254900

Py

M06-2X/6-31+g(d,p),

el. energy = -248.197867 a.u.

C	1.14383500	-0.72117000	0.00006200
C	1.19750900	0.67155600	-0.00005500
C	-0.00010400	1.38227000	0.00000700
C	-1.19759300	0.67139000	0.00002700
C	-1.14374500	-0.72132900	-0.00009300

N	0.00010800	-1.41582000	0.00002000
H	-0.00021000	2.46821200	0.00004900
H	2.06045400	-1.30593200	-0.00000600
H	2.15618500	1.17936800	-0.00004100
H	-2.15635000	1.17906600	0.00010900
H	-2.06025000	-1.30626700	0.00006500

TS-conf

M06-2X/6-31+g(d,p),

el. energy = -467.120942 a.u.

im. frequency -47.31

C	3.45401100	0.80593700	0.39120500
C	3.26926300	-0.56476300	0.58656700
C	2.10490700	-1.18492600	0.13779700
C	1.10598800	-0.44810300	-0.51179800
C	1.30181300	0.92304900	-0.70310600
C	2.46766600	1.54852400	-0.25579400
H	4.36283100	1.28891600	0.73715100
H	4.03611200	-1.15091800	1.08458900
H	1.96810600	-2.25376100	0.28843600
H	0.53741700	1.50498300	-1.21466600
H	2.60592000	2.61353800	-0.41812700
C	-0.17057100	-1.12054700	-0.96099300
H	-0.69869400	-0.44616900	-1.64308200
H	0.07200800	-2.01471300	-1.54359200
C	-1.07723000	-1.53136800	0.22428000
H	-0.68812500	-1.14022900	1.16855600
H	-1.11267500	-2.61809500	0.32293900
C	-2.57320700	-1.08649200	0.06754100
H	-2.95412900	-1.40038900	-0.90653300
H	-3.13349100	-1.55966200	0.88139000
C	-2.64889400	0.36487400	0.23663400
C	-2.92669700	1.23143300	-0.89876400
H	-2.62008000	0.79794200	-1.85304800
H	-4.03649000	1.23912300	-0.91531600
H	-2.59734500	2.26144200	-0.75484500
C	-2.43116000	0.96389200	1.55135400
H	-2.47710000	0.24952000	2.37249700
H	-1.41777300	1.40212200	1.50552300
H	-3.10182000	1.81727900	1.69858100

INT-1

M06-2X/6-31+g(d,p),

el. energy = -467.133408 a.u.

C	-2.60135200	-0.84049400	0.04689500
C	-2.47531600	0.28714500	0.86871600
C	-1.48457200	1.23052500	0.61646600
C	-0.60059600	1.06820900	-0.45985600
C	-0.74655800	-0.05476600	-1.28581000
C	-1.74222300	-1.00486900	-1.03588500
H	-3.37601000	-1.57455300	0.24636500
H	-3.15413900	0.42496900	1.70518400
H	-1.38546200	2.10088200	1.26118000
H	-0.08488600	-0.17406000	-2.14157600
H	-1.84180500	-1.86744400	-1.68834300
C	0.54571800	2.02178600	-0.66042400
H	0.85667100	2.02145200	-1.71054400
H	0.24186300	3.04079200	-0.40139100
C	1.74302100	1.63037900	0.22326000
H	1.46740500	1.70243900	1.28008500
H	2.56665500	2.32914400	0.05529200
C	2.24982400	0.22287500	-0.10924800
H	2.53479300	0.13082300	-1.16116900
H	3.17207900	0.04071500	0.48445200
C	1.46527000	-0.94155500	0.31929700
C	1.53886400	-2.18119400	-0.46834300
H	1.59180200	-1.99707700	-1.54170400
H	2.50149200	-2.63330000	-0.16866200
H	0.75116400	-2.88929100	-0.20654800
C	0.81951400	-1.00880700	1.63254000
H	0.94200000	-0.11574300	2.24123500
H	-0.25123500	-1.21412800	1.47020300
H	1.19804300	-1.90102700	2.15028500

INT-1–Py Adduct

M06-2X/6-31+g(d,p),

el. energy = -715.337504 a.u.

C	3.17684700	-1.69293000	-1.36404100
C	3.86197100	-1.40993500	-0.17525200
C	3.16636400	-0.97001300	0.94642100
C	1.77516500	-0.80084100	0.90336900
C	1.09719900	-1.09861500	-0.28658500
C	1.79364400	-1.54551900	-1.41450300
H	3.72290200	-2.03670300	-2.23730600
H	4.93972000	-1.53594000	-0.12894500
H	3.70265500	-0.74559100	1.86584400

H	0.01582400	-0.97626600	-0.32694200
H	1.25175700	-1.77197000	-2.32842400
C	1.03767700	-0.20941000	2.07439400
H	-0.01078000	-0.52777900	2.05883300
H	1.48036000	-0.55330400	3.01449700
C	1.09725700	1.32754900	2.03761900
H	2.13643800	1.66413100	2.10885200
H	0.56384600	1.73569500	2.90018000
C	0.43079700	1.87995500	0.77330800
H	-0.60595400	1.54103200	0.68247200
H	0.40436600	2.98840400	0.85029600
C	1.12222000	1.74682700	-0.51573900
C	-2.74792700	-1.30158300	0.18633000
C	-4.09292300	-1.59694100	0.40017100
C	-5.04204900	-0.62040600	0.10861000
C	-4.60791800	0.60820300	-0.38358600
C	-3.24030900	0.80519200	-0.56207300
N	-2.31858500	-0.12489200	-0.28544600
H	-6.09958500	-0.81313400	0.26164600
H	-1.98072600	-2.04279400	0.40247200
H	-4.38177400	-2.56910700	0.78501400
H	-5.30833100	1.40022600	-0.62595800
H	-2.86779500	1.75410600	-0.94433100
C	0.31040700	1.64163800	-1.73643600
H	-0.54302200	0.97253400	-1.59191300
H	-0.10060300	2.65672700	-1.88103100
H	0.90234500	1.38821900	-2.61667500
C	2.56485000	1.95993900	-0.65828200
H	2.99818600	1.06206000	-1.12821000
H	2.70984700	2.76006000	-1.39760900
H	3.08079000	2.18497600	0.27300700

TS-cycl

M06-2X/6-31+g(d,p),

el. energy = -715.334118 a.u.

im. frequency -178.50

C	-2.93995600	1.82702800	-1.24265200
C	-3.67309900	1.62276500	-0.05820200
C	-3.08465600	1.03910400	1.05734100
C	-1.74540200	0.63438300	1.01635700
C	-1.02379000	0.78717400	-0.19039600
C	-1.61948900	1.42744400	-1.30188000

H	-3.41219000	2.30449200	-2.09502700
H	-4.71237500	1.93542000	-0.01348400
H	-3.65898500	0.89841200	1.96902600
H	0.05145100	0.61024800	-0.18866600
H	-1.03298300	1.58617100	-2.20222900
C	-1.09575800	-0.07605800	2.16219000
H	-0.04846600	0.23271800	2.24929200
H	-1.60723600	0.15803500	3.09966800
C	-1.15034300	-1.59738800	1.90792200
H	-2.18540800	-1.94778000	1.97192500
H	-0.58396100	-2.11732100	2.68503400
C	-0.54789000	-1.93220200	0.54897700
H	0.51044400	-1.65413800	0.50578900
H	-0.60226400	-3.02411100	0.38906900
C	-1.24647300	-1.41183500	-0.66453400
C	2.75373700	1.30456600	0.18454600
C	4.10051800	1.57956600	0.41331800
C	5.03393200	0.57615300	0.16562100
C	4.58329400	-0.65720300	-0.29939000
C	3.21531300	-0.83277600	-0.49632100
N	2.30923100	0.12386700	-0.26171600
H	6.09247800	0.75180600	0.33175300
H	1.99738400	2.06567900	0.36744600
H	4.40282500	2.55625500	0.77580200
H	5.27201100	-1.46915400	-0.50697300
H	2.82903700	-1.78372400	-0.85873900
C	-0.44433900	-1.39870500	-1.92390600
H	0.52439600	-0.91263100	-1.78794300
H	-0.25765100	-2.45865400	-2.15489600
H	-0.99202200	-0.96090400	-2.75930200
C	-2.70648500	-1.63461700	-0.82022400
H	-3.16275300	-0.88855300	-1.47675700
H	-2.79304900	-2.59984300	-1.34229500
H	-3.24998900	-1.69388300	0.12091200

2

M06-2X/6-31+g(d,p),

el. energy = -466.754896 a.u.

C	-2.50351100	-1.26278000	0.08077800
C	-3.02548700	0.03074200	0.02011400
C	-2.15387700	1.11089200	-0.05612400

C	-0.76244400	0.93419800	-0.08250500
C	-0.23229800	-0.36808500	-0.03544600
C	-1.12526200	-1.44861600	0.05629300
H	-3.16594200	-2.12083700	0.14933000
H	-4.09906000	0.19417300	0.04004200
H	-2.55079400	2.12350300	-0.09133300
H	-0.73286300	-2.46066100	0.11301200
C	0.12443800	2.15905900	-0.16728000
H	0.15801000	2.50089000	-1.21139700
H	-0.32954500	2.97127400	0.41059500
C	1.54599900	1.87483900	0.30540700
H	1.55531000	1.72677200	1.39238500
H	2.19096000	2.73367200	0.09292800
C	2.06692200	0.62915200	-0.40295200
H	2.00060200	0.79433000	-1.48808100
H	3.12489900	0.45522500	-0.17190000
C	1.27623800	-0.64302500	-0.04296800
C	1.62808300	-1.72384100	-1.07780700
H	1.26439600	-1.44720200	-2.07331700
H	2.71704700	-1.83855900	-1.13180000
H	1.20603700	-2.69901900	-0.81709100
C	1.69979200	-1.14380000	1.35005700
H	1.15453800	-2.05479300	1.61866100
H	2.77159200	-1.37443900	1.35682300
H	1.50325300	-0.39674000	2.12573600

Py-H

M06-2X/6-31+g(d,p),

el. energy = -248.643935 a.u.

C	-0.66698100	-1.18402200	0.00000400
C	0.71490100	-1.20876800	-0.00000100
C	1.41179000	-0.00058100	-0.00000400
C	0.71591500	1.20819200	0.00000400
C	-0.66599200	1.18456500	-0.00000400
N	-1.30204800	0.00053300	0.00000300
H	2.49691600	-0.00104100	-0.00000700
H	-1.29108800	-2.06881700	0.00000800
H	1.22989200	-2.16139000	0.00000000
H	1.23168500	2.16039100	0.00001100
H	-1.28938500	2.06987800	0.00000300
H	-2.32148600	0.00093300	-0.00003000

TS-elim

M06-2X/6-31+g(d,p),

el. energy = -715.332160 a.u.

im. frequency -8.13

C	4.82248100	-0.56115500	0.51496400
C	3.69381300	-1.30325400	0.86521100
C	2.44130900	-0.94954300	0.36351900
C	2.29633100	0.14722300	-0.49374900
C	3.43509800	0.88374200	-0.83884900
C	4.68990400	0.53382400	-0.33969600
H	5.79898200	-0.83734900	0.90129200
H	3.78908100	-2.16041200	1.52550500
H	1.56390000	-1.53406200	0.63363900
H	3.33722200	1.73467700	-1.50966900
H	5.56449300	1.11293000	-0.62169500
C	0.93184900	0.55230300	-0.99563100
H	1.01780000	0.99098100	-1.99648000
H	0.29279000	-0.33449500	-1.07847900
C	0.26133000	1.56647700	-0.05921500
H	0.86849600	2.47878300	-0.00936000
H	0.21687900	1.15132800	0.95419400
C	-1.14212900	1.90706400	-0.54440900
H	-1.22690200	2.08724000	-1.62217400
H	-1.79411200	0.98154400	-0.37698300
C	-1.96551700	2.80781600	0.20953400
C	-3.15331800	3.40384600	-0.40783200
H	-3.38611800	2.98770600	-1.38782200
H	-4.00752800	3.36579100	0.27557300
H	-2.90957300	4.47472100	-0.51828500
C	-1.66177900	3.09895600	1.61619900
H	-2.39530100	3.75241500	2.08532400
H	-1.59132000	2.14671000	2.16130100
H	-0.65439000	3.53479300	1.67107500
C	-2.36406700	-1.63979300	-1.15611600
C	-2.33966300	-3.03164600	-1.19149300
C	-2.16728700	-3.72316000	0.00542900
C	-2.02898600	-2.99711400	1.18598400
C	-2.06871900	-1.60618400	1.11981300
N	-2.23289100	-0.93463800	-0.02607000
H	-2.14109500	-4.80853700	0.01774200
H	-2.48880600	-1.06516200	-2.07144300
H	-2.45182700	-3.55375100	-2.13551600

H -1.89237200 -3.49221200 2.14133900

H -1.96396400 -1.00758200 2.02144600

O1a

M06-2X/6-31+g(d,p),

el. energy = -466.723279 a.u.

C 4.09648400 0.34181600 -0.26466900

C 3.20594400 1.39344000 -0.04398700

C 1.87436200 1.12700200 0.27486500

C 1.40981600 -0.18957700 0.37977100

C 2.31240400 -1.23558600 0.15472000

C 3.64522900 -0.97488200 -0.16445400

H 5.13440800 0.54681600 -0.50960000

H 3.54915900 2.42155300 -0.11649800

H 1.18383800 1.94982700 0.44936900

H 1.96576000 -2.26378200 0.23465600

H 4.33220700 -1.79969100 -0.33128500

C -0.04319200 -0.47019600 0.67275600

H -0.13865500 -1.41645800 1.21793300

H -0.45292100 0.31865300 1.31450400

C -0.88886300 -0.54468600 -0.61598300

H -0.47240100 -1.32737800 -1.26109200

H -0.78325600 0.39959500 -1.16109200

C -2.33514500 -0.84926700 -0.32776300

H -2.59334100 -1.90676800 -0.25416900

C -3.31161900 0.04509700 -0.11284500

C -4.72161200 -0.38957600 0.19162800

H -4.81765800 -1.47870200 0.20062600

H -5.04358500 -0.00461200 1.16703000

H -5.41947300 0.01384300 -0.55245900

C -3.11128100 1.53775400 -0.14042300

H -3.75937900 1.99698300 -0.89695800

H -3.39977600 1.97139900 0.82495400

H -2.08008500 1.83069400 -0.34763400

4 References

1 Faraday M. Siebente Reihe von Experimental-Untersuchungen Über Elektricität. *Ann. Phys.* **1834**, *109*, 481–520.

2 Kolbe H. Beobachtungen Über Die Oxydirende Wirkung Des Sauerstoffs, Wenn Derselbe Mit Hülfe Einer Elektrischen Säule Entwickelt Wird. *J. Prakt. Chem.* **1847**, *41*, 137–139.

3 Simons, J. H. The Electrochemical Process for the Production of Fluorocarbons. *Journal of Electrochemical Society* **1949**, *95*, 47–67.

4 Berson, J. A.; Donald, D. S.; Libbey, W. J.; Am Chem SOC, J.; Crandall, J. K.; Crawby, L. C.; Lin, L. C.; Weinberg, H. E.; Fawcett, F. S.; Mochel, W. E.; Theobald, C. W.; Shono, T.; Hamaguchi, H.;

5 Savéant J.M. *Elements of Molecular and Biomolecular Electrochemistry*; Wiley: Hoboken, Ed.; NJ, 2006.

6 Sperr, J. B.; Wright, D. L. The Application of Cathodic Reductions and Anodic Oxidations in the Synthesis of Complex Molecules. *Chemical Society Reviews* **2006**, *35* (7), 605–621.

7 Yoshida, J. I.; Suga, S.; Suzuki, S.; Kinomura, N.; Yamamoto, A.; Fujiwara, K. Direct Oxidative Carbon-Carbon Bond Formation Using the “cation Pool” Method. 1. Generation of Iminium Cation Pools and Their Reaction with Carbon Nucleophiles. *J. Am. Chem. Soc.* **1999**, *121*

8 Yoshida, J. I.; Shimizu, A.; Hayashi, R. Electrogenerated Cationic Reactive Intermediates: The Pool Method and Further Advances. *Chemical Reviews* **2018**, *118* (9), 4702–4730.

9 Yoshida; Jun-Ichi; Suga, S. Basic Concepts of “Cation Pool” and “Cation Flow” Methods and Their Applications in Conventional and

Combinatorial Organic Synthesis. *Chemistry - A European Journal* **2002**, *8* (12), 2650–2658

10 Itami, K.; Yoshida, J. I. 2-Pyridylsilyl Group: A Useful Multifunctional Group in Organic Synthesis. *Synlett* **2006**, No. 2, 157–180.

11 Roth, H. G.; Romero, N. A.; Nicewicz, D. A. Experimental and Calculated Electrochemical Potentials of Common Organic Molecules for Applications to Single-Electron Redox Chemistry. *Synlett* **2016**, *27* (5), 714–723.

12 Yoshida, J.-I.; Murata, T.; Lsoe, S. Electrochemical Oxidation of Organosilicon Compounds I. Oxidative Cleavage of Carbon-Silicon Bond in Allylsilanes and Benzylsilanes. *Tetrahedron Letters* **1986**, *27* (29), 3373–3376.

13 Fukui, K.; Yonezawa, T.; Shingu, H. A Molecular Orbital Theory of Reactivity in Aromatic Hydrocarbons. *The Journal of Chemical Physics* **1952**, *20* (4), 722–725.

14 Yoshida, J. I.; Kataoka, K.; Horcajada, R.; Nagaki, A. Modern Strategies in Electroorganic Synthesis. *Chemical Reviews* **2008**, *108* (7), 2265–2299

15 Hintz, H. A.; Sevov, C. S. Catalyst-Controlled Functionalization of Carboxylic Acids by Electrooxidation of Self-Assembled Carboxyl Monolayers. *Nature Communications* **2022**, *13* (1).

16 Schafer, H. J. Recent Synthetic Applications of the Kolbe Electrolysis. *Chemistry and Physics of Lipids* **1979**, *24*, 321–333.

17 Leech, M. C.; Lam, K. Electrosynthesis Using Carboxylic Acid Derivatives: New Tricks for Old Reactions. *Accounts of Chemical Research* **2020**, *53* (1), 121–134.

18 Schfifer, H.-J. Recent Contributions of Kolbe Electrolysis to Organic Synthesis. *Top. Curr. Chem* **1990**, *152*, 91–151.

19 Hofer H; Moest M. Ueber Die Bildung von Alkoholen Bei Der Elektrolyse Fettsaurer Salze. *Justus Liebigs Ann. Chem.* **1902**, *323*, 284–323

20 Corey, J. E.; Sauers, R. R.; Ruzicka, L.; Eschenmoser, A.; Heusser, H.; Jeger, O.; Arigoni, D.; R Barton, D. H.; McGhie, J. F.; Pradhan, K.; Knight, S. A.; Menard, E.; Wyler, H.; Hiestand, A.; Beaton, J. M.; Spring, F. S.; Stewart, J. L.; Beaton, M.; Stevenson, R.; Stewart, J. M.; Overton, K. H. The Synthesis of Pentacyclosqualene (8,8'-Cycloónocerene) and the a- and ß Onoceradienes1. *J. Am. Chem. Soc* **1959**, *78* (4), 3925.

21 Baran, P. S.; Xiang, J.; Shang, M.; Kawamata, Y.; Lundberg, H.; Reisberg, S. H.; Chen, M.; Mykhailiuk, P.; Beutner, G.; Collins, M. R.; Davies, A.; del Bel, M.; Gallego, G. M.; Spangler, J. E.; Starr, J.; Yang, S.; Blackmond, D. G. Hindered Dialkyl Ether Synthesis with Electrogenerated Carbocations. *Nature* **2019**, *573* (7774), 398–402.

22 Francke, R.; Little, D. Redox catalysis in organic electrosynthesis: basic principles and recent development. *Chem. Soc. Rev.*, **2014**,43, 2492-2521.

23 D. J. Mazur, P. M. Kendall, C. W. Murtiashaw, P. Dunn, S. L. Pezzullo, S. W. Walinsky and J. B. Zung Electrochemical Deacetoxylation: Synthesis of 11-Ketotigogenin, *J. Org. Chem*., **1996**, 61, 405–407.

24 J. H. Chapman, J. Elks, G. H. Phillipps and L. J. Wyman, Synthesis of Gymnomitrol *J. Am. Chem. Soc*., **1956**, 4344–4350.

25 D. Chai, D. Genders, N. Weinberg, G. Zappi, E. Bernasconi, J. Lee, J. Roletto, L. Sogli, D. Walker, C. R. Martin, V. Menon, P. Zelenay and

H. Zhang, Ceftibuten: Development of a Commercial Process Based on Cephalosporin C. Part III. Process for the Conversion of 3-Exomethylene-7(*R*)-glutaroylaminocepham-4-carboxylic Acid 1(*S*)-Oxide to Ceftibuten *Org. Proc. Res. Dev.*, **2002**, 6, 178–183.

26 T. W. Kang, K. J. Jeon, W. K. Choi, H. N. Song and Y. K. Park, 7-Glutaryl imide cephalosporanic acid derivatives and process for preparing it, WO2004101572A1, **2004**.

27 A. Aliyenne, F. Pin, V. D. Nimbarte, A. M. Lawson, S. Comesse, M. Sanselme, V. Tognetti, L. Joubert and A. Daı¨ch, Autotandem Catalysis: Inexpensive and Green Access to Functionalized Ketones by Intermolecular Iron-Catalyzed Amidoalkynylation/Hydration Cascade Reaction via N-Acyliminium Ion Chemistry *Eur. J. Org. Chem.*, **2016**, 3592–3602.

28 L. Labanauskas, R. Mazeikaite, R. Striela, O. Gedrimaite, G. Urbelis and A. Zilinskas, Nucleophilic substitution of the acetoxy group in 3-methylbenzoylaminomethyl acetate *Russ. Chem. Bull.*, **2011**, 60, 1672–1676.

29 J. K. Kochi, A New Method for Halodecarboxylation of Acids Using Lead(IV) Acetate *J. Am. Chem. Soc.*, **1965**, 87, 2500–2502.

30 J. K. Kochi and A. Bemis, Carbonium ions from alkyl radicals by electron transfer *J. Am. Chem. Soc.*, **1968**, 90, 4038–4051.

31 J. D. Bacha and J. K. Kochi, Oxidation of alkyl radicals from decarboxylation of acids by lead(IV) and copper(II) *J. Org. Chem.*, **1968**, 33, 83–93.

32 M. Ko¨ckinger, P. Hanselmann, D. M. Roberge, P. Geotti-Bianchini, C. O. Kappe and D. Cantillo, Sustainable electrochemical decarboxylative acetoxylation of aminoacids in batch and continuous flow *Green Chem.*, **2021**, 23, 2382–2390.

33 D. Pletcher and F. C. Walsh, *Industrial Electrochemistry*, Springer, Dordrecht, Netherlands, 2nd edn, **1993**.

34 F. Goodridge and K. Scott, *Electrochemical Process Engineering – A Guide to the Design of Electrolytic Plant*, Springer Science + Business Media, New York, **1995**.

35 D. Pletcher, R. A. Green and R. C. D. Brown, Flow Electrolysis Cells for the Synthetic Organic Chemistry Laboratory *Chem. Rev*., **2018**, 118, 4573–4591.

36 N. Tanbouza, T. Ollevier and K. Lam, Understanding flow chemistry for the production of active pharmaceutical ingredients *iScience*, **2020**, 23, 101720.

37 J. Wetter, *Improvements in Electrolysing Processes and Appliances*, GB190228353A, **1902**.

38 D. S. P. Cardoso, B. Sˇljukic´, D. M. F. Santos and C. A. C. Sequeira, Organic Electrochemistry: Molecular Syntheses with Potential *Org. Process Res. Dev.*, **2017**, 21, 1213–1226.

39 C. A. C. Sequeira and D. M. F. Santos, Electrochemical Routes for Industrial Synthesis *J. Braz. Chem. Soc.*, **2009**, 20, 387–406.

40 H. Pu¨tter, in Organic Electrochemistry, ed. H. Lund, O. Hammerich, *Industrial Electroorganic Chemistry*, Marcel Dekker Inc., New York, 4th edn, **2001**.

41 A. Theoret, Challenge and Commercial Opportunities in Organic Electrosynthesis: The case of Anthraquinone, *9th Int. Forum on Electrolysis*, Electrosynthesis Company, Clearwater, FL, E. Amherst, NJ, **1995**, pp. 5–9.

42 M. M. Baizer, Electrolytic Reductive Coupling: I . Acrylonitrile *J. Electrochem. Soc*., **1964**, 111, 215.

43 D. Hoormann, H. Pu¨tter and J. Jo¨rissen, Elektrochemische Verfahren – Neuentwicklungen und Tendenzen *Chem. Ing. Tech*., **2005**, 77, 1363–1376.

44 A. A. Folgueiras-Amador, A. E. Teuten, D. Pletcher and R. C. D. Brown, A design of flow electrolysis cell for 'Home' fabrication *React. Chem. Eng.*, **2020**, 5, 712–718.

45 A. A. Folgueiras-Amador, K. Philipps, S. Guilbaud, J. Poelakker and T. Wirth, An Easy-to-Machine Electrochemical Flow Microreactor: Efficient Synthesis of Isoindolinone and Flow Functionalization *Angew. Chem., Int. Ed.*, **2017**, 56, 15446–15450.

46 M. Lehmann, C. C. Scarborough, E. Godineau and C. Battilocchio, An Electrochemical Flow-Through Cell for Rapid Reactions *Ind. Eng. Chem. Res.*, **2020**, 59, 7321–7326.

47 M. R. Chapman, Y. M. Shafi, N. Kapur, B. N. Nguyen and C. E. Willans, Electrochemical flow-reactor for expedient synthesis of copper–N-heterocyclic carbene complexes *Chem. Commun.*, **2015**, 51, 1282–1284.

48 W. Jud, C. O. Kappe and D. Cantillo, Development and Assembly of a Flow Cell for Single-Pass Continuous Electroorganic Synthesis Using Laser-Cut Components *Chem. Methods*, **2021**, 1, 36–42.

49 G. Laudadio, W. de Smet, L. Struik, Y. Cao and T. Noe¨l, Design and application of a modular and scalable electrochemical flow microreactor *J. Flow Chem.*, **2018**, 8, 157–165.

50 Y. Cao, C. Soares, N. Padoin and T. Noe¨l, Gas bubbles have controversial effects on Taylor flow electrochemistry *Chem. Eng. J*., **2021**, 406, 126811.

51 W. Jud, C. O. Kappe and D. Cantillo, A Continuous Flow Cell for High-Temperature/High-Pressure Electroorganic Synthesis *ChemElectroChem*, **2020**, 7, 2777–2783.

52 D. Cantillo, Synthesis of active pharmaceutical ingredients using electrochemical methods: keys to improve sustainability *Chem. Commun*., **2022**, 58, 619.

53 Bu, F.; Lu, L.; Hu, X.; Wang, S.; Zhang, H.; Lei, A., Electrochemical oxidative decarboxylation and 1,2-aryl migration towards the synthesis of 1,2-diaryl ethers, *Chem. Sci.*, **2020**, *11*, 10000-10004.

54 a) Atobe, M.; Tateno, H.; Matsumura, Y., Applications of Flow Microreactors in Electrosynthetic Processes, *Chem. Rev.*, **2018**, *118*, 4541-4572; b) Pletcher, D.; Green, R. A.; Brown, R. C. D., Flow Electrolysis Cells for the Synthetic Organic Chemistry Laboratory, *Chem. Rev.*, **2018**, *118*, 4573-4591; c) Noël, T.; Cao, Y.; Laudadio, G., The Fundamentals Behind the Use of Flow Reactors in Electrochemistry, *Acc. Chem. Res.*, **2019**, *52*, 2858-2869.

55 a) Atobe, M.; Tateno, H.; Matsumura, Y., Applications of Flow Microreactors in Electrosynthetic Processes, *Chem. Rev.*, **2018**, *118*, 4541-4572; b) Pletcher, D.; Green, R. A.; Brown, R. C. D., Flow Electrolysis Cells for the Synthetic Organic Chemistry Laboratory, *Chem. Rev.*, **2018**, *118*, 4573-4591; c) Noël, T.; Cao, Y.; Laudadio, G., The Fundamentals Behind the Use of Flow Reactors in Electrochemistry, *Acc. Chem. Res.*, **2019**, *52*, 2858-2869.

56 Kagechika, H.; Shudo, K., Synthetic Retinoids: Recent Developments Concerning Structure and Clinical Utility, *J. Med. Chem.*, **2005**, *48*, 5875-5883.

57 a) Tanbouza, N.; Ollevier, T.; Lam, K., Bridging Lab and Industry with Flow Electrochemistry, *iScience*, **2020**, *23*, 101720 b) Lee, D. S.; Love, A.; Mansouri, Z.; Waldron Clarke, T. H.; Harrowven, D. C.; Jefferson-Loveday, R.; Pickering, R. J.; Poliakoff, M.; George, M. W., High-Productivity Single-Pass Electrochemical Birch Reduction of Naphthalenes in a Continuous Flow Electrochemical Taylor

Vortex Reactor, *Org. Process Res. Dev.*, **2022**, *26*, 2674-2684 and references cited therein.

58 a) Hintz, H. A.; Sevov, C.S. Catalyst-controlled functionalization of carboxylic acids by electrooxidation of self-assembled carboxyl monolayers, *Nat. Commun.*, **2022**, *13*, 1319; b) Leech, M. C.; Lam, K., Electrosynthesis Using Carboxylic Acid Derivatives: New Tricks for Old Reactions, *Acc. Chem. Res.*, **2020**, *53*, 121-134; c) Martínez, Á. M.; Hayrapetyan, D.; van Lingen, T.; Dyga, M.; Gooßen, L. J., Taking electrodecarboxylative etherification beyond Hofer–Moest using a radical C–O coupling strategy, *Nat. Commun.*, **2020**, *11*, 4407 and references cited therein).

59 Frisch, M.J.; Trucks, G- W.; Schlegel, H. B.; Scuseria, G. E.; Robb, M. A.; Cheeseman, J. R.; Scalmani, G.; Barone, V.; Petersson, G. A.; Nakatsuji, H.; Li, X.; Caricato, M.; Marenich, A. V.; Bloino, J.; Janesko, B. G.; Gomperts, R.; Mennucci, B.; Hratchian, H. P.; Ortiz, J. V.; Izmaylov, A. F.; Sonnenberg, J. L.; Williams-Young, D.; Ding, F.; Lipparini, F.; Egidi, F.; Goings, J.; Peng, B.; Petrone, A.; Henderson, T.; Ranasinghe, D.; Zakrzewski, V. G.; Gao, J.; Rega, N.; Zheng, G.; Liang, W.; Hada, M.; Ehara, M.; Toyota, K.; Fukuda, R.; Hasegawa, J.; Ishida, M.; Nakajima, T.; Honda, Y.; Kitao, O.; Nakai, H.; Vreven, T.; Throssell, K.; Montgomery, Jr. J. A.; Peralta, J. E.; Ogliaro, F.; Bearpark, M. J.; Heyd, J. J.; Brothers, E. N.; Kudin, K. N.; Staroverov, V. N.; Keith, T. A.; Kobayashi, R.; Normand, J.; Raghavachari, K.; Rendell, A. P.; Burant, J. C.; Iyengar, S. S.; Tomasi, J.; Cossi, M.; Millam, J. M.; Klene, M.; Adamo, C.; Cammi, R.; Ochterski, J. W.; Martin, R. L.; Morokuma, K.; Farkas, O.; Foresman, J. B.; Fox, D. J. Gaussian16, Revision C.01; Gaussian, Inc., Wallingford, CT, **2019**.

60 a) Grimme, S.; Neese, F., Fully Automated Quantum-Chemistry-Based Computation of Spin–Spin-Coupled

Nuclear Magnetic Resonance Spectra, *Angew. Chem. Int. Ed*., **2017**, *56*, 14763-14769; b) Bannwarth, C.; Ehlert, S.; Grimme, S., GFN2-xTB–An Accurate and Broadly Parametrized Self-Consistent Tight-Binding Quantum Chemical Method with Multipole Electrostatics and Density-Dependent Dispersion Contributions, *J. Chem. Theory Comput*., **2019**, *15*, 1652−1671; c) Pracht, P.; Bohle, F.; Grimme, S., Automated exploration of the low-energy chemical space with fast quantum chemical methods, *Phys. Chem. Chem. Phys.*, **2020**, *22*, 7169-7192.

61 Zhao, Y.; Truhlar, D. G., The M06 suite of density functionals for main group thermochemistry, thermochemical kinetics, noncovalent interactions, excited states, and transition elements: two new functionals and systematic testing of four M06-class functionals and 12 other functionals, *Theor. Chem. Acc.*, **2008**, *120*, 215-241.

62 a) Clark, T.; Chandrasekhar, J.; Spitznagel, G. W.; Schleyer, P. V. R., Efficient diffuse function-augmented basis sets for anion calculations. III. The 3-21+G basis set for first-row elements, Li-F, *J. Comput. Chem*., **1983**, *4*, 294-301; b) Ditchfield, R.; Hehre, W. J.; Pople, J. A., Self-Consistent Molecular-Orbital Methods. IX. An Extended Gaussian-Type Basis for Molecular-Orbital Studies of Organic Molecule, *J. Chem. Phys.*, **1971**, *54*, 724-728; c) Hariharan, P. C.; Pople, J. A., The influence of polarization functions on molecular orbital hydrogenation energies, *Theor. Chim. Acta*, **1973**, *28*, 213-222; d) Hehre, W. J.; Ditchfield, R.; Pople, J. A., Self-Consistent Molecular Orbital Methods. XII. Further Extensions of Gaussian-Type Basis Sets for Use in Molecular Orbital Studies of Organic Molecules, *J. Chem. Phys*., **1972**, *56*, 2257-2261.

63 Marenich, A. V.; Cramer, C. J.; Truhlar, D. G., Universal Solvation Model Based on Solute Electron Density and on a Continuum Model

of the Solvent Defined by the Bulk Dielectric Constant and Atomic Surface Tensions, *J. Phys. Chem. B*, **2009**, *113*, 6378-6396.

64 (a) Gonzalez, C.; Schlegel, H. B. Reaction path following in mass-weighted internal coordinates. *J. Chem. Phys*., **1990**, *94*, 5523-5527; (b) Gonzalez, C.; Schlegel, H. B. An improved algorithm for reaction path following. *J. Chem. Phys*., **1989**, *90*, 2154.

65 Cala L, Rubio-Presa R, García-Pedrero O, Fañanás FJ, Rodríguez F. Synthesis of Spirocyclic Compounds by a Ring-Expansion/Cationic Cyclization Cascade Reaction of Chlorosulfate Derivatives. *Org Lett*. , **2020,** 10, 3846-3849.

66 Natori, Y.; Sakuma, T.; Yoshimura, Y.; Kinami, K.; Hirokami, Y. Bioorganic & Medicinal Chemistry Letters Arabinoiminofuranoses , a New Class of a -Glucosidase Inhibitors. *Bioorg. Med. Chem. Lett.* **2014**, *24* (15), 3298–3301.

67 Cheung, F. K.; Lin, C.; Minissi, F.; Criville, A. L.; Graham, M. A.; Fox, D. J.; Wills, M.; Park, A. An Investigation into the Tether Length and Substitution Pattern of Arene-Substituted Complexes for Asymmetric Transfer Hydrogenation of Ketones. *Org.Lett*., **2007**, 4, 2005–2008.

68 Herold, S.; Bafaluy, D.; Muñiz, K. Anodic Benzylic C(Sp3)–H Amination: Unified Access to Pyrrolidines and Piperidines. *Green Chem.***, 2018**, 20, 3191–3196.

69 Nieman, J. A.; Coleman, J. E.; Wallace, D. J.; Piers, E.; Lim, L. Y.; Roberge, M.; Andersen, R. J. Synthesis and Antimitotic / Cytotoxic Activity of Hemiasterlin Analogues. *J. Nat. Prod.,* **2003**, 66, 183–199.

70 Bartkovitz, D. J.; Brook, P.; Us, N. J.; Liu, J.; Ross, M. (19) United States (12) Patent Application Publication. **2010**, *1* (12).

71 Chen, W.; Walker, J. C. L.; Oestreich, M. Metal-Free Transfer Hydroiodination of C − C Multiple Bonds. *J. Am. Chem. Soc.*, **2019**, 141, 1135-1140.

72 Hao, H.; Mao, Y.; Xu, Z.; Lou, S.; Xu, D. Selective Cross-Dehydrogenative C (Sp 3) − H Arylation with Arenes. *Org. Lett.,* **2020**, 22, 2396-2402.

73 Dabrowski, J. A.; Villaume, M. T.; Hoveyda, A. H. Angewandte Enantioselective Synthesis of Quaternary Carbon Stereogenic Centers through Copper-Catalyzed Conjugate Additions of Aryl- and Alkylaluminum Reagents to Acyclic Trisubstituted Enones. *Angew. Chem. Int*. **2013**, 52, 8156–8159.

74 Yu, X.; Wang, P.; Yan, D.; Lu, B.; Chen, J. Photocatalytic Neophyl Rearrangement and Reduction of Distal Carbon Radicals by Iminyl Radical-Mediated C-C Bond Cleavage. *Adv. Synth. Catal.*, **2018**, 360, 3601–3606.

75 Plamondon, S. J.; Gleason, J. L. Total Synthesis of (−)-3-Oxoisotaxodione. *Org. Lett.,* **2022**, 24, 2305-2309.

76 Süleyman Y.; Süleyman G.; First Synthesis of Dopamine and Rotigotin Analogue2-Amino-6,8-dimethoxy-1,2,3,4-tetrahydronaphthalene. *Synthetic Communications*., **2014**, 44, 1058-1065.

77 Yao, Y.-X.; Zhang H.-W.; Lu, C.-B.; Shang H.-Y., Tian Y.-Y.; Highly Selective and Practical Iron-Catalyzed Formal Hydrogenation of Epoxides to Primary Alcohols Using Formic Acid, *Eur. J. Org. Chem*. **2023**, 26..

78 Huang, H.; Jia, K.; Chen, Y. Hypervalent Iodine Reagents Enable Chemoselective Deboronative/Decarboxylative Alkenylation by Photoredox Catalysis. *Angew. Chem. Int*. **2015,** 54, 1881-1884.

79 Ledneczki, I.; Forgo, P.; Molnar, A.; Fused Polycyclic Hydrocarbons Through Superacid-Induced Cyclialkylation of Aromatics. *Catal. Lett.* **2007**, 119, 296-303.

5. *Aknowledgements*

At the end of this long journey, there are a few people i'd like to thank:

First of all, my mom, my dad and my brother. Making you proud is the only thing i live for. I love you.

To my best friends Edo, Catta, Simo, Gabo, Ale, Andre, Ste, that have been by my side for all my life. I wish i could be a friend as good as you.

To my supervisor Prof. Zanoni for the support he gave me during these years and for the challenges he put me in front of: it helped me to become a better and more mature chemist.

Thanks to Prof. Porta for all the tips and tricks he taught me and always worked. It's hard to find a more experienced chemist than you.

Thanks to Prof. Sarlah for his presence, that raised the overall level of all the students here.

Thanks to all the Flamma group, in particular Federico and Beatrice that have always believed in me and in the chemistry we were doing, even when i had trouble in believing myself. Thanks also to Massimo for his revolutionary ideas and his faith in electrochemistry.

A big thank to Pietro: there are a lot of things i'd like to say, but for now i'll say that you are the most gifted chemist (and person) i've ever known in my life. Wherever you go, they will be blessed to have you.

To Gio, Ghe and Ele for all the time we spent together. Nothing would be the same without you.

To Zigo just for being my friend and for having always a good advice for me. Sharing the fumehood was the best thing that happened to me during these years.

To Chad, that has been by my side from the first day i entered this lab. Working with you made me the better version of myself as a chemist and as a man. I hope one day our paths will meet again.

To Stef, for every day we spent 12+ hours in the lab from early morning to late evening, it's been a hell of a ride.

To Matteo for introducing me to Bar Italia.

To all the people that have been part of the B2 lab since i started, too many to mention individually.

To Milla, the first person i met at the university ten years ago. We already know everything.

To all my friends from the department, in particular Fra, Pancio and Matte for everything we experienced together.

To all my friends from Graz: Nikola, Bence, Pippo and Bhanwar that accepted me from the very beginning as a colleague and a brot. I will never forget you wherever you are in the world.

To Prof. Cantillo for the excellent supervision during my time in Austria.